RISK ASSESSMENT AND MITIGATION ON FREQUENCY STABILITY FOR OPERATIONAL PLANNING

WEN JIAXIN

PhD

The Hong Kong Polytechnic University

2021

The Hong Kong Polytechnic University

Department of Electrical Engineering

Risk Assessment and Mitigation on Frequency Stability for Operational Planning

Wen Jiaxin

A thesis submitted in partial fulfillment of the requirements for the degree of Doctor of Philosophy

August 2021

CERTIFICATE OF ORIGINALITY

I hereby declare that this thesis is my own work and that, to the best of my knowledge and belief, it reproduces no material previously published or written, nor material that has been accepted for the award of any other degree or diploma, except where due acknowledgment has been made in the text.

_____(Signed)

__WEN Jiaxin___(Name of student)

Abstract

The integration of renewable energy sources (RES) brings more uncertain active power supply into the system and reduces the system inertia, which incurs more severe frequency fluctuation and obvious heterogeneity of frequency responses in different areas. Thus, the risk of system and area-level frequency instability, represented by two indices, i.e., rate of change of frequency (RoCoF) and frequency nadir/vertex (FN/FV), requires to be assessed and mitigated in operational planning. Firstly, the cumulant-based assessment framework is proposed to efficiently assess system RoCoF and FN/FV, which includes analytical sensitivity and numerical sensitivity. Secondly, a linear sensitivity-based method with a straightforward calculation process is proposed to achieve fast and effective area-level RoCoF assessment, where two kinds of sensitivities are proposed, analytical sensitivity and integrated sensitivity. Then, the evaluated high risk of area-level RoCoF violation is mitigated by increasing inertia, and a probabilistic enhancement strategy is proposed to identify the required inertia demand for different levels of enhancement, where a small percentage of violation is allowed. Moreover, six allocation plans are proposed to distribute the area-level inertia to individual power plants in the region according to different considerations, i.e., technical feasibility and individual cost, and RoCoF performance. The multi-sensitivity and multi-interval methods are proposed to assess the risk of area-level FN/FV violation by additionally considering the impact of the RES locations and excitation system

compared with the widely employed system frequency response (SFR) model, where the multi-interval method can achieve more accurate evaluation due to the additional consideration of generator frequency oscillation. The effectiveness and efficiency of the proposed frameworks are validated by numerical scenario-based simulation (SBS).

Acknowledgments

First and foremost, I would like to express my most sincere gratitude to my chief supervisor, Dr. Siqi. Bu, for his continuous support, care, and encouragement throughout my PhD study and research. It is my honor to be supervised by Dr. Bu for my PhD, and I learnt large amount of knowledge, think patterns, writing skills, and so on from Dr. Bu, which benefits my future life. I also appreciate the support, encouragement, and assistance from my co-supervisor, Dr. Kevin K. W. Chan.

I would like to express my special appreciation to my research group Dr. Jianqiang Luo, Ms. Qian Hu, Mr. Yong Hu, Dr. Qi Wang, Dr. Shiwei Xia, Mr. Ruoheng Wang, Ms. Jiangfeng Zhang, Ms. Chaoyun Wang, for the patient support throughout my entire PhD study.

My thanks also go to my friends Mr. Zilin Li, Dr. Xiang Gao, Dr. Da XU, Ms. Lei Meng, Dr. Xiaoshun Zhang, Mr. Kuang Zhang, Ms. Ling ZHENG. They have given me much valuable advice and practical helps on my life and research. I will never forget this marvelous research journey in Hong Kong.

Moreover, I would like to thank my dear parents for their selfless and unconditional love and support for my study.

Last but not least, I would like to acknowledge the support from The Hong Kong Polytechnic University.

Table of Contents

Lists of Figures

Lists of Tables

Lists of Abbreviations

ACOI	Area-level center of inertia
AID-AP	Average inertia-based distributed AP
AP	Allocation plan
AS	Analytical sensitivity
BID-AP	Balanced inertia-based distributed AP
BSD-AP	Balanced sensitivity-based distributed AP
CBM	Cumulant-based method
CDF	Cumulative distribution function
COI	Center of inertia
DFT	Discrete Fourier transform
DG	Distributed generators
FN/FV	Frequency nadir/vertex
FSMI	Frequency stability margin index
IC-AP	Inertia-based centralized AP
IS	Integrated sensitivity
LSM	Linear-sensitivity method
MIS	Multi-interval sensitivity
MPS	Multi-point sensitivity
NC-AP	Network-based centralized AP
NS	Numerical sensitivity
PCA	Principal component analysis
PDF	Probability distribution function
PMU	Phasor measurement unit
PSO	Particle swarm optimization
PVP	Photovoltaic plant

RAM	Risk assessment matrix
RES	Renewable energy source
RIIM	RAM-based inertia identification method
RoCoF	Rate of change of frequency
SBS	Scenario-based simulation
SC-AP	Sensitivity-based centralized AP
SFR	System frequency response
VSG	Virtual synchronous generator
WAMS	Wide area measurement system
WF	Wind farm

Chapter 1

Introduction

1.1 Background

The rapid development of industry and commerce has led to a substantial increase in the demand for electricity supply, which will exacerbate the rate at which limited fossil energy is consumed and further produce a large number of greenhouse gases[1]. To improve this situation, a low-carbon energy system is required to gradually replace the currently fossil-based energy system as the main power generation system [2], which can be achieved by increasing the proportion of renewable energy source (RES)-based generation in the future power system [3-5]. Hence, quite a few countries have been studying how to make full use of natural resources, such as wind and solar, for electricity supply and further building a large number of RES-based plants [6, 7]. For example, the installed wind energy capacity in China, the USA, Germany, Spain, India, UK, Italy, France, Canada, Brazil, and Pakistan continues to increase from 2000 to 2018, as presented in Fig. 1.1 [8]. The figure also exhibits that China occupies the largest share of installed wind power capacity in all countries.

In [9], the development trend of the future power grid is predicted, as shown in Fig. 1.2. The percentage of RES-based generation in the total electricity generation is forecasted to be 50%, 80%, 95%, and eventually 100% in 2025, 2030, 2040, and 2050, respectively. Wind energy and solar energy account for 37% and 57% of total

generation, respectively, where onshore wind energy holds the largest share, i.e., 23.52%. Thereby, it is necessary to face the opportunities and challenges brought by the RES-based power generation system.

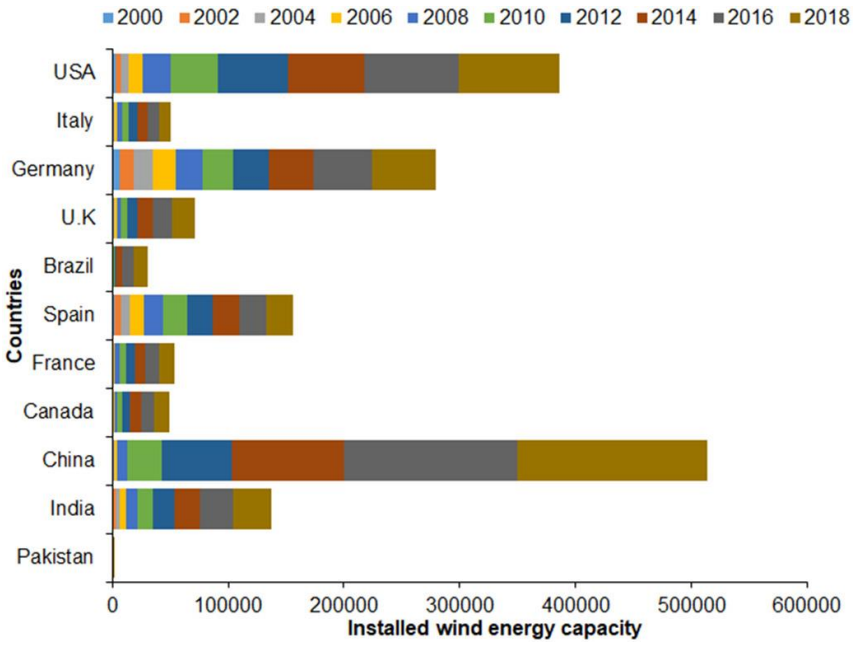

Fig. 1.1 The installed wind energy capacity of different countries from 2000 to 2018 [8].

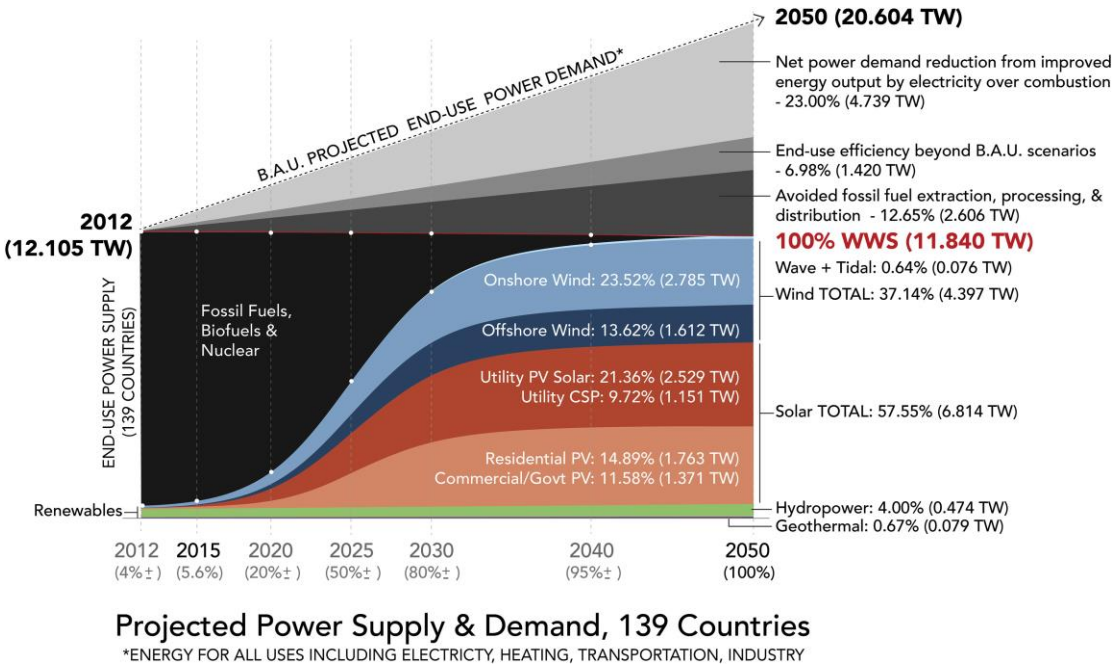

Fig. 1.2 The forecasted development trend of RESs in the future [9].

1.2 Research Motivations

The integration of the RES can effectively alleviate the problem of energy shortage and environmental pollution, while it also brings an increasing number of stochastic disturbances into power systems [10-13]. Moreover, replacing conventional power plants with RES-based plants leads to a reduction in system inertia which is a critical parameter participating in the stable regulation of a power system [14-16]. The above two changes in a modern power system will more easily incur the risk of system instability than ever before, including power angle instability [17-19], voltage instability [20-22], and frequency instability [23-26].

The stochastic active power output of RESs breaks the balance between the power supply and the load demand, which directly causes the frequency deviation and triggers the action of some control systems such as the excitation system or governor droop control system [27]. When the frequency fails to be regulated within a safe range preset by grid code, the protective measures are triggered, such as under frequency load shedding [28, 29] and over frequency generator tripping [30, 31], which would cause the power supply interruption for consumers and power oscillation in the grid and thus should be avoided in practice if possible [32, 33]. The London blackout on 9 August 2019 drew wide attention, and the official investigation report [34] indicates that a sudden reduction in the power output of the Hornsea offshore wind farm worsened the frequency response (the high RoCoF, i.e., rate of change of frequency and the large FN, i.e., frequency nadir) considerably, which furthered the enormous loss of both generations and demands. Therefore, it is necessary to assess and mitigate the potential

risks of frequency instability caused by the stochastic variation of RESs in operational planning.

To address this challenge brought by the integration of the RES into the grid, the current practice of most electricity companies is to contract on additional conventional generation, which is mostly more than actual needs to accommodate the predicted arbitrary "worst-case scenario." However, the "worst-case scenario" where the uncertain disturbances of all the RESs reach maximum simultaneously rarely happens in a highly RES-penetrated power system because of spatiotemporal uncorrelation among the same or different types of the RESs in the network [35]. For different kinds of RESs, wind farms (WFs) often reach the maximal output in the night while the photovoltaic plants (PVPs) only generate during the daytime. The same type of RESs located in different places could follow the same distribution, such as wind speed following Weibull distribution but with different parameters such as average wind speed. Moreover, the correlation of wind speed received by two remote WFs is quite low. These factors would result in a relatively low probability of simultaneously maximal or minimal power supply from converter-interfaced RESs. Hence, the "worst-case scenario"-based deterministic assessment, which can only determine whether an event is secure or not [36], is not suitable to cope with such a situation since it fails to discover the degree of risk, i.e., the occurrence probability of an event. Therefore, a two-dimensional (probabilistic/risk) evaluation including both the severity and the occurrence probability of the event is more beneficial for the system planner to make a decision, which may further increase the allowed penetration level of RESs.

The two-dimensional evaluation can achieve this goal in three steps: 1) to model the stochastic output of uncertainties, 2) to compute the probability distribution of the interested indices (i.e., RoCoF and FN/FV, i.e., frequency nadir/vertex, in this thesis), and 3) to assess the result based on the risk assessment matrix (RAM) [37, 38].

The stochastic models of uncertainties can be divided into three types according to power system structure: generation, demand, and network.

1) The uncertainty of power generation is mainly caused by the stochastic output of the WFs, PVPs, and conversational plants. The uncertain wind power follows discrete normal distribution [39] and normal distribution [40]. The wind speed follows Weibull distribution [41], normal distribution [42], discrete normal distribution [43], joint Gaussian distribution [44], log-normal distribution [45], and gamma distribution [46]. The Beta distribution [47] and Weibull distribution [48] can be adapted for solar power, which can also be modeled using past data [49]. The stochastic model of power generation can be expressed using normal distribution [50] and historical data [51].

2) The uncertainty model of system demand can be expressed as a normal distribution [52], Gumbel distribution [53], discrete distribution [39], joint normal distribution [54]. The historical data can also be used to establish related probability distribution function (PDF) [55], and the load change is described using the Poisson jump process [56, 57].

3) The fault incident follows Poisson distribution [58] and binomial distribution [59]. The exponential distribution is applied for time to failure [58], and the fault location can be modeled using uniform distribution [56] or historical data [60]. The

Rayleigh distribution [53, 61] is suitable for fault duration time, and the fault clearing is described using normal distribution [53, 62] or the Poisson jump process [57].

The assessment method is divided into two main categories according to the process of acquiring the desired PDF curve, i.e., numerical method and analytical method.

The numerical method aims to compute the probabilistic distribution of the concerned indices by generating a large number of random variables and thus, simulation results, which mainly refers to the Monte Carlo simulation [63, 64] including sequential Monte Carlo [65, 66], pseudo sequential Monte Carlo [67], nonsequential Monte Carlo [68], and Markov chain Monte Carlo [69, 70]. In [63], a scenario-based simulation (SBS), similar to sequential Monte Carlo, is employed to calculate the maximal renewable energy penetration limits to maintain the frequency performance by considering a large number of potential operational scenarios. The results are accurate, but its calculation procedure is very time-consuming, which is usually regarded as a verification tool

The analytical method calculates the distribution of the concerned indices based on the statistic theory and sensitivity or a limited number of simulation results, including cumulant-based method (CBM) [41], Taylor series expansion[71, 72], first-order second-moment method [73, 74], point estimation method [75, 76], unscented transformation method (UT) [77]. The CBM can comfortably accommodate arbitrary types of continuous or noncontinuous distribution and correlation of stochastic variables [41], which is proven to be the most efficient and accurate way to conduct probabilistic small-signal stability analysis in [78]. Moreover, the CBM has not been

employed for probabilistic assessment on frequency stability [79].

The grid frequency essentially reflects the rotational speed of the synchronous generators [80], which can be estimated using system bus measurement by phasor measurement unit (PMU) [81]. On this basis, the RoCoF can be computed as the incremental ratio of two consecutive frequency estimates according to either P-class or M-class models given in IEEE Standards [82]. Many technologies are applied for frequency estimation, including zero-crossing detection, Kalman filter [83, 84], discrete Fourier transform (DFT) [85-87], and their extended methods. The zero-crossing detection is usually applied to obtain the frequency, while the accuracy is low when the signal is distorted caused by disturbances or faults. The Kalman filter is widely applied in power system frequency estimation, based on the identification theory and the relationship among sampled voltage signals in time series. The method depends on the initial conditions largely, and the calculation procedure is complicated [83, 84]. The DFT is easy to implement where the frequency is estimated based on the phase angle difference of two consecutive phasors, but the phasor requires to be updated continuously with rolling data windows, which indicates a large amount of computational burden [85-87].

Normally, the most critical system RoCoF occurs right after the instant of disturbance without yet triggering any control actions [88-90], which is the focus of the thesis. At the moment of the disturbance occurring (t=0^+), the grid frequency changes smoothly, owing to resistance from the inertia of synchronous machines [32], while the voltage phase angle of the bus has a sudden jump [91], which finally leads to an

inconsistency between the estimated RoCoF and the genuine value associated with synchronous generators[80, 92, 93]. Reference [80] reports that when there is a 20O phase jump in bus voltage after a disturbance, the estimated frequency and RoCoF by PMU would be 45Hz and 500Hz/s respectively for the next half-cycle, which is far from relevant generator values and could lead to a misalarm. This estimation inconsistency has been dealt with by several measures in [81, 92]. One of the most common solutions is to intentionally fix the estimate as the last valid RoCoF, i.e., the value before the event occurrence [92], which actually ignores the initial RoCoF response. In [81], an advanced interpolation technique is proposed to estimate average RoCoF, which corresponds to a longer interval containing the disturbance instant rather than the instant at $t=0^+$. To calculate RoCoF over a time window could underestimate the power grid security risk, which is not desirable from a system operators' perspective.

Moreover, the system operator considers the system frequency and RoCoF as global variables for operational planning [94], which is usually aggregated based on the center of inertia (COI) or employs a typical bus measurement [91]. However, the fact of uneven distributions of inertia in the system and increasing heterogeneity of the network due to the growing integration of distributed RESs can actually lead to drastically different frequency responses in different areas [95], which deserves careful monitoring and studies but cannot be easily accommodated by conventional planning analysis, where only a uniform frequency response is assumed [96].

On the premise of unchanged capacity and steady output power of the RES and the network structure, increasing the inertia is an effective solution to mitigate the risk of

RoCoF violation. The concept of the virtual synchronous generator (VSG) [97], also called a virtual synchronous machine [98] or synchronverter [99], is introduced to emulate the behavior of a synchronous generator, including the emulation of inertia by controlling the operation of an inverter and the connected energy storage system properly. In addition, virtual inertia is realized by different control strategies on the energy storage equipment and applied in different fields such as the microgrid, wind turbines, and HVDC [100-103].

The VSG can be employed for the improvement of risky RoCoF conditions. In [104], a VSG is introduced for grid frequency support, which lowers the RoCoF risk caused by the stochastic output of distributed generators. In [105], the RoCoF performance is enhanced by a VSG emulated by controlling a microgrid-forming inverter for the supercapacitor. In [106], a power electronic converter-connected capacitor is installed in parallel with the generator to emulate inertia by regulating the DC-link voltage in order to reduce RoCoF.

RoCoF is an essential indicator of determining the required inertia of the system and area in operational planning. In [107], particle swarm optimization (PSO) is applied to calculate the virtual inertia constant with the consideration of the RoCoF-based protection scheme. In [108] and [109], RoCoF limitation is considered to determine the minimal level of system inertia for unit commitment in the worst-case scenario. The critical value of RoCoF is applied to limit the system inertia as a constraint in a commitment-and-dispatch issue [110] and economic dispatch [90]. In [63], a dynamic inertia constraint is proposed to guarantee the stability of area-level RoCoF by

maintaining the inertia no less than a specific value that is calculated based on the critical value of RoCoF.

However, in a multi-RES penetrated power system, the 'worst-case scenario' caused by the simultaneously maximal or minimal output of all RESs rarely happens, as analyzed before. Moreover, it is reasonable to assume that the cost increases with the size of required inertia, and thus, less required inertia is preferred by electric companies due to less cost. Thereby, it is necessary and practical to trade off the risk of RoCoF violation and the cost for reducing the required inertia, which is the motivation to propose probabilistic mitigation on the risk of RoCoF violation. It should be noted that the detailed cost analysis is not the focus of the thesis, and this simple assumption is sufficient for the following analysis. The RAM is suitable to coordinate both factors by relaxing the constraint from severity (i.e., RoCoF limits) and meanwhile considering the constraint from occurrence probability, which can be adjusted manually according to different requirements in operational planning. Therefore, it is practical and economic to provide the system operator with a series of options on mitigating the risk of RoCoF violation, each of which is a pair of the selectable risk degree and corresponding required inertia or cost.

After acquiring the area-level inertia demand, i.e., the total inertia required to be added in the area for security concerns, it is necessary to allocate the inertia demand to individual conventional power plants properly. For instance, the area-level inertia demand can be allocated to a single big power plant directly or multiple generators dispersedly in the region, the sum of which should be equal to the area-level inertia

demand calculated in the previous step. However, few pieces of literature present a detailed distribution plan.

For current pieces of literature, two types of coherency identification methods are applied: model-based method and measurement-based method.

The model-based coherency identification [111-113] groups the regions according to the similar frequency dynamic response of generators during the low-frequency oscillation, which can be presented by eigenvalue and eigenvectors of the linearized system. Thus, this method requires the classical generator model and the network information.

The measurement-based method requires a part of the system response data, such as the rotor angle curve or frequency deviation signal, as the input for coherency identification, which is extracted from the monitoring equipment such as PMU and Wide Area Measurement System (WAMS). Then a specific classification criterion is employed on these data to acquire the partition results. In [114], the relative correlation of the rotor angle curves is taken as a standard for coherency identification. While in [115], the principal component analysis (PCA) is applied to obtain the proper coherent generators based on rotor angle curves. In [116], frequency deviation signals of both generators and buses are used for coherent identification base on relative correlation.

Both methods require different kinds of data for coherency identification, i.e., system parameters and measurement data, and hence, the method can be determined according to the available data.

Another vital index quantifying the risk of frequency stability is the FN/FV, which

is the bottom/peak of a frequency response curve in a period of time [117]. Numerous investigations on FN/FV have been conducted. In [118], the classical system frequency response (SFR) model is proposed to derive the system FN/FV w.r.t a disturbance, which treats the whole system as a mass and ignores the impacts of the electric distance, generator excitation system, and the interaction among the outputs of individual generator in the system. Although these assumptions seem less accurate, the SFR model provides a clear understanding and foundation for frequency stability analysis and thus is widely adopted. Quite a few improvement methods are developed to achieve better performance. In [119], the short-term first-order model for governors and prime movers in the SFR model is approximated by an aggregated constant that considers the impacts of individual generators. On this basis, the maximal frequency deviation of a small isolated system is estimated, while the excitation system is not considered. In [120], the excitation system is involved in predicting the system FN after a large disturbance, where a constant ramp rate of the overall mechanical power response is approximated to fit the response of each governor response. However, only one disturbance is considered, and the impacts of disturbance locations, especially in a multi-RES penetrated power system on system FN/FV, have not been investigated. To sum up, system FN/FV is investigated widely based on the SFR model, improved SFR model, and fitting method, in which the impact of frequency oscillation of individual generators can be offset when computing the system-level frequency response and thus can be ignored. However, few literature assesses the area-level FN/FV.

Based on the above analysis, it is necessary to probabilistically assess the risk of

system and area-level RoCoF and FN/FV violation using a more efficient and effective method and mitigate the high risk in a probabilistic manner rather than the ‘worst-case scenario’-based deterministic manner.

1.3 Primary Contributions

The integration of the RESs incurs more severe the issue of frequency instability, which requires to be evaluated for operational planning. This thesis aims to probabilistically assess and enhance the risk of system and area-level frequency violation using several effective and efficient methods compared with traditionally employed SBS.

1) The CBM-based assessment is firstly employed to achieve an efficient risk assessment on system frequency stability margins, i.e., system RoCoF and system FN/FV, where two types of sensitivities are adopted. The analytical sensitivity (AS) is derived based on an aggregated SFR model, which ignores the impacts from the network information and excitation system. The proposed numerical sensitivity (NS) is obtained using a perturbation method, which does not require information on power flow and network structure. The number of the required simulation equals the number of the RES in the system. The proposed framework can significantly facilitate the system planner’s decision-making process in operational planning and effectively mitigate the renewable curtailments.

2) The AS-LSM (linear-sensitivity method) is proposed to achieve a fast calculation on probabilistic distribution of the area-level RoCoF, where required AS of area-level

RoCoF w.r.t stochastic output of the RES is derived based on the classical generator model and the network information. The proposed AS-LSM and AS-CBM can achieve similar evaluation accuracy verified by SBS in uncorrelated wind speed-based scenarios and correlated wind speed-based scenarios. While the proposed AS-LSM has a higher computing efficiency than SBS and a more straightforward calculation procedure compared with AS-CBM.

3) A perturbation method is introduced to quantify the relationship between RES variation and the compensation of a conventional plant (i.e., power distribution coefficient) for integrating the proposed integrated sensitivity (IS), which does not require information on power flow and network structure. The proposed IS-LSM achieves a fast assessment of the risk of area-level RoCoF violation in operational planning. The area-level RoCoF calculated by the proposed method is proven to be consistent with the aggregated generator RoCoF according to the conventional definition of area center frequency but with less computational time. Based on the IS and the assessment results by IS-LSM, the RAM-based inertia identification method (RIIM) is proposed to determine the inertia demand for enhancement of the risky RoCoF condition in a probabilistic manner for the first time. The merit of the method can effectively reduce the cost of investment on improving risky RoCoF (i.e., reducing the size of the area-level inertia demand) and increase the penetration level of the RES. Moreover, different levels of probabilistic enhancement can be selected by manually setting different values of defined probabilistic enhancement coefficient according to different requirements within limits from the given RoCoF RAM. Six allocation plans

(APs), including centralized and distributed plans, are proposed to distribute the area-level inertia demand calculated by the proposed RIIM to individual plants in the area according to technical feasibility and individual cost & RoCoF performance, which provides more options for system operational planners' decision making.

4) A multi-point sensitivity (MPS) is established based on the classical generator model to describe the relationship between the system FN/FV and the stochastic output of multiple RESs, which can reflect the impacts of RES locations on system FN/FV and further be extended for area-level evaluation. The method is easy to implement, and only limited data are required. Based on MPS, a multi-interval sensitivity (MIS) is further proposed considering the impacts of generator frequency oscillation on area-level FN/FV according to different output ranges (i.e., above or below the steady output) of individual RES. The proposed MPS method and MIS method are superiority over SBS in time consumption and are also more accurate than SFR model-based method when assessing system FN/FV. Both MPS and MIS methods can accommodate any arbitrary distribution of RESs. The MIS -based assessment is more accurate while more data are required. The system operator can select either method for risk assessment in operational planning according to practical needs.

1.4 Thesis Layout

The rest of this thesis consists of five Chapters. Chapter 2 firstly presents a cumulant-based framework of risk assessment of system RoCoF and FN/FV for operational planning, some of which are further utilized in the following chapters,

including the stochastic modelling of the uncertainties and established assessment tool, i.e., RoCoF RAM and FN/FV RAM. Chapter 3 firstly briefly reviews the slow coherency identification method, which is treated as a basis for following area-level assessment, and then proposes the AS-LSM to achieve a fast calculation on probabilistic distribution of area-level RoCoF, which is compared with AS-CBM. Chapter 4 develops a framework for probabilistically assess and mitigate the risk of area-level RoCoF violation, which contains the six APs distributing the area-level inertia demand to the individual generator in the region. Chapter 5 presents an MIS method to achieve an effective and efficient evaluation on area-level FN/FV considering the generator frequency oscillation. Finally, the conclusions and future work of the thesis are drawn in Chapter 6.

Chapter 2

Cumulant-based Risk Assessment on System RoCoF and FN/FV

In view of modern power systems characterized by significant inertia reduction and booming uncertainty, this chapter proposes an important operational planning tool to comprehensively analyze frequency stability via representative indices, RoCoF, and FN/FV in a probabilistic manner for the first time. The proposed generic framework can tackle various frequency-related uncertainties and accommodate different system frequency response models. The proposed framework consisted of four parts: stochastic modeling of frequency-related uncertainties, the computing sensitivities of RoCoF and FN/FV, cumulant-based identification for probabilistic distribution of RoCoF and FN/FV, and assessment tools, which will be elaborated in sequence. The results of case studies prove the effectiveness of the proposed framework.

2.1 Modeling Power System Frequency-related Uncertainties

The major uncertainties related to power system frequency stability refer to the stochastic active power disturbance in the system, which could be caused by the fluctuation of renewable energy and system loads or system faults such as generation loss. Since the former cause is a comparatively new issue and happens much more frequently with an increasing impact, it is the main focus of this chapter. Therefore, the stochastic modeling of wind and solar power and demand are presented here. The

impact of system faults can also be modeled and assessed by the framework according to the assessment need. It is reported that wind and solar power follow different distributions according to different assessment timescales and demand generally follows normal distribution, as shown in Fig. 2.1. For instance, Beta distribution should be adopted for the wind and solar power during day-ahead planning, while for year-ahead planning, the Weibull distribution is applied for wind power and normal distribution is suitable for solar power. The spatiotemporal correlations between different renewable energy sources and system loads can be properly modeled by the correlation coefficient matrix [41].

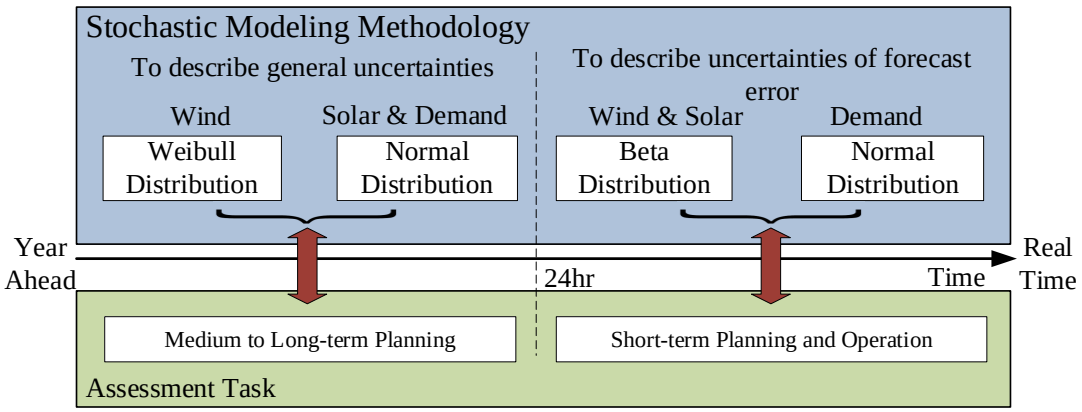

Fig. 2.1 Stochastic modelling of uncertainties from different RESs and system loads in different assessment tasks/timescales.

2.2 Computing the Sensitivity of RoCoF and FN/FV w.r.t Active Power Disturbance

2.2.1 AS of System RoCoF and FN/FV

The AS of RoCoF and FN/FV can be derived based on the SFR model aggregated by the method in [121], which averages the dynamic behavior of each generator. It is

considered a useful and simple model to express the behavior of the frequency response. The simplified model is shown in Fig. 2.2. According to the structure, the frequency response is calculated:

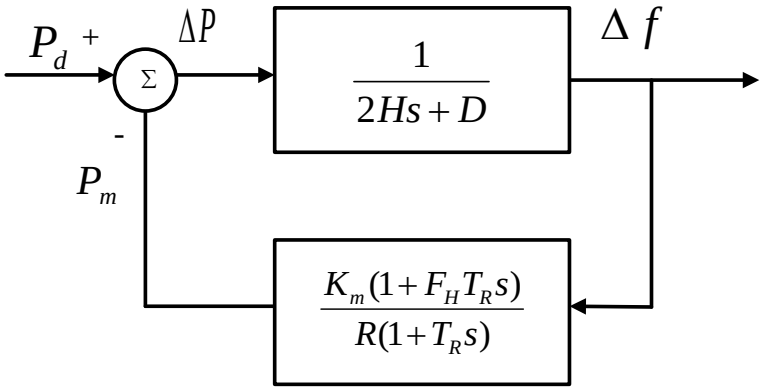

Fig. 2.2 A simplified SFR model with a single disturbance.

$$\Delta f = \left(\frac{R\omega_n^2}{DR+K_m}\right)\left(\frac{(1+T_R s)}{s^2+2\xi\omega_n s+\omega_n^2}\right)P_d \tag{2.1}$$

where R is governor speed droop constant, D is load damping constant, and H is system inertial constant. K_m is mechanical power gain, T_R is reheat time constant F_H, is high-pressure turbine fraction, P_d is the system active power disturbance.

$$\omega_n^2 = \frac{DR+K_m}{2HRT_R} \tag{2.2}$$

$$\varsigma = \frac{2HR+DRT_R+K_m F_H T_R}{2(DR+K_m)}\omega_n \tag{2.3}$$

In the Laplace domain, the disturbance is expressed as:

$$P_d(s) = \frac{\Delta P}{s} \tag{2.4}$$

where ΔP is the magnitude of the P_d. Substituted (2.4) into (2.1), and the result is shown below:

$$\Delta f = \left(\frac{R\omega_n^2}{DR+K_m}\right)\left(\frac{(1+T_R s)}{s^2+2\xi\omega_n s+\omega_n^2}\right)\frac{\Delta P}{s} \tag{2.5}$$

The equation is expressed in the time domain:

$$\Delta f(t) = \frac{R\Delta P}{DR+K_m}(1 + ae^{-\varsigma\omega_n t}\sin(\omega_r t + \phi)) \tag{2.6}$$

where,

$$a = \sqrt{\frac{1-2T_R\varsigma\omega_n+T_R^2\omega_n^2}{1-\varsigma^2}} \tag{2.7}$$

$$\omega_r = \omega_n\sqrt{1-\varsigma^2} \tag{2.8}$$

$$\phi = tan^{-1}\left(\frac{\omega_r T_R}{1-\varsigma\omega_n T_R}\right) - tan^{-1}\left(\frac{\sqrt{1-\varsigma^2}}{-\varsigma}\right) \tag{2.9}$$

The worst RoCoF happens right after the system disturbance (at $t = 0^+$) before the governor responds. Thus, if the worst RoCoF can be kept within the standard, the system can be secured for other RoCoF conditions. To study the SFR model without the governor, let mechanical power variation $\Delta P_m = 0$ in (or simply set $K_m = 0$), (2.6) becomes

$$\Delta f(t) = \frac{\Delta P}{D} = \left(1 - e^{-\frac{D}{2H}t}\right) \tag{2.10}$$

The (2.10) demonstrates that $\Delta f(t)$ only depends on D, H and ΔP before the governor is in service. Based on (2.10), the worst and biggest RoCoF is proved to be at $t = 0^+$

$$\frac{d\Delta f(0^+)}{dt} = \frac{1}{2H}\Delta P \tag{2.11}$$

From the above analysis, it is easy to find the different signs of the ΔP would lead

to different frequency characteristic ($\Delta P < 0$ will lead to FN and $\Delta P > 0$ will lead to FV). Based on (2.6), let $\frac{d\Delta f(t)}{dt} = 0$, so that FN/FV $\left(\Delta f_{\frac{n}{v}}\right)$ and the time to reach FN/FV $\left(t_{\frac{n}{v}}\right)$ can be calculated

$$t_{n/v} = \frac{1}{\omega_r} tan^{-1}\left(\frac{\omega_r T_R}{\varsigma\omega_n T_R - 1}\right) \tag{2.12}$$

$$\Delta f_{n/v} = \left(\frac{R}{DR + K_m}\left(1 + ae^{-\varsigma\omega_n t_{n/v}}\sqrt{1-\varsigma^2}\right)\right)\Delta P \tag{2.13}$$

FN/FV (the worst steady-state frequency condition) normally occurs before the supplementary control (automatic generation control (AGC)) starts to operate. Hence the function of AGC is not considered for FN/FV analysis, which is mainly used to eliminate the steady-state frequency deviation.

2.2.2 NS of System RoCoF and FN/FV

Obviously, the so-called AS (FN/FV or RoCoF) computed from the analytical SFR model is identical for all the disturbances with different locations. The uncertainties occurring in different locations of the network might have slightly different impacts on the system center frequency, which implies that the network could be considered in the sensitivity calculation to enhance the assessment accuracy in this case.

Therefore, a concept of NS is defined here to characterize and quantify the network impact of frequency-related uncertainties, which can be simply computed by the perturbation approach in the following.

$$NS = \frac{X_m}{\Delta P_t} \tag{2.14}$$

Where X_m refers to $RoCoF_S$ or $\frac{FN}{FV_S}$ of the frequency response of system center (f_{COI}), which could be easily obtained from:

$$f_{COI} = \frac{\sum_{i=1}^{N} f_i H_i}{\sum_{i=1}^{N} H_i} \tag{2.15}$$

where f_i is the frequency response of the i^{th} generator, N is the number of generators in the system, H_i is the inertia constant of the i^{th} generator based on a common base. Hence, there is no need of SFR model in the NS computation.

2.3 Cumulant-based Identification for Probabilistic Distribution of RoCoF and FN/FV

The CBM can directly obtain the PDF of RoCoF and FN/FV, the calculation process of which is described in detail as follows:

The wind energy transferred from wind speed following the Weibull distribution is selected as the typical RES for demonstration purposes. The relationship between wind speed and wind power is illustrated in Fig. 2.3 and described from:

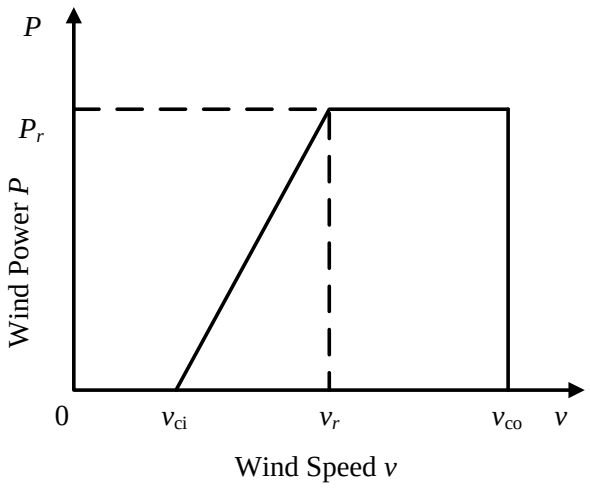

Fig. 2.3 The relationship between wind speed and wind power.

$$P_w = \begin{cases} 0 & v \le v_{ci} \\ k_1 v + k_2 & v_{ci} \le v \le v_r \\ P_r & v_r \le v \le v_{co} \\ 0 & v \ge v_{co} \end{cases} \tag{2.16}$$

where v_{ci}, v_{co} and v_r are cut-in wind speed, cut-out wind speed, and rated wind speed, respectively, and P_r is the rated power of a wind turbine generator.

$$k_1 = \frac{P_r}{v_r - v_{ci}} \tag{2.17}$$

$$k_2 = -k_1 v_{ci} \tag{2.18}$$

The Weibull distribution is presented from

$$f_p(P_w) = \begin{cases} \left(1 - \left(F_s(v_{co}) - F_s(v_{ci})\right)\right)\delta(P_w) & P_{wi} = 0 \\ \frac{b}{d}\left(\frac{P_w - k_2}{d}\right)^{b-1} e^{-\left(\frac{P_w - k_2}{d}\right)^b} & 0 < P_w < P_r \\ \left(F_s(v_{co}) - F_s(v_r)\right)\delta(P_w - P_r) & P_w = P_r \\ 0 & P_w < 0 \; or \; P_w > P_r \end{cases} \tag{2.19}$$

where,

$$b = \left(\frac{\sigma}{\mu}\right)^{-1.086} \tag{2.20}$$

$$d = \frac{P_r \mu}{(v_r - v_{ci})\Gamma\left(1 + \frac{1}{b}\right)} \tag{2.21}$$

where $\Gamma(\cdot)$ is a Γ function, μ and σ are the mean and standard deviation of wind speed, respectively.

The CBM is applied to obtain the PDF of the frequency characteristics. Firstly, the moment and cumulant of the wind power generation is derived below:

$$\alpha^n_{\Delta P_w} = \int_{-P_{w0}}^{P_r - P_{w0}} x^n dF_p(x) = \int_{-P_{w0}}^{P_r - P_{w0}} x^n f_p(x)\, dx$$

$$= \left(1 - \left(F_s(v_{co}) - F_s(v_{ci})\right)\right)(-P_{w0})^n + \left(F_s(v_{co}) - F_s(v_{ci})\right)(P_r - P_{w0})^n$$

$$+ \sum_{k=0}^{n} C_n^k\,(d)^k (k_2 - P_{w0})^{n-k} \times \int_{\left(\frac{-k_2}{d}\right)^b}^{\left(\frac{P_r - k_2}{d_i}\right)^b} \tau^{\frac{k}{d}} e^{-\tau} d\tau \qquad (2.22)$$

where, $C_n^k = \frac{n!}{k!(n-k)!}$ and $\int_{\left(\frac{-k_2}{d}\right)^b}^{\left(\frac{P_r - k_2}{d_i}\right)^b} \tau^{\frac{k}{d}} e^{-\tau} d\tau$ is an incomplete Γ function.

The n^{th} order cumulant, $\gamma_{\Delta P_w}^n$, as the semi-invariant, is the polynomial in $\alpha_{\Delta P_w}^1$, $\alpha_{\Delta P_w}^2$,…$\alpha_{\Delta P_w}^n$ for example from [122, 123]:

$$\gamma_{\Delta P_w}^1 = \alpha_{\Delta P_w}^1$$

$$\gamma_{\Delta P_w}^2 = \alpha_{\Delta P_w}^2 - \left(\alpha_{\Delta P_w}^1\right)^2$$

$$\gamma_{\Delta P_w}^3 = \alpha_{\Delta P_w}^3 - 3\alpha_{\Delta P_w}^1 \alpha_{\Delta P_w}^2 + 2\left(\alpha_{\Delta P_w}^1\right)^3 \qquad (2.23)$$

Therefore, the n^{th} order cumulant, $\gamma_{\Delta P_w}^n$ can be calculated from the various-order moment.

According to the probability theory in [122, 123], if the relationship between a random variable ρ and m other independent random variables $\eta_j, j = 1,2 \ldots \text{m}$ is linear, that is $\rho = a_1\eta_1 + a_2\eta_2 + \cdots + a_{\text{m}}\eta_{\text{m}}$, their n^{th} order cumulants satisfy the following equation:

$$\gamma_\rho^n = \alpha_1^n \gamma_{\eta_1}^n + \alpha_2^n \gamma_{\eta_2}^n + \cdots + \alpha_{\text{m}}^n \gamma_{\eta_{\text{m}}}^n \qquad (2.24)$$

If m wind generation sources are connected into the grid, and the relationship between the FSMIs (frequency stability margin index) referring to RoCoF or FN/FV and the wind farm is established as the following:

$$\Delta FSMI = \sum_{i=1}^{m} \left(\frac{\partial FSMI}{\partial P_{wi}}\right) \Delta P_{wi} \tag{2.25}$$

From (2.24) and (2.25), it can be obtained:

$$\gamma_{\Delta FSMI}^{n} = \sum_{i=1}^{m} \left(\frac{\partial FSMI}{\partial P_{wi}}\right)^{n} \gamma_{\Delta P_{wi}}^{n} \tag{2.26}$$

where $\gamma_{\Delta \mathrm{FSMI}}^{n}$ is the n^{th} order cumulant of the random variation of the *FSMI*. The mean of $\Delta FSMI$ is $\mu_{\Delta FSMI} = \gamma_{\Delta FSMI}^{1}$. The derivation of the (2.26) is based on the assumption that wind speed is no relationship between either two wind farms. With the consideration of correlation coefficients, the (2.26) should be modified to:

$$\gamma_{\Delta FSMI}^{n} = \sum_{i_1=1}^{m} \sum_{i_2=1}^{m} \cdots \sum_{i_n=1}^{m} \left(\left(\frac{\partial FSMI}{\partial P_{wi1}}\right) \times \cdots \times \left(\frac{\partial FSMI}{\partial P_{win}}\right) \gamma_{\Delta P_{wi1 \cdots in}}^{n} \right) \tag{2.27}$$

where $\gamma_{\Delta P_{wi1 \cdots in}}^{n}$ denotes the n^{th} order cross cumulants of the multiple wind power variations.

There is less influence on the accuracy of the PDF and CDP result of $FSMI$ from high order of the $\Delta FSMI$. Therefore, only the first several order cross cumulants of $\Delta FSMI$ are calculated by (2.27) to consider the correlation. The other cumulants of high orders can be computed by (2.26) to reduce the calculating burden. The first order cross cumulant of wind power variation is unchanged. The second and the third-order cross cumulants can be computed from the following equations by [122, 123]:

$$\gamma_{\Delta P_{wi1i2}}^{2} = \beta_{\Delta P_{wi1i2}}^{2} = E[(\Delta P_{wi1} - \mu \Delta P_{wi1})(\Delta P_{wi2} - \mu \Delta P_{wi2})]$$

$$\gamma_{\Delta P_{wi1i2i3}}^{2} = \beta_{\Delta P_{wi1i2i3}}^{3}$$

$$= E[(\Delta P_{wi1} - \mu \Delta P_{wi1})(\Delta P_{wi2} - \mu \Delta P_{wi2})(\Delta P_{wi3} - \mu \Delta P_{wi3})] \tag{2.28}$$

where $\beta^{n}_{\Delta P_{wi1\cdots in}}$ is the n^{th} order cross central moment and $\mu\Delta P_{win}$ is the mean of ΔP_{win}. The value in (2.28) could be calculated by the wind power variation sample series. Therefore, the first three order cross cumulants of $\Delta FSMI$ can be obtained.

The sensitivities for both FN/FV and RoCoF w.r.t system active power disturbance are obtained in the previous step.

The n^{th} central moment, $\beta^{n}_{\Delta FSMI}$, of ΔFSMI is calculated from its cumulants [122, 123]:

$$\beta^{1}_{\Delta\text{FSMI}} = 0$$

$$\beta^{2}_{\Delta\text{FSMI}} = \gamma^{2}_{\Delta\text{FSMI}} = \sigma^{2}_{\Delta\text{FSMI}}$$

$$\beta^{3}_{\Delta\text{FSMI}} = \gamma^{3}_{\Delta\text{FSMI}}$$

$$\beta^{4}_{\Delta\text{FSMI}} = \gamma^{4}_{\Delta\text{FSMI}} + 3(\gamma^{2}_{\Delta\text{FSMI}})^{2} \tag{2.29}$$

where, $\sigma_{\Delta\text{FSMI}}$ is the standard deviation of $\Delta FSMI$.

From the cumulants and central moments of $\Delta FSMI$, the cumulative distribution function (CDF) of the standardized $\Delta FSMI$, $\Delta\overline{FSMI} = (\Delta FSMI - \mu_{\Delta FSMI})/\sigma_{\Delta FSMI}$, can be obtained by using the following well-known Gram-Charlier expansion:

$$F_{\Delta\overline{FSMI}}(x) = g_0\Phi(x) + \frac{g_1}{1!}\Phi'(x) + \frac{g_2}{2!}\Phi''(x) + \frac{g_3}{3!}\Phi'''(x) + \cdots \tag{2.30}$$

where, $F_{\Delta\overline{\text{FSMI}}}(x)$ is the CDF of $\Delta\overline{FSMI}$ and $\Phi(x)$ is the CDF of standard normal distribution separately. The prime symbol denotes various order derivatives of $\Phi(x)$. Coefficients in the Gram-Charlier expansion of (2.30) are polynomial in the central moments of $\Delta FSMI$ can be found in [122, 123]:

$$g_0 = 1$$

$$g_1 = g_2 = 0$$

$$g_3 = -\frac{\beta_{\Delta FSMI}^3}{\sigma_{\Delta FSMI}^3}$$

$$g_4 = \frac{\beta_{\Delta FSMI}^4}{\sigma_{\Delta FSMI}^4} - 3 \tag{2.31}$$

Obviously, the CDF of $\Delta FSMI$ can easily be obtained from that of $\Delta\overline{FSMI}$ to be:

$$F_{\Delta FSMI}(x) = F_{\Delta\overline{FSMI}}\left(x\frac{x-\Delta\mu_{\Delta FSMI}}{\sigma_{\Delta FSMI}}\right) \tag{2.32}$$

Due to $\Delta FSMI = FSMI - FSMI_0$ ($\mathrm{FSMI}_0$is the deterministic value of the $FSMI$), the CDF of $FSMI$ can be obtained from:

$$F_{FSMI}(x) = F_{\Delta FSMI}(x - FSMI_0) \tag{2.33}$$

The PDF of $f_{\mathrm{FSMI}}(x)$ is the derivative of the CDF of $FSMI$ obtained in (2.33). Since the distribution of the wind speed is not continuous as given by (2.16), and hence $f_{\mathrm{FSMI}}(x) \neq 0$ only exists over a certain interval of $FSMI$ within $[FSMI_l, FSMI_r]$. The CDF and PDF given by (2.33) is for $FSMI$ within $[FSMI_l, FSMI_r]$, and the boundary value should be calculated separately. Therefore, the (2.33) is modified to (2.34), and the CDF is derived from:

$$f_{FSMI}(x) = \begin{cases} \left(1 - \left(F_s(v_{co}) - F_s(v_{ci})\right)\right)\delta(x - \mathrm{FSMI}_l) & x = \mathrm{FSMI}_l \\ derivate\ of\ (2.28) & \mathrm{FSMI}_l < x < \mathrm{FSMI}_r \\ \left(F_s(v_{co}) - F_s(v_{ri})\right)\delta(x - \mathrm{FSMI}_r) & x = \mathrm{FSMI}_r \\ 0 & x < \mathrm{FSMI}_l\ or\ x > \mathrm{FSMI}_r \end{cases} \tag{2.34}$$

$$F_{FSMI}(x) = \begin{cases} 0 & x \leq FSMI_l \\ (2.29) & \text{FSMI}_l < x < FSMI_r \\ 1 & x \geq FSMI_r \end{cases} \tag{2.35}$$

2.4 Assessment Tool

The RAM can provide a two-dimensional assessment result with severity and occurrence probability comprehensively, which is a practical tool to evaluate the risk of an event. Three levels of risk are provided considering both the severity and the occurrence probability, which are labeled as 'L' (i.e., low risk in green part), 'M' (i.e., middle risk in yellow part), and 'H' (i.e., high risk in red part). The severity of RoCoF and FN/FV RAM is established according to an industrial standard [18], and the occurrence probability can be determined and adjusted manually according to grid code. In this thesis, the RoCoF and FN/FV RAM are formed in Table 2.1 and Table 2.2 to evaluate the risk of system RoCoF and FN/FV.

Table 2.1 The RoCoF RAM.

Probability \ Hz/s	<-0.5	-0.5~-0.4	-0.4~0.4	0.4~0.5	>0.5
0-1%	M	L	L	L	M
1%-30%	H	M	L	M	H
30%-100%	H	H	L	H	H

Table 2.2 The FN/FV RAM.

Probability \ Hz	<49.5	49.5~49.8	49.8~50.2	50.2~50.5	>50.5
0-1%	M	L	L	L	M
1%-30%	H	M	L	M	H
30%-100%	H	H	L	H	H

2.5 Framework of Risk Assessment on Frequency Stability

The framework of the risk assessment on frequency stability based on the above subchapters is illustrated in Fig. 2.4.

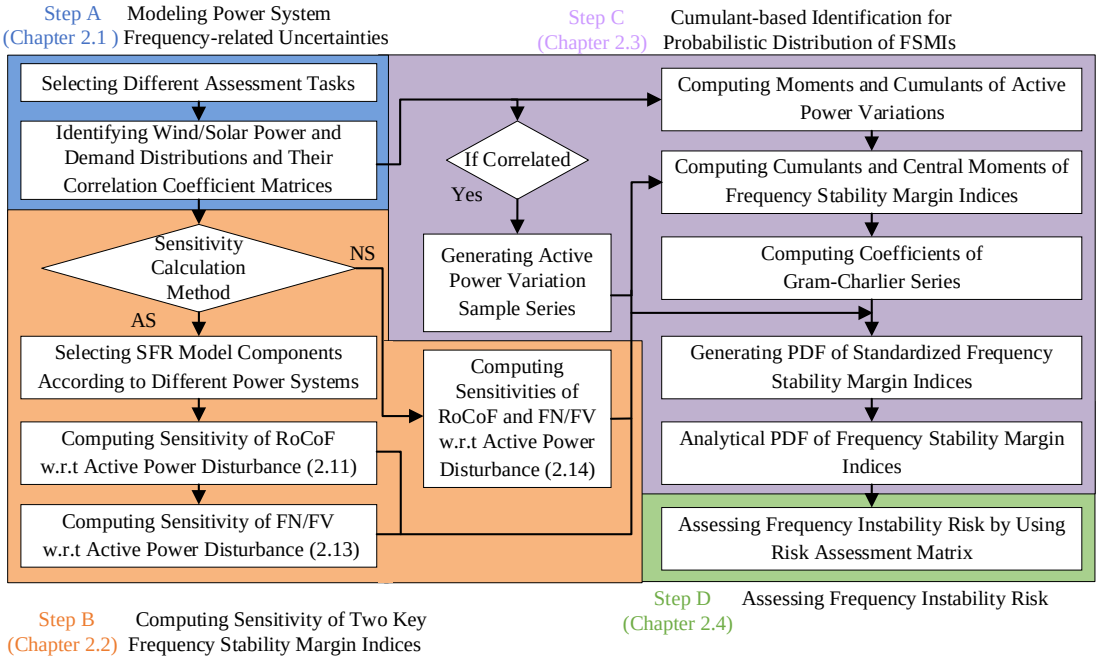

Fig. 2.4 The proposed framework of risk assessment on frequency stability.

In Step A, according to the chosen assessment task, the wind/solar power and demand distributions and their correlation coefficient matrices are determined. Then by selecting different calculation methods, the sensitivity of frequency stability margin indices is computed based on (2.11), (2.13), or (2.14) in Step B. The results of above Step A and B are sent into Step C as the inputs to obtain the PDF of RoCoF or FN/FV by adopting the cumulant-based approach, and the procedure is briefly described as follows: 1) Generate active power variation sample series according to the correlation coefficient matrices among each disturbance source. 2) Compute moments and cumulants of active power variations. 3) Compute the cumulants and central moments

of frequency stability margin indices. 4) Calculate coefficients of Gram-Charlier Series. 5) Generate PDFs of standardized RoCoF or FN/FV and then adjust them to the desired PDFs. The last step is to assess the frequency instability risk using RAM. The RAM can provide a two-dimensional assessment, i.e., occurrence probability and severity, and hence can provide a comprehensive and visible risk-based evaluation on stability, which has been applied to assess the risk of small disturbance security issues [37].

2.6 Case Study

The proposed assessment framework is verified on a modified IEEE 10-machine 39-bus test system with three wind farms connected to buses 6, 23, and 29, respectively, as shown in Fig. 2.5. The wind speed distribution is employed with the correlation coefficient matrix [124].

$$[\rho_{ij}]_{3\times3} = \begin{bmatrix} 1 & 0.5 & 0 \\ 0.5 & 1 & 0 \\ 0 & 0 & 1 \end{bmatrix} \tag{2.31}$$

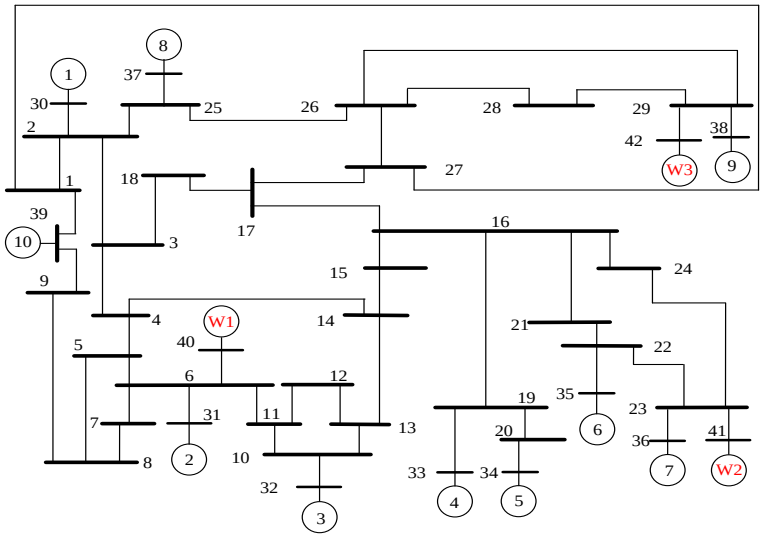

Fig. 2.5 A modified IEEE 10-machine test system involving three WFs in different locations.

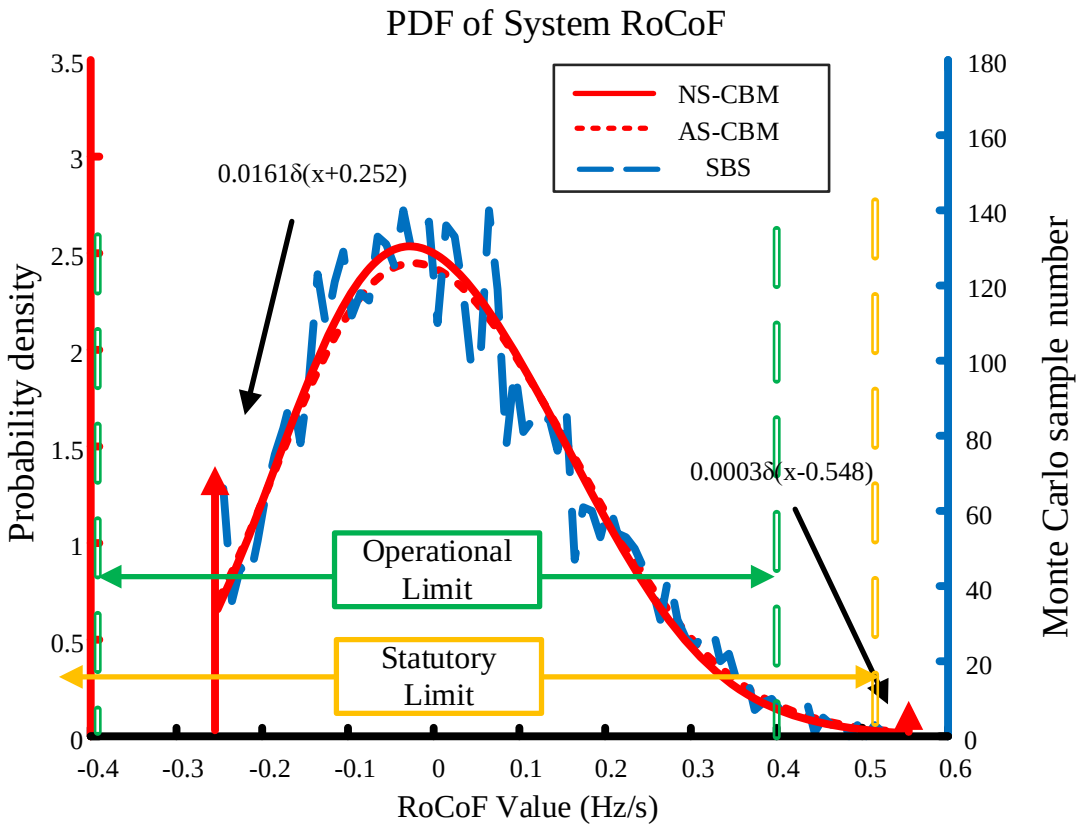

Fig. 2.6 The PDFs of RoCoF assessed by CBM-based assessment and SBS.

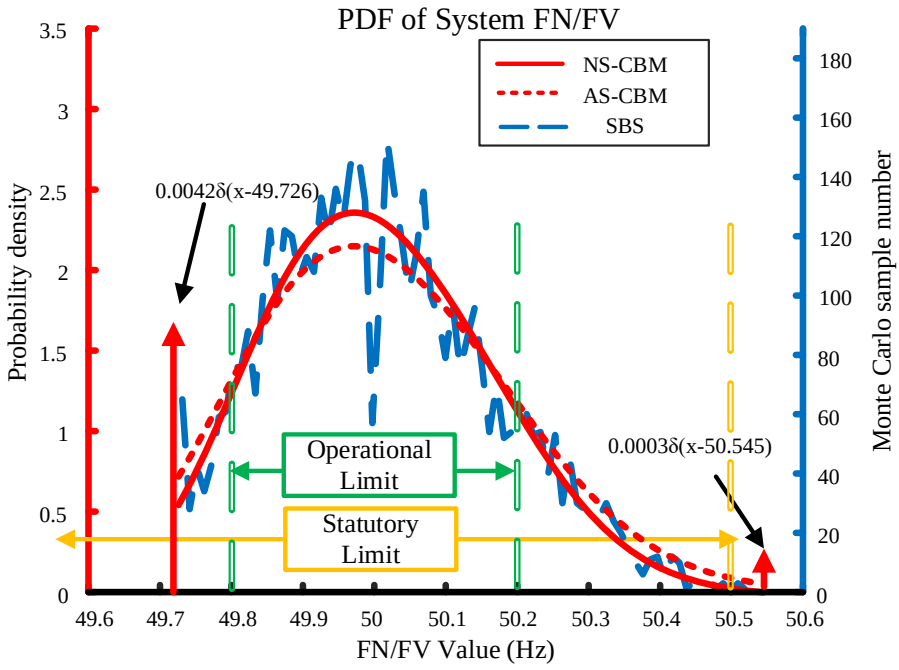

Fig. 2.7 The PDFs of FN/FV assessed by CBM-based assessment and SBS.

The proposed CBM-based assessment is carried out according to the steps introduced in the previous subchapter, i.e., Fig. 2.4, and the SBS is also conducted 5000 times as the benchmark to test the accuracy and efficiency of the proposed assessment. The PDF results of both RoCoF and FN/FV produced by three methods are given in Fig. 2.6 and Fig. 2.7 respectively, where both UK operational (green) and statutory (yellow) limit standard for frequency stability is applied as an example. It can be verified by Fig. 2.6 and 2.7, the PDF curves by proposed CBM with NS and AS are consistent with the ones by SBS for both RoCoF and FN/FV. Take the probability within the operational limits for further demonstration. The NS-CBM has a marginal superiority over AS-CBM when compared with SBS results shown in Table 2.3. It is also proved by Table 2.3 that the proposed CBM-based assessments have satisfactory performances. Meanwhile, the computational time of the three methods is also compared and displayed in Table 2.4. It can be seen that the proposed AS-CBM and NS-CBM are around 8800 and 1500 times faster than SBS, where the NS-CBM cost more computational time compared with AS-CBM since it requires three simulations to obtain the associated NS.

Finally, the RAM of UK SQSS [125] (Table 2.1 & 2.2) is applied as an example to evaluate whether the system is stable or not. The RAM is filled with the probability results obtained by the proposed NS-CBM in Table 2.5-2.6. As revealed by the risk assessment in Table 2.5-2.6, the system has around 81% probability to remain in the safe state in terms of steady-state frequency stability and around 99% for RoCoF. Although there are some circumstances for the frequency to breach the operational or

even statutory limits, as shown in Fig. 2.5-2.6, the chances are quite low, as indicated in Table 2.5-2.6. Therefore, the alert is on, but no actual actions are needed, which demonstrates a typical case where the wind curtailments can be avoided.

Table 2.3 The frequency stability probabilities within operational limits evaluated by AS-CBM, NS-CBM, and SBS (%).

	FN/FV	RoCoF
AS-CBM	77.462%	98.231%
NS-CBM	80.808%	99.015%
SBS	79.640%	98.840%

Table 2.4 The computational time of AS-CBM and NS-CBM.

SBS	AS-CBM	NS-CBM
48569.54s	5.5s	32.56s

Table 2.5 RoCoF RAM evaluated by NS-CBM.

Probability \ Hz/s	<-0.5	-0.5~-0.4	-0.4~0.4	0.4~0.5	>0.5
0-1%	0%	0%		0.774%	0.210%
1%-30%					
30%-100%			99.015%		

Table 2.6 FN/FV RAM evaluated by NS-CBM.

Probability \ Hz	<49.5	49.5~49.8	49.8~50.2	50.2~50.5	>50.5
0-1%	0%				0.197%
1%-30%		7.881%		11.113%	
30%-100%			80.808%		

2.7 Summary

This chapter proposes a CBM-based risk assessment framework to comprehensively and efficiently evaluate system frequency stability margins for the

first time, which can significantly facilitate the system planner's decision-making process in the operational planning and effectively mitigate the renewable curtailments. The RAM is practically applied to assess the risk of frequency stability (FN/FV and RoCoF) by incorporating a specific industrial standard for the first time. The simulation results demonstrate that when comparing with the NS-based assessment considering the network impact and the existing scenario-based simulation, the performance of AS-based assessment is also quite satisfactory in the application of probabilistic stability analysis.

Chapter 3

A Fast-Algorithmic Risk Assessment on Area-level RoCoF

Due to the heterogeneity of different area-level frequency responses caused by increasing penetration level of distributed RESs and uneven distribution of inertia sources, the severe fluctuation of regional frequency responses (i.e., area-level RoCoF) concerned by system operators could be concealed by the conventional assessment based on aggregated system frequency response. Moreover, the occurrence probability of a high RoCoF issue is vital during the system planner's decision-making. Therefore, it is necessary to assess the risk of area-level RoCoF violation for the operational planning of a RES penetrated power system.

Due to excellent performance in system-level assessment verified in the previous chapter, the CBM is employed to conduct the evaluation, where the required AS quantifying the relationship between the area-level RoCoF and the stochastic output of the RES is derived based on the classical generator model and network information. However, the computational process is very complicated, as presented in the previous chapter. Hence, a straightforward algorithm is proposed to achieve a fast and effective evaluation on the area-level RoCoF compared with CBM, verified by SBS. The effectiveness and efficiency of the proposed method are verified in a modified 16-machine 5-area IEEE benchmark system

3.1 Slow Coherency Identification Method

Slow coherency identification was proposed by Chow [111] to identify the low-frequency oscillation areas. The method initially only partitions the generators, which is further extended to accommodate the load bus [112]. There are two advantages of this method: 1) it neglects the type and location of the fault, 2) it neglects the accuracy of the generator model and control system. The method considers the classical model of generators, network connection, and power flow, which is straightforward and easy to implement.

The model of a power system with N generators and P load buses could be described as below:

$$\mathbf{M}\ddot{\delta} = f(\delta, V) \tag{3.1}$$

$$0 = \mathrm{g}(\delta, V) \tag{3.2}$$

where δ is an N-vector of the machine angles, V is a P-vector of the complex load bus voltage, M is the diagonal inertia matrix, f is a vector of acceleration torques, and g is the load flow function of the power system. Linearized system model at the balance point (δ_0, V_0) could be rewritten as follow:

$$\mathbf{M}\Delta\ddot{\boldsymbol{\delta}} = \mathbf{K_1}\Delta\boldsymbol{\delta} + \mathbf{K_2}\Delta\boldsymbol{V} \tag{3.3}$$

$$0 = \mathbf{K_3}\Delta\boldsymbol{\delta} + \mathbf{K_4}\Delta\boldsymbol{V} \tag{3.4}$$

where Δδ is an N-vector of the machine angle deviations from δ_0 and ΔV is a 2P-vector of the real and imaginary parts of the load bus voltage deviations from V_0. ΔV in (3.3)-

(3.4) is eliminated, and the system is written:

$$\mathrm{M}\Delta\ddot{\delta} = \mathrm{K}\Delta\delta \tag{3.5}$$

where $\mathrm{K} = \mathrm{K}_1 - \mathrm{K}_2\mathrm{K}_4^{-1}\mathrm{K}_3$ and *K* is also the synchronizing torque coefficients.

The eigenvectors of $M^{-1}K$ describe the mode shapes of the electromechanical modes, which are coherent with that mode if two machines have similar entries of the mode k. In other words, if Vs is the matrix of the eigenvectors corresponding to the small eigenvalues of $\mathrm{M}^{-1}\mathrm{K}$, a slow coherent group of machines have similar row vectors in Vs, and thus, a practice algorithm to identify the slow coherent group is to first find the r most linearly independent vectors w_α from *Vs* and treat them as reference vectors. Then a machine with the row w_i will be grouped in the same area with the reference machine whose row vector w_α is closest to w_i. *Vs* is rewritten in a new form for the simplification:

$$\mathbf{V_s} = \begin{bmatrix} \mathbf{V_{s1}} \\ \mathbf{V_{s2}} \end{bmatrix} \tag{3.6}$$

where V_{s1} contains the reference rows. Then the row vectors of V_{s1} are used as unit coordinate vectors in a new coordinate system, which can be expressed as (3.7) transferred from (3.6):

$$\begin{bmatrix} \mathbf{V_{s1}} \\ \mathbf{V_{s2}} \end{bmatrix} \mathbf{V_{s1}^{-1}} = \begin{bmatrix} \mathbf{I} \\ \mathbf{L} \end{bmatrix} \tag{3.7}$$

where *L* is the matrix for assigning non-reference machines to referenced machines.

The calculation step could be described as follows:

1) Choose the number of area r,

2) Calculate eigenvalues of $\mathrm{M}^{-1}\mathrm{K}$,

3) Compute a matrix *Vs* of the eigen subspace of the r smallest eigenvalues in magnitude in step 2),

4) Gaussian elimination is applied in *Vs* to obtain the r reference machines,

5) Order the machines such that rows of V_{s1} of (3.7) correspond to the reference machines and solve for *L* form:

$$\mathbf{V_1^T L^T = V_2^T} \tag{3.8}$$

6) Use *L* to assign the machines to the coherent areas. That, if the largest positive entry in a row of L is the a[th] entry, then the machine corresponding to that row is grouped into the area a.

The method could also be extended to the whole system. The load bus is attached to a machine with a small inertial uM and no transient reactance. The linearized electromechanical model of the artificial system is

$$\mathbf{M}\Delta\ddot{\boldsymbol{x}} = \begin{bmatrix} \mathbf{M} & \mathbf{0} \\ \mathbf{0} & \boldsymbol{uM} \end{bmatrix} \begin{bmatrix} \ddot{\boldsymbol{x}}_1 \\ \ddot{\boldsymbol{x}}_2 \end{bmatrix} = \begin{bmatrix} \mathbf{K_{11}} & \mathbf{K_{12}} \\ \mathbf{K_{21}} & \mathbf{K_{22}} \end{bmatrix} \begin{bmatrix} \mathbf{x_1} \\ \mathbf{x_2} \end{bmatrix} = \mathbf{K_N x} \tag{3.9}$$

where, x_1 and *M* are Δδ and inertial matrix of the real machines respectively, x_2 and uM are Δδ and inertial matrix of the virtual machines respectively and K_N is the synchronizing torque coefficients with consideration of virtual machines. The calculation steps, including load bus, are the same as the previous one. This coherency identification method is used as a basis for further investigation of area-level frequency stability.

3.2 AS of Area-Level RoCoF w.r.t a Single Disturbance

The RoCoF of a system or a generator can be directly derived as below according to the SFR model or a classical generator model in [90]:

$$RoCoF = \frac{\Delta f(t)}{dt} = \frac{1}{2H}\Delta P(t) \tag{3.10}$$

where H is the inertia, $\Delta f(t)$ is the frequency deviation from the nominal frequency f_0, and $\Delta P(t)$ is the imposed active power disturbance.

3.2.1. Generator-level Power Disturbance Propagation and Its Distribution Coefficient

The system active power disturbance (ΔP_{Dist}) caused by the sudden change of RES at t=0^+ would propagate in the system and distribute to each generator bus $\Delta P_i(0^+)$ according to the synchronizing power coefficients (P_{sik}) between the location of the RES and the individual generator [91], which is illustrated in Fig. 3.1.

Firstly, the original network structure is simplified to a reduced network that only contains the N generators and one disturbance source, i.e., RES. Secondly, the synchronizing power coefficients (P_{sik}) between RES, i.e., bus *k* and, the i^{th} generator bus is calculated according to [91].

$$P_{sik} = V_i V_k (B_{ik}\cos\delta_{ik0} - G_{ik}\sin\delta_{ik0}) \tag{3.11}$$

where V_i and V_k are the voltage magnitude of bus *i* and bus *k*, respectively. B_{ik} and G_{ik} are the imaginary and real parts of the equivalent admittance between bus *i* and bus *k* separately. δ_{ik0} is the steady angle difference between bus *i* and bus *k*.

Then the distribution coefficient of power disturbance (P_c) is defined as (3.12) to quantify the propagating relationship of active power in the grid between the RES and the generator buses [91], based on which analytical distributed active power of each generator bus, i.e., $\Delta P_i(0^+)$ from the stochastic output of the RES (P_{Dist}) can be expressed as below.

$$P_{ci} = \frac{P_{sik}}{\sum_{i=1}^{N} P_{sik}} \tag{3.12}$$

$$\Delta P_i(0^+) = P_{ci} P_{Dist} \tag{3.13}$$

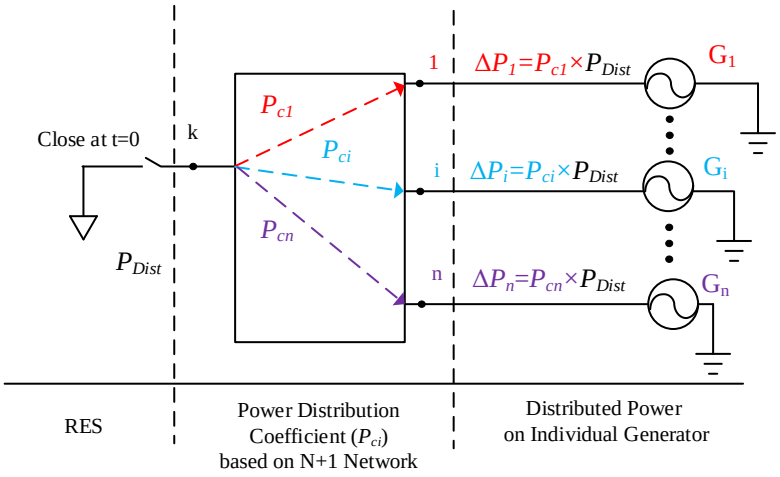

Fig. 3.1 The active power disturbance propagation from RES (i.e., bus *k*) to each generator bus.

3.2.2. Area-level Power Disturbance Propagation and Its Distribution Coefficient

Based on the above analysis, the active power disturbance component allocated to a region equals the sum of the active power disturbance distributed to the individual generator bus in this region.

$$\Delta P^j(0^+) = \sum_{i=1}^{G} \Delta P_i^j(0^+) \tag{3.14}$$

where $\Delta P^j(0^+)$ and ΔP_i^j are the allocated active power to the j^{th} area and the i^{th} generator bus in the region, respectively, and G is the number of generators in the j^{th} area. Thus, the distributed area-level active power disturbance from the RES can be obtained as (3.15) by substituting (3.13) into (3.14) with the assist of the defined area-level distribution coefficient of power disturbance in (3.16).

$$\Delta P^j(0^+) = \sum_{i=1}^{G} P_{ci}^j \, P_{Dist} = P_c^j \, P_{Dist} \tag{3.15}$$

$$P_c^j = \frac{\sum_{i=1}^{G} P_{sik}}{\sum_{i=1}^{N} P_{sik}} \tag{3.16}$$

where, P_c^j the is the j^{th} area P_c, and N is the total number of the generators in the system.

3.2.3. AS of Generator-level RoCoF

The generator-level RoCoF can be expressed as (3.17) by substituting (3.13) into (3.10) with the assist of the defined generator-level AS in (3.18).

$$RoCoF_i = \frac{1}{2H_i} P_{ci} P_{Dist} = AS_i P_{Dist} \tag{3.17}$$

$$AS_i = \frac{1}{2H_i} \times \frac{P_{sik}}{\sum_{i=1}^{N} P_{sik}} \tag{3.18}$$

where $RoCoF_i$ is the RoCoF of the i^{th} generator and the AS_i is the AS of $RoCoF_i$w.r.t the output of the RES.

3.2.4. AS of Area-level RoCoF

In a multi-machine system, owning to different locations and control parameters of individual generators in the system, the frequency responses of these generators are various when suffering an active power disturbance.

Conventionally, system frequency response, as the overall performance of all the frequency responses in the system, is aggregated based on COI, where all generators are integrated into one equivalent generator with the sum of inertia under a base power capacity [91]. Hence, a similar method is applied here to calculate the area-level center of inertia (ACOI), which is defined as follows.

Firstly, the individual inertia constant is converted based on a common base power capacity as below.

$$H_i = H_{i,o} \times \left(\frac{S_i}{S_{base}}\right) \tag{3.19}$$

where $H_{i,o}$ is the i^{th} inertia constant w.r.t its rated power capacity S_i, and S_{base} is the base power capacity.

Then the ACOI of the j^{th} area (H^j) is defined as below.

$$H^j = \sum_{i=1}^{G} H_i^j \tag{3.20}$$

Where H_i^j is the i^{th} generator inertia in the j^{th} area, and G is the number of generators in the j^{th} region. The superscript refers to the number of the area.

The system frequency response based on the COI is the average weighted frequency responses of individual generator where the weight coefficient is the ration of the single generator inertia and the sum of generator inertia [91]. Based on the concept of the COI, ACOI is established and employed to represent the area-level frequency response, i.e., ACOI frequency response (f_{ACOI}^j), as below.

$$f_{ACOI}^j = \frac{\sum_{i=1}^{G} H_i^j f_i^j}{\sum_{i=1}^{G} H_i^j} \tag{3.21}$$

where f_i^j is the frequency response of the i^{th} generator in the j^{th} area, and G is the number of the generators in the j^{th} area.

Based on ACOI, the area-level RoCoF ($RoCoF^j$) is derived in (3.22) by substituting (3.15) and (3.20) into (3.10) with the assist of the defined area-level analytical sensitivity (AS^j) in (3.23).

$$RoCoF^j = \frac{1}{2H^j}\Delta P^j(0^+) = \frac{1}{2\sum_{k=1}^{G} H_k^j} P_c^j \, P_{Dist} = AS^j P_{Dist} \tag{3.22}$$

$$AS^j = \frac{1}{2\sum_{k=1}^{G} H_k^j} \times \frac{\sum_{i=1}^{G} P_{sik}}{\sum_{i=1}^{N} P_{sik}} \tag{3.23}$$

where the AS^j is the sensitivity of $RoCoF^j$ and G is number of the generators in the j^{th} area.

3.3 AS-LSM-based Risk Assessment on Area-level RoCoF in a Multi-RES Penetrated Power System

3.3.1 Area-level Active Power Disturbance Integration

From the above analysis, the propagation and distribution of system active power disturbance from the RES depend on the 'electrical distance' between the RES and each generator bus at t=0+ demonstrated by (3.13). In a multi-RES penetrated power system, it is reasonable to assume that the active power disturbance distributed to a generator bus from various RESs equals the sum of the active power disturbance distributed to the bus from individual RESs, described as (3.24). Hence, the area-level active power disturbance in a multi-RESs penetrated system can be expressed as (3.25).

$$\Delta P_i(0^+) = \sum_{l=1}^{M} P_{cil} P_{Distl} \tag{3.24}$$

$$\Delta P^{j}(0^{+}) = \sum_{i=1}^{G} \Delta P_i\,(0^{+}) = \sum_{i=1}^{G}\sum_{l=1}^{M} P_{cil} P_{Distl} \tag{3.25}$$

where, P_{cil} are the distribution coefficient between the i^{th} generator bus and the l^{th} RES. P_{Distl} is the stochastic output of the l^{th} RES. M and G are the number of the RES in the system and generators in the j^{th} area.

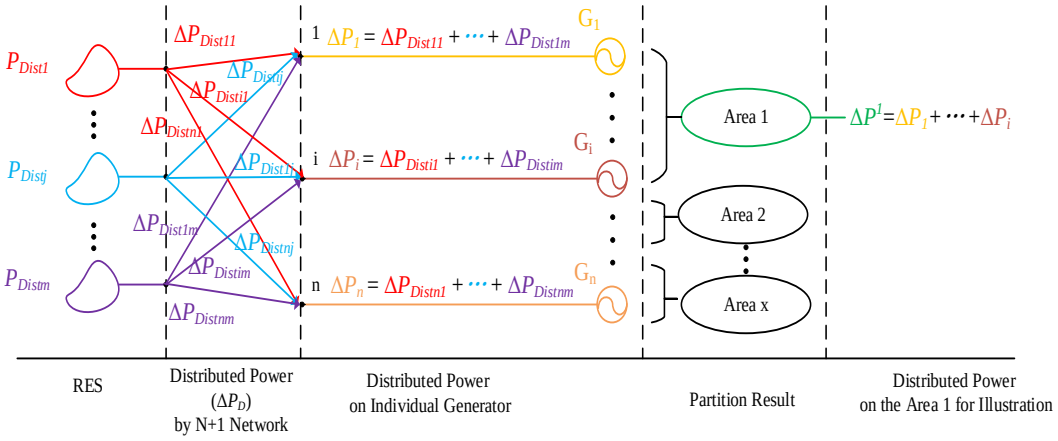

Fig. 3.2 The propagating procedure of the active power disturbances in the multi-RES penetrated power system and the derivation of the area-level active power disturbance.

The propagating procedure of the active power disturbance from multiple RESs to the generator buses is illustrated in Fig. 3.2. Assume there are M RESs and N generators in the system. Firstly, each RES propagates the active power disturbance to individual generator buses via the reduced N+1 network, where ΔP_{Distij} is the active power allocated to the i^{th} generator bus from the j^{th} RES. Then, the total active power (ΔP_i) spreads to a single generator bus equals the sum of the active power disturbance propagated to this bus from stochastic output of different RESs. Moreover, the area-level active power disturbance equals the sum of the active power disturbance distributed to the generator bus in the coherent region. For instance, the first *i* generators are into Area 1, the active power disturbance propagated to Area 1 (ΔP^1) is equivalent

to the sum of the active power allocated to all generator buses in Area 1, i.e., $\Delta P_k, k = 1 \cdots i$, as shown in Fig. 3.2.

3.3.2 Area-level RoCoF Integration based on AS and LSM

To accommodate multiple stochastic variables (i.e., active power disturbance from RESs), the LSM is proposed here to calculate the critical index (i.e., area-level RoCoF) with the assist of AS. Hence, the area-level RoCoF can be calculated using the AS-LSM in (3.26), where the full expression is given as (3.27).

$$RoCoF^j = \sum_{l=1}^{M} AS_l^j P_{Distl} \tag{3.26}$$

$$RoCoF^j = \frac{1}{2\sum_{k=1}^{G} H_k^j} \sum_{i=1}^{G} \sum_{l=1}^{M} P_{cil}\ P_{Distl} \tag{3.27}$$

where G and N are the number of the generator in the j^{th} area and the system, respectively, and M is the number of RES in the system. AS_l^j stands for AS of $RoCoF^j$ w.r.t the output of the l^{th} RES.

The system-level RoCoF can be treated as a special form of area-level RoCoF when there is only one area, i.e., G=N, and the (3.27) degrades to (3.28). Furthermore, when there is only one disturbance in the system, the (3.28) further degrades to (3.10).

$$RoCoF = \frac{1}{2\sum_{k=1}^{N} H_k} \sum_{l=1}^{M} \Delta P_{Distl} \tag{3.28}$$

3.3.3 Calculation Procedure of Probabilistic Distribution of Area-level RoCoF by AS-LSM

The flow chart of the calculation procedure of probabilistic distribution of regional RoCoF by AS-LSM is illustrated in Fig. 3.3 and described as follows:

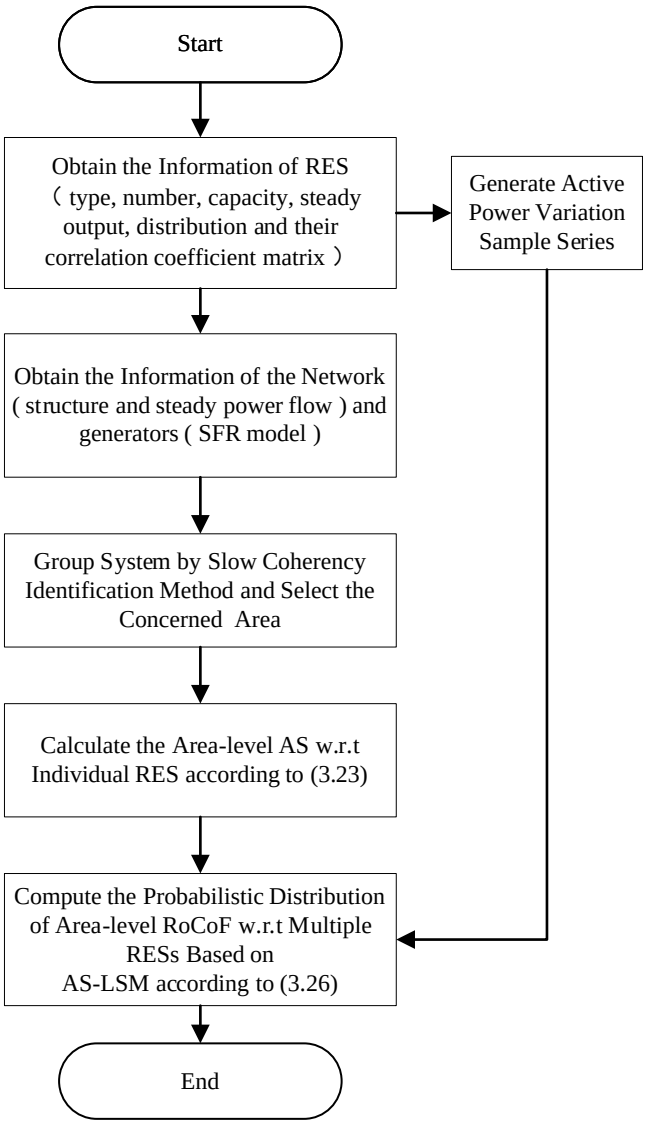

Fig. 3.3 The flowchart of the probability calculation for area-level RoCoF by AS-LSM.

1) The information of the RES is obtained, including type, number, capacity, steady output, probabilistic distribution of the natural source, and the correlation coefficient matrix, based on which active power variation sample series is generated; 2) The information of the generator and the network is acquired; 3) On the basis of the above data, the slow coherency identification described in Chapter 3.2 is implemented to divide the system into several areas, and the interested region is selected; 4) The concerned area-level AS w.r.t the output of individual RES is calculated according to

(3.23), and 5) AS-LSM is employed to determine regional RoCoF based on the stochastic output of individual RES and the related regional AS by (3.26). Repeat the above process to acquire the probabilistic distribution of the area-level RoCoF until all the generated scenarios are considered.

3.4 Case Studies

The effectiveness and efficiency of the proposed AS-LSM for calculating the probabilistic distribution of area-level RoCoF are demonstrated by comparing with the 5000 numerical SBSs and analytical AS-CBM due to its satisfactory performance on system-level assessment verified in the previous chapter. A modified IEEE 16-machine 68-bus system is employed as Fig. 3.4, where three WFs are connected to buses 29, 32, and 41, respectively, and the system is partitioned by the slow coherency identification method in Chapter 3.2. The area that includes more than one single generator is the focus of the thesis, which are Area 4 and Area 5. There are two scenarios studied in this section, i.e., with and without the correlations of wind speed. The base capacity of the system is 100MVA. The operational state of the employed benchmark system changes to half the original level (total generation and associated inertia, and load demand). The capacity of each wind plant is 600MVA, and the steady output is 200MVA with the Weibull distribution employed in [124]. The penetration of wind energy is 19.7%, i.e., the proportion of the total capacity of three WFs over the system load according to [126].

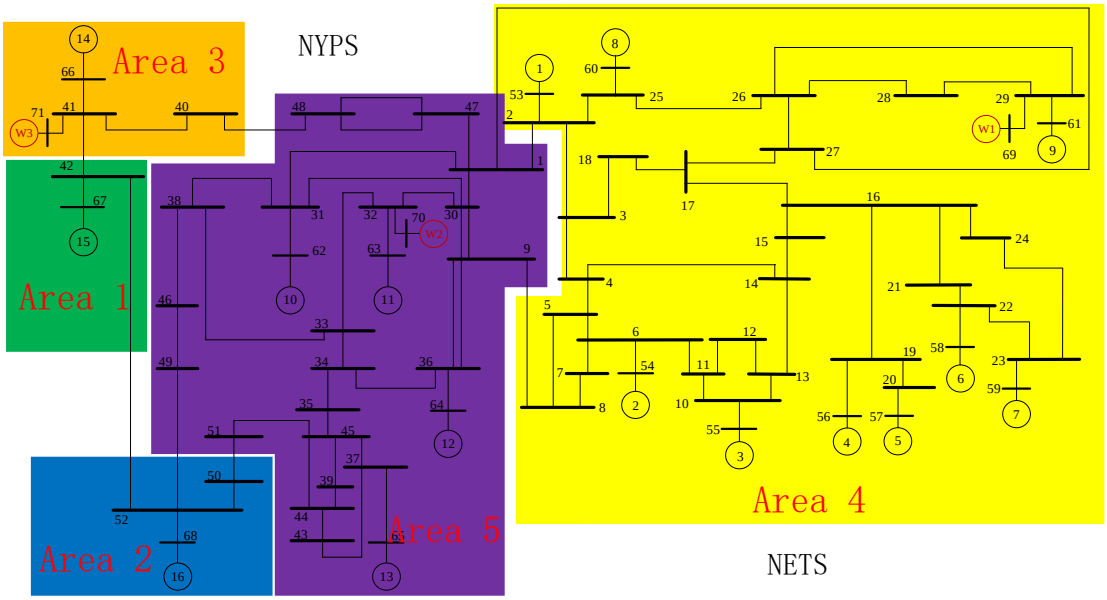

Fig. 3.4 A modified IEEE 16-machine 5-area test system involving three WFs in different locations (for AS-LSM and AS-CBM).

Table 3.1 The AS of system/area-level RoCoF w.r.t the output of individual WFs.

	WF1	WF 2	WF 3
System	0.050502	0.050502	0.050502
Area 1	0.000983	0.003597	0.019503
Area 2	0.003680	0.017777	0.001502
Area 3	0.006693	0.013478	0.299779
Area 4	0.294051	0.049267	0.004431
Area 5	0.019988	0.112672	0.003533

According to the calculation procedure described in Fig. 3.3, the area-level ASs w.r.t the output of WFs 1-3 computed according to (3.23) are given in Table 3.1. As illustrated in Table 3.1, the system ASs w.r.t the output of WFs 1-3 are all 0.050502, since the SFR model ignores the impact of the 'electric distance.' However, there is a significant difference between the AS of area-level RoCoF w.r.t the WFs 1-3 due to complex impacts from both 'electric distance' and defined area-level inertia. In detail, the AS of Area 4 RoCoF w.r.t WF2 and 3 are small (i.e., 0.049267 and 0.004431),

whereas the sensitivity w.r.t WF1 is relatively large (i.e., 0.294051), which is caused by different 'electric distance.' Furthermore, the maximal and minimal ASs of all area-level RoCoFs w.r.t WF1 are 0.294051 and 0.000983, respectively, and the difference originates from the various regional inertia.

3.4.1 Uncorrelated Wind Speed

The correlation between two wind power sources is closely related to their geographical distance, based on which correlation coefficient matrix $[\rho_{ij}]_{m\times m}$ for m grid-connected wind power sources is established [127]. In this scenario, the correlation among the wind speed sources is not considered due to the assumed long distance among each WFs. Based on the AS in Table 3.1, AS-LSM and AS-CBM are employed to calculate the probabilistic distribution of the system, Area 4 and Area 5 RoCoF, further verified by SBS as Fig. 3.5(a)-(c). The detailed probabilistic results of RoCoF within the operational limits (i.e., ±0.4Hz/s according to Table 2.1) are presented in Table 3.2 and Table 3.3.

The AS-LSM and AS-CBM have satisfactory performance in evaluating the probabilistic distribution of the RoCoF in the system, Area 4 and Area 5 intuitively, as exhibited in Fig.3.5. An interesting phenomenon is that the shapes of the probabilistic distributions of the system RoCoF and the area-level RoCoFs are different, which can be approached by both methods according to Table 3.2 and Table 3.3. Table 3.3, i.e., the absolute errors of the probabilistic results by both AS-LSM and AS-CBM, indicates that probabilistic results of system RoCoF evaluated by both methods are relatively stable compared with that of area-level RoCoFs. For example, AS-LSM has better

performances better than AS-CBM in estimating the probabilistic distribution of Area 4 RoCoF due to smaller errors (0.48% vs. 2.2733%). However, when assessing Area 5 RoCoF the AS-CBM performs better than AS-LSM (0.1451% vs. 2.14%).

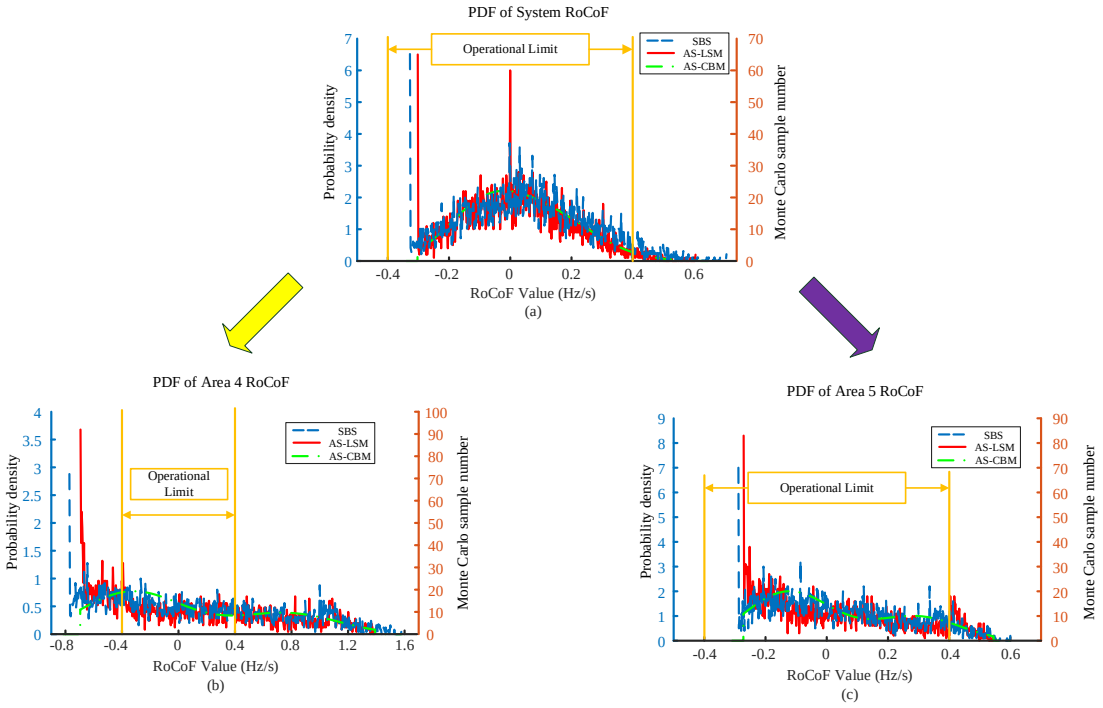

Fig. 3.5 The PDFs of system/area-level RoCoF by SBS, AS-LSM, and AS-CBM; (a) system, (b) Area 4, and (c) Area 5.

Table 3.2 The probabilistic distribution of the system, Area 4, and Area 5 RoCoF using SBS, AS-LSM, and AS-CBM within operational limits (uncorrelated wind speed).

No	SBS	AS-LSM	AS-CBM
System	96.9200%	98.0800%	98.0307%
Region 4	41.3200%	40.8400%	43.5933%
Region 5	92.8400%	90.7000%	92.9851%

The computational time of the three methods is displayed in Table 3.4. Both AS-LSM and AS-CBM can save more than 99.9% of computational time by SBS, where the AS-LSM is faster than AC-CBM owning to the simple calculation procedure.

Table 3.3 The absolute error of probabilities for the system, Area 4, and Area 5 RoCoF by AS-LSM and AS-CBM within operational limits (uncorrelated wind speed).

No	AS-LSM	AS-CBM
System	1.1600%	1.1107%
Region 4	0.4800%	2.2733%
Region 5	2.1400%	0.1451%

Table 3.4 The computational time of SBS, AS-LSM, and AS-CBM.

	SBS	AS-LSM	AS-CBM
Computational Time	2691.72s	1.95s	2.57s

3.4.2 Correlated Wind Speed

In this scenario, the correlation coefficient between WF2 and WF3 is set to be 0.8 (highly correlated) as below.

$$[\rho]_{3\times3} = \begin{bmatrix} 1 & 0 & 0 \\ 0 & 1 & 0.8 \\ 0 & 0.8 & 1 \end{bmatrix} \tag{3.29}$$

The PDFs of RoCoF on the system and Area 4 are given in Fig. 3.6 and Fig. 3.7, respectively, for demonstration purposes. The assessment result of Area 5 RoCoF is not presented due to similar results. The detailed probabilistic results and errors are also listed in Table 3.5 and Table 3.6, respectively.

The probabilistic distributions of system RoCoF assessed by SBS, AS-LSM, and AS-CBM are exhibited in Fig. 3.6. Compared with the probabilistic results of system RoCoF computed by SBS in Fig. 3.5 (a), there are a few noticeable ‘impulses’ at a few points on the horizontal ordinate (i.e., RoCoF value) in Fig. 3.6, which leads a relatively high probability of the ‘worst-case scenario’ and needs to be carefully evaluated in operational planning. The most obvious ‘impulse,’ i.e., the occurrence probability, in

Fig. 3.6 occurs at the minimal RoCoF value. On the other hand, due to the fact that the sum of the probability corresponding to each RoCoF value is 1, the probabilities of RoCoF corresponding to the non-'impulse' points would decrease and present a smooth curve in Fig. 3.6. Table 3.5 and Table 3.6 further evaluate the effectiveness of the AS-LSM and AS-CBM.

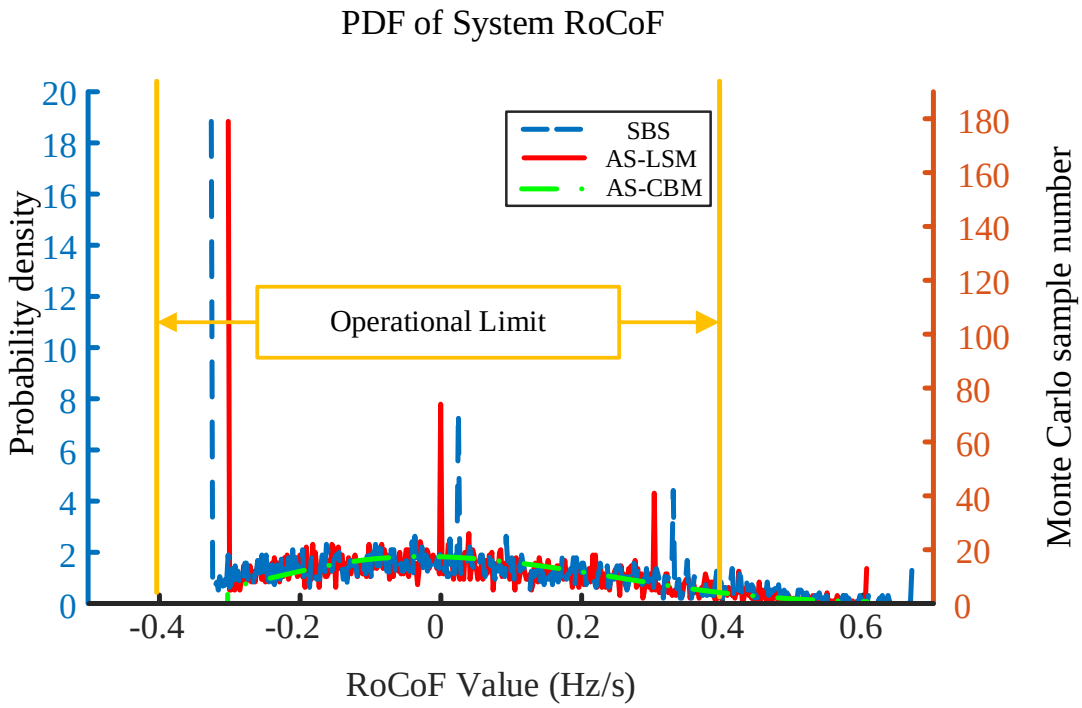

Fig. 3.6 The PDF of system RoCoF by SBS, AS-LSM, and AS-CBM.

In Fig. 3.7, there are still some 'impulses' in the probabilistic distribution of Area 4 RoCoF by SBS, and the curve is relatively smooth compared with that in Fig. 3.5 (b), i.e., the uncorrelated wind speed situation. The probabilistic distribution of area-level RoCoF obtained by SBS is not bell-shaped, which can be approached by both methods effectively, while the AS-LSM performs better than AS-CBM due to more minor errors, i.e., 0.9% vs. 1.2902% in Area 4 RoCoF and 0.54% vs. 1.255% in Area 5 RoCoF as given in Table 3.6.

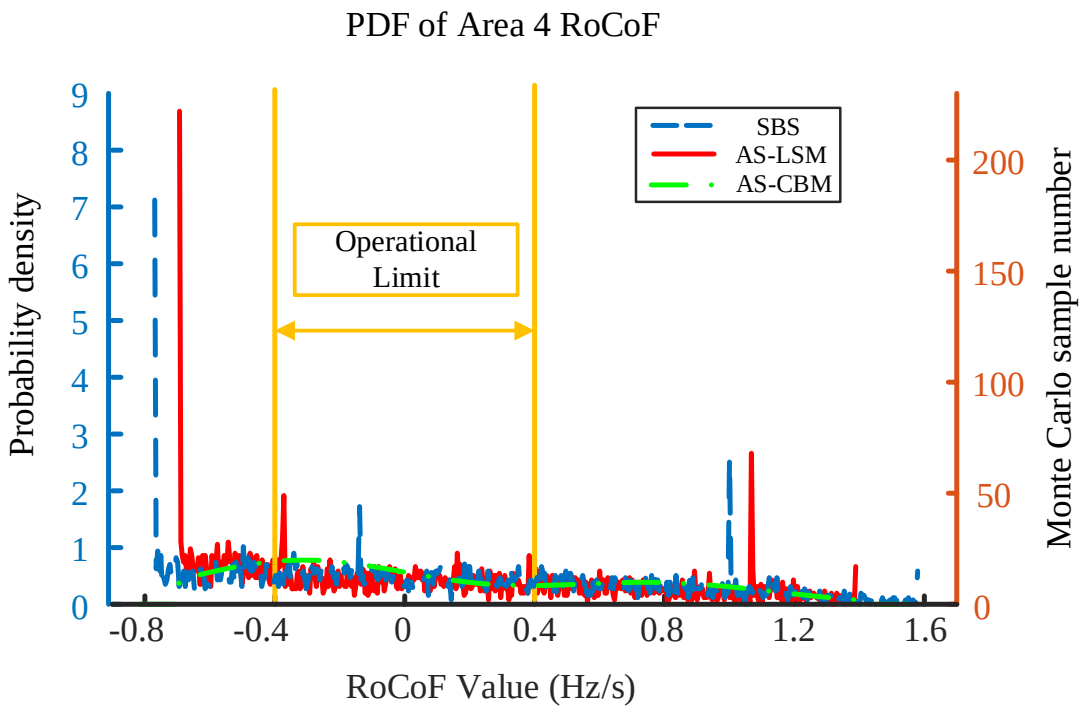

Fig. 3.7 The PDF of Area 4 RoCoF by SBS, AS-LSM, and AS-CBM.

Table 3.5 The probabilistic distribution of the system, Area 4, and Area 5 RoCoF using SBS, AS-LSM, and AS-CBM within operational limits (correlated wind speed).

No	SBS	AS-LSM	AS-CBM
System	93.6600%	94.9800%	95.2664%
Region 4	42.7000%	41.8000%	43.9902%
Region 5	91.4600%	90.9200%	92.7150%

Table 3.6 The absolute error of probabilities for the system, Area 4, and Area 5 RoCoF by AS-LSM and AS-CBM within operational limits (correlated wind speed).

No	AS-LSM	AS-CBM
System	1.3200%	1.6064%
Region 4	0.9000%	1.2902%
Region 5	0.5400%	1.2550%

3.5 Summary

The probabilistic distributions of system RoCoF and area-level RoCoF are different, i.e., bell-shaped vs. non-bell-shaped, which proves the necessity of area-level RoCoF evaluation for operational planning. The proposed AS-LSM can achieve accurate assessment on area-level RoCoF validated by SBS, which needs less time than SBS and can also provide a more straightforward calculating procedure than CBM. Some apparent ‘impulses’ occur in the probabilistic distributions of both system and area-level RoCoF when the wind speed correlation is considered. This phenomenon could be correctly reflected by AS-LSM and AS-CBM, while AS-LSM performs better, demonstrating the flexibility and robustness of the proposed AS-LSM.

Chapter 4

IS-LSM based Risk Assessment and Enhancement on Area-Level RoCoF

In the previous chapter, the proposed AS-LSM can be treated as an alternative to AS-CBM to calculate the probabilistic distribution of the area-level RoCoF due to the accurate assessment result and the straightforward calculation process. In this chapter, an IS based on the measurement and generator inertia is proposed to replace the AS to achieve the risk assessment on area-level RoCoF, i.e., IS-LSM. The proposed method only requires a limited number of measurement results of active power and can avoid the derivation process of the AS, which can be regarded as a model-free method. The calculated probabilistic distribution of area-level RoCoF is further evaluated by the associated RAM.

Moreover, the assessed high risk is mitigated by increasing inertia determined by the proposed RIIM, which allows a small probability of RoCoF violation according to the RAM and further reduces the required inertia demand and thus the cost for enhancement. Finally, six different APs are proposed to distribute the calculated area-level inertia demand to individual plants in the region according to various considerations, i.e., technical feasibility and individual cost, and RoCoF performance. The risk assessment and mitigation are critically validated via SBS, and the results based on the proposed methods are carefully discussed.

4.1 IS-LSM-based Risk Assessment on Area-level RoCoF

4.1.1 The Acquisition of IS of Area-level RoCoF

According to the swing equation, the RoCoF is determined as below [88, 90, 128].

$$RoCoF = \frac{\Delta f(t)}{dt} = \frac{1}{2H} P_{imb}(t) \tag{4.1}$$

where H is the inertial, $\Delta f(t)$ is the frequency deviation from the nominal frequency f_0, and $P_{imb}(t)$ is the imbalanced power between generation and load demand, which is caused by the stochastic output of the RESs in this thesis.

At the moment of a disturbance occurring, the active power disturbance (P_{Dist}) propagates to each generator bus ($\Delta P_i, i = 1, \cdots, N$ where N is the number of generators in the system) in the network at the related power distribution coefficient (C_i), which is depicted as below.

$$\Delta P_i = C_i \times P_{Dist} \tag{4.2}$$

It is noted that the (4.2) and (3.13) are similar since they express the same propagation process, while the difference is that the C_i in (4.2) replace the P_{ci} in (3.13) due to different acquisition methods, where the complicated derivation process is simplified by limited test data.

Without the loss of generality, the calculation steps for the power distribution coefficient are exhibited in Fig. 4.1 using an N-generator two-area system, where Generators $1, \cdots, i+1$ are in Area 1 and Generators $i+1, \cdots, N$ are in Area 2, which are detailed as follows.

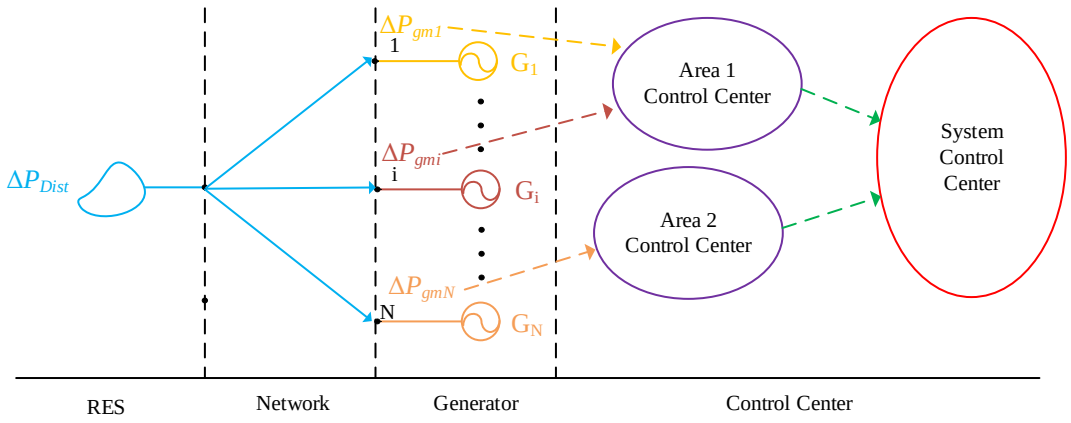

Fig. 4.1 The integration process of the area-level power distribution coefficient.

First, an active power disturbance (P_{Dist}) is imposed on a single RES at t=0, and the change in active power on the transmission line connecting the individual generator bus and the network (i.e., $\Delta P_{gmi}, i = 1, \cdots, N$) is obtained.

Second, the generator-level power distribution coefficient (C_i) is computed in (4.3) by changing the form of (4.2) where ΔP_{gmi} is considered as an approximation to ΔP_i.When the C_i is determined according to (4.3), the value is fixed in the following assessment since the impact of changed C_i on risk assessment for operational planning is marginal.

$$C_i = \frac{\Delta P_{gmi}}{P_{Dist}} \tag{4.3}$$

Third, the recorded data of an individual plant (C_i) are sent to the area control center to integrate the area-level power distribution coefficient (C^j) by summing up the C_i in the coherent area using (4.4). As illustrated in Fig. 4.1, the power distribution coefficients of the first i generators are submitted to the Area 1 Control Center, and the power distribution coefficient of Area 1 (C^1) can be acquired by (4.4). Furthermore, the

system power distribution coefficient can be acquired via the same idea by collecting and aggregating the area-level power distribution coefficients (C^j) in the system.

$$C^j = \sum_{i=1}^{G} C_i^j \tag{4.4}$$

where, C^j is the power distribution coefficient of the j^{th} area, C_i^j is the power distribution coefficient of the i^{th} generator bus in the jth area, and G is the number of generators in the j^{th} area. The superscript refers to the number of the area.

The concept of ACOI defined in the previous chapter is employed in this chapter, which can be expressed as below.

$$H^j = \sum_{i=1}^{G} H_i^j \tag{4.5}$$

where, H_i^j is the inertia of the i^{th} generator in the j^{th} area, and G is the number of generators in the j^{th} area.

Submitting (4.2) into (4.1) with imbalanced power equaling active power variation, i.e., $P_{imb} = \Delta P_i$A simple expression of RoCoF is derived in (4.6), which can also be expressed as the product of sensitivity defined in (4.7) and the disturbing active power. The IS of RoCoF will be used for RAM-based mitigation in the next step.

$$RoCoF_{Simple} = \frac{1}{2H} \times C \times P_{Dist} = IS \times P_{Dist} \tag{4.6}$$

$$IS = \frac{1}{2H} \times C \tag{4.7}$$

The (4.6) is derived for generator-level RoCoF, but the form of (4.6) can also be employed for the calculation of area-level RoCoF, verified as follows.

The conventional system center frequency is defined as the aggregation of the frequency responses of the individual generator with a weight coefficient that is the ratio between the inertia of the individual generator and the COI based on a common power capacity [91], and a similar idea can be applied to compute the area-level frequency response (f^j) as below.

$$f^j = \sum_{i=1}^{G} \frac{H_i}{H^j} \times f_i^j \tag{4.8}$$

where f_i^j is the frequency response of the ith generator in the j^{th} area, and G is the number of the generator in the j^{th} area. With a similar assumption applied to (4.8) and the same initial steady state value, i.e., the nominal frequency f_0, the conventional area-level RoCoF based on the proposed a COI is given by

$$RoCoF_{ACOI}^j = \sum_{i=1}^{G} \frac{H_i}{H^j} \times RoCoF_i^j \tag{4.9}$$

where $RoCoF_i^j$ is the RoCoF of the ith generator in the j^{th} area.

With the assistance of the aggregation method in (4.9), the area-level result ($RoCoF_{simple}^j$) can be acquired as (4.10) by substituting (4.6) into (4.9) with $RoCoF_{Der,i}^j = RoCoF_i^j$.

$$RoCoF_{ACOI}^j = \sum_{i=1}^{G} \frac{H_i}{H^j} \times \frac{1}{2H_i} \times C_i^j \times P_{Dist} = \frac{1}{2H^j} \sum_{i=1}^{G} C_i^j \times P_{Dist}$$

$$= \frac{1}{2H^j} \times C^j \times P_{Dist} = RoCoF_{simple}^j \tag{4.10}$$

Hence, (4.6) is proved to be a generic form of the calculation for generator/area-level RoCoF, which also demonstrates the generality of the corresponding sensitivity in (4.7).

Comparing the proposed and conventional calculation of the area-level RoCoF by (4.6) and (4.9), we can discover that the traditional method needs to obtain the RoCoF of the individual generator while the proposed method in (4.6) requires sensitivity and the stochastic output of the RES (P_{Dist}). When there is a change on P_{Dist}, the conventional method needs to collect the RoCoF of all generators again for computation of area-level RoCoF, whereas the proposed method only requires P_{Dist} with the assumption of an unchanged sensitivity already acquired in the previous calculation, avoiding the time-domain simulation and saving calculation time.

4.1.2 The Framework of Risk Assessment on Area-level RoCoF by IS-LSM

In a multi-RES penetrated power system, it is assumed that there is a linear superposition relationship between area-level RoCoF caused by the stochastic output of all RESs and individual RES. Hence, LSM is introduced and combined with (4.6) to form the IS-LSM for the computation of the area-level RoCoF as below.

$$RoCoF = \sum_{i=1}^{\mathrm{M}} S_i \times P_{Dist,i} \tag{4.11}$$

where M is the number of RESs in the system and $P_{Dist,i}$ is the stochastic active power disturbance (P_{Dist}) of the ith RES.

For a given network, the S_i (i=1…M) are considered constant, and thus the RoCoF variation depends on a different combination of the $P_{Dist,i}$ ($i = 1 \ldots \mathrm{M}$), which can be easily transferred from the stochastic model of individual RESs according to historical data in the planning stage. Thereby, a large amount of area-level RoCoFs are generated according to (4.11), and the number of area-level RoCoF belongs to a specific interval

is counted as $N_{interval}$. Then the probability distribution of the area-level RoCoF within the concerned interval is calculated by (4.12), where N is the total number of generated RoCoF, and then evaluated by the RAM of RoCoF in Table 2.1.

$$P_{interval} = \frac{N_{interval}}{N} \tag{4.12}$$

Based on the above analysis, the flowchart of the risk assessment on area-level RoCoF by the IS-LSM is illustrated in Fig. 4.2, and the detailed description is as follows:

A) To obtain the RES information, including the number, type, steady output, max fluctuating active power, and characteristic distribution of RESs, such as wind speed, and then generate the active power variation sample series according to the correlation coefficient matrices among each RES, where the probabilistic distribution of RES can be any type as illustrated in Fig. 2.1, including Normal distribution, Weibull distribution, and so on.

B) To obtain the changing active power on the transmission line connecting the individual generator bus and the network after an active test power imposed on a single RES, and then calculate the generator-level power distribution coefficient according to (4.3) and aggregate area/system-level power distribution coefficient according to (4.4). After acquiring generator inertia, area/system-level inertia is integrated by (4.5), based on which the sensitivity of the area-level RoCoF w.r.t a single RES is computed by (4.7). In the following, the computation procedure is repeated until the concerned IS of area-level RoCoF w.r.t each RES in the system is gained.

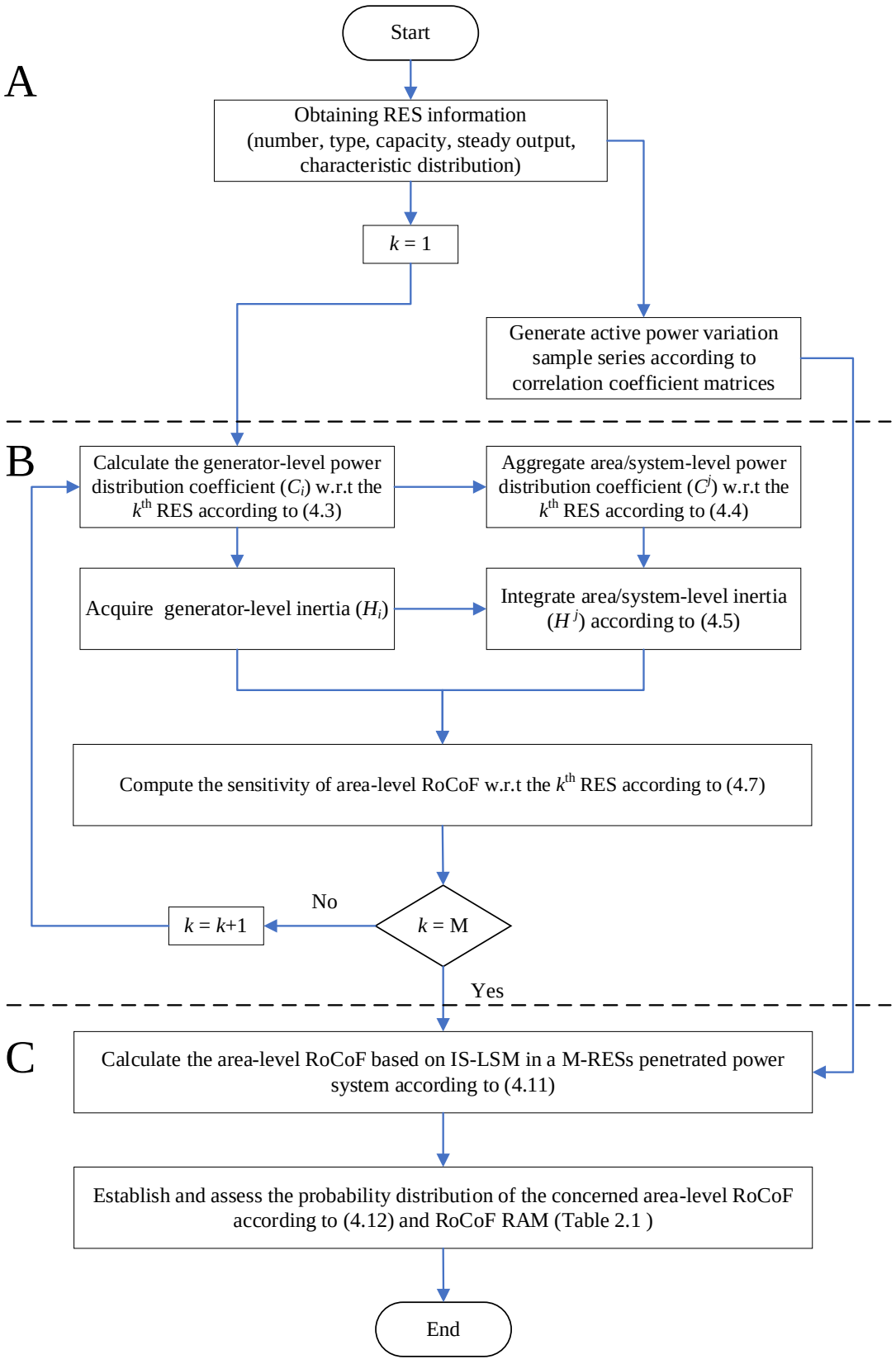

Fig. 4.2 The flowchart of risk assessment on area-level RoCoF by IS-LSM.

C) To calculate the area-level RoCoF and establish the related probability distribution with the assistance of the generated active power variation sample series from the RESs using (4.11) and (4.12), which is further evaluated by the RoCoF RAM. If the high risk of RoCoF is identified, the assessment results and inertia are sent to RIIM for further probabilistic enhancement.

4.2 Probabilistic Risk Mitigation on Area-level RoCoF

According to (4.6), under the premise of not changing the existing network structure (C) and the output of RES (P_{Dist}), increasing the inertia in operational planning can reduce the risk of RoCoF violation effectively. Typically, the inertia demand is determined based on the 'worst-case scenario,' where the worst RoCoF corresponding to simultaneous maximal active power disturbance of all RESs is improved to the critical RoCoF value (e.g., normally 0.5 Hz/s). However, the active power disturbances (P_{Dist}) of RESs, which brings about the 'worst-case scenario' before and after the enhancement (i.e., increasing the inertia demand), are the same. Hence, based on (4.6) the total inertia demand (H_{total}) can be identified by (4.13) when the worst RoCoF is enhanced to a target value.

$$H_{total} = \frac{RoCoF_w}{RoCoF_t} H \tag{4.13}$$

where, $RoCoF_w$ is the worst RoCoF before increasing inertia and $RoCoF_t$ is the target worst RoCoF after increasing inertia.

To achieve the goal of enhancing risky RoCoF, the inertia should increase from the original H to the current H_{total} after enhancement, and the inertia demand (H_{demand}) is obtained by

$$H_{demand} = H_{total} - H \tag{4.14}$$

Moreover, it is discovered that in the process of calculating H_{total} by (4.14), the C representing the network information in (4.6) is eliminated, which means the enhancement of RoCoF could ignore the impacts of the network information. In other words, the enhancement of the risky RoCoF in a specific area by increasing inertia does not impact the RoCoF in other areas and vice versa, which forms a 'risk-oriented' enhancement. The above features enable an easy inertia identification method and a RoCoF enhancement on the risky area only.

It should be noted that the aim of the above method is to handle the problem in only one dimension, i.e., the severity of an event. The other assessment dimension, i.e., occurrence probability, is taken into account in the following. This two-dimensional enhancement permits the occurrence of some stability violation within an acceptable probability according to a pre-defined evaluation criterion and thus could decrease the investment in reducing the high instability risk, which forms the proposed RIIM. The concept of the RIIM is described with the assist of the RoCoF RAM in Table 2.1 in the following.

As displayed in the table, the most concerning part is the 'red region,' which must be avoided to maintain a healthy RoCoF, and thus the evaluated results within these parts must be moved to other regions. In view of the probabilistic stability, the 'yellow

region' displayed in both upper corners of the table is the target region, in which the event breaching the critical value (±0.5Hz/s) within a small probability (1%) is allowed. Therefore, the objective of the RIIM is to move the evaluation results from a highly risky area (red region) to a middle-risk area (yellow region) to achieve probabilistic enhancement and further reduce the cost of investment. The calculation procedure is described in the following and as illustrated in Fig. 4.3.

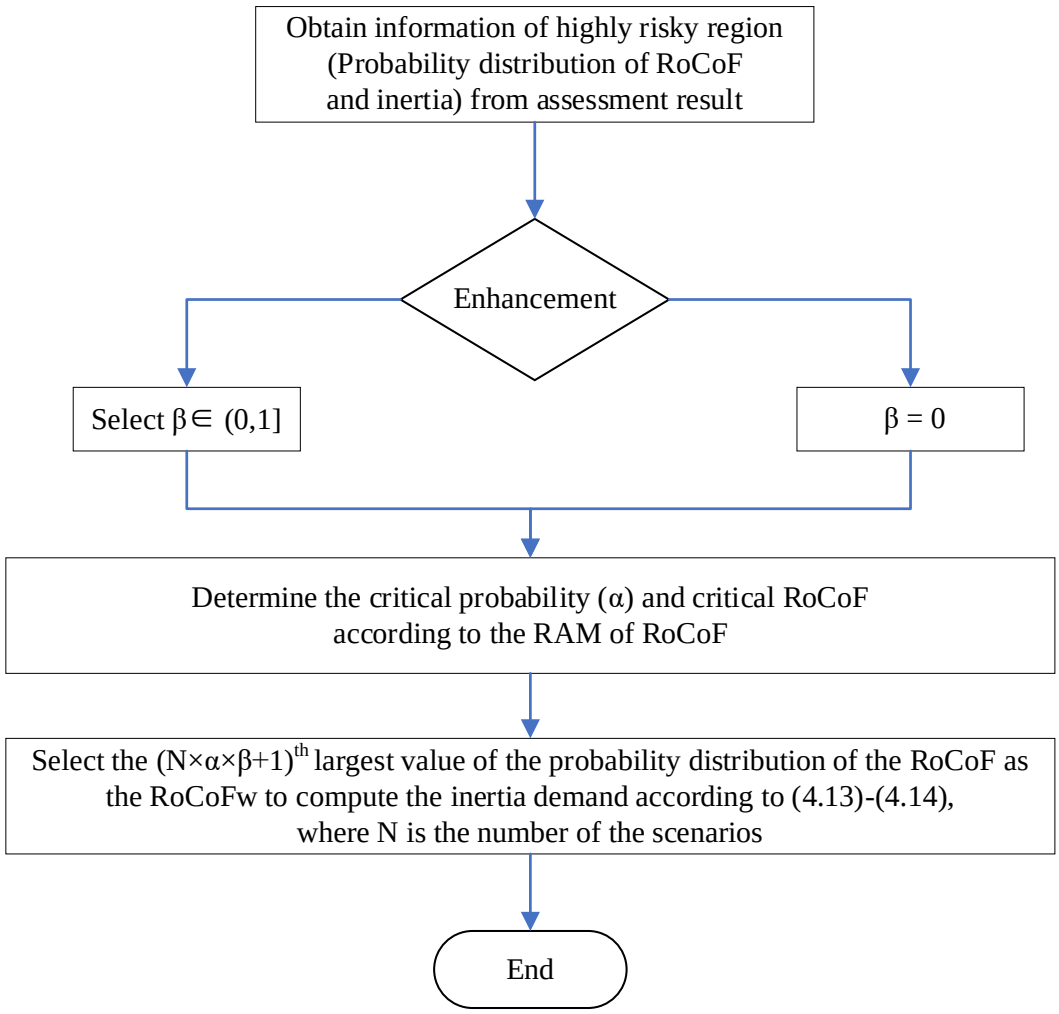

Fig. 4.3 The calculation procedure of RIIM.

1) Obtain the information of the highly risky region, including the probability distribution of the concerned area-level RoCoF from risk assessment result in the previous section and related inertia.

2) Choose the probabilistic enhancement coefficient β, which is between 0 and 1.

The value of β determines the degree of probabilistic enhancement, and the larger value represents the higher level. Value '1' indicates an extreme scenario for probabilistic enhancement. When the value decreases to '0', the probabilistic enhancement (two dimensions) degrades to deterministic enhancement (one dimension), which indicates the generality of the proposed RIIM.

3) According to the RAM of RoCoF, the critical RoCoF (±0.5Hz/s) and the critical probability α (1%) are acquired. Note here the critical probability α is the maximal acceptable probability of the scenario in which RoCoF will violate the critical RoCoF.

4) Pick up the $(N \times \alpha \times \beta + 1)^{\text{th}}$ largest value of the probability distribution of the concerned area-level RoCoFs obtained in the first step (including repeating ones) as the $RoCoF_w$ in (4.13) to calculate the total inertia demand and further the inertia demand according to (4.14), where N is the total number of the scenarios.

The introduction of β is an important part of the proposed RIIM since it provides a chance for the system planner and operator to select the desired value manually from a series of inertia demands, which are determined according to different levels of probabilistic enhancement and the related investment for improving risky area-level RoCoF conditions.

4.3 Allocation Plans of Required Inertia to Individual Generator in the Area

Six APs (including centralized and distributed APs) are proposed to distribute the area-level inertia demand to individual plants in the area according to technical feasibility and individual cost and RoCoF performance, as illustrated in Fig. 4.4.

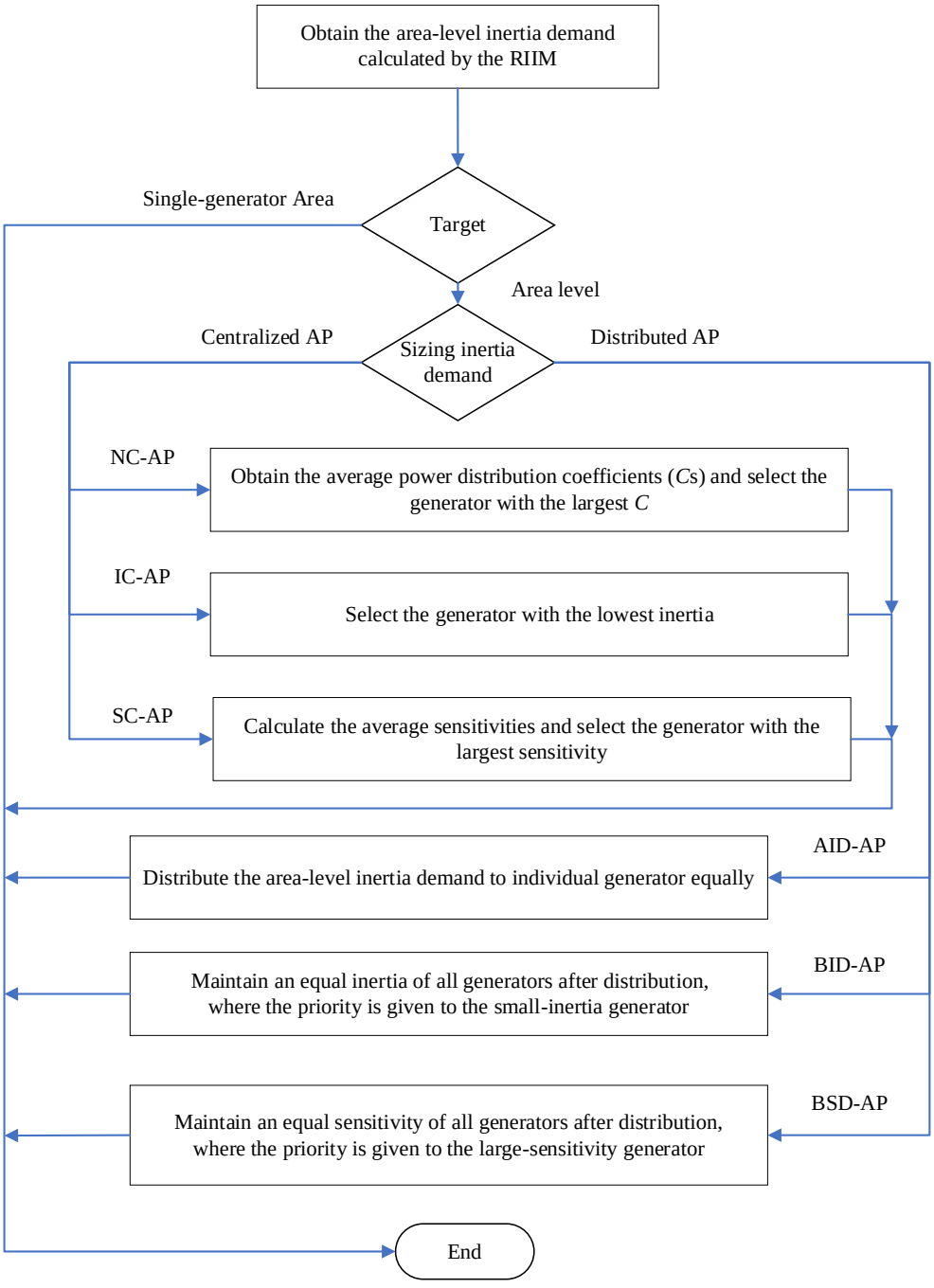

Fig. 4.4 The brief introduction of six APs of inertia demand.

The proposed APs are network-based centralized AP (NC-AP), inertia-based centralized AP (IC-AP), sensitivity-based centralized AP (SC-AP), average inertia-based distributed AP (AID-AP), balanced inertia-based distributed AP (BID-AP), and balanced sensitivity-based distributed AP (BSD-AP), respectively. If there is only one generator in the area, the inertia demand is installed on the generator directly.

4.3.1 Centralized AP for Inertia Demand

Centralized AP for inertia demand simply allocates the area-level inertia demand to only one generator directly, and the selection of the generator for installation of additional inertia is the primary concern. Three APs are proposed based on different considerations, i.e., network, inertia, and sensitivity.

1) NC-AP. At the instance of disturbance occurrence, the active power disturbance is propagated to an individual generator bus according to the 'electric distance,' and usually, the nearer a RES is, the larger the active power that is allocated to the generator bus. Therefore, the generator for the installation of additional inertia is selected based on network information, i.e., the power distribution coefficient (C), and the generator with the largest C is chosen.

2) IC-AP. Conventionally, a power station with low inertia may turn unstable more easily than a power station with high inertia when suffering a disturbance. Thus, small-inertia plants should be the target, and a station with the lowest inertia is selected for increasing inertia.

3) SC-AP. According to (4.6), sensitivity is the direct factor for the RoCoF. This plan aims to alleviate the worst generator-level RoCoF in a region, and hence, the

generating station with the largest sensitivity of RoCoF is the first choice to install additional inertia.

4.3.2 Distributed APs for Inertia Demand

The centralized AP is straightforward and easy to understand, but when the system requires an extremely large inertia injection, it is challenging to implement due to the technical difficulty, huge cost of investment, and the related responsibility. Hence, dispersedly allocating inertia demand to the individual plants makes the enhancement more acceptable and feasible, and three distributed APs of inertia demand are proposed according to various concerns (i.e., cost, inertia, and RoCoF performance of individual conventional plants):

1) AID-AP. To tradeoff the cost of investment for the reduction of risks and improve technical feasibility, area-level inertia demand is allocated to individual plants equally.

2) BID-AP. Currently, some small-inertia power plants are reducing competitive strength compared with large-inertia plants gradually in the expanding grid due to safety concerns. Thereby, more contributions should be made by small plants to increase the competitive power, and thus the total inertia of each plant in the region after enhancement aims to be equal. The calculation procedure of the plan is described as follows and illustrated in Fig. 4.5.

A) Obtain the information of generators in the region (i.e., number N and inertia) and the area-level inertia demand, which is determined by the RIIM. B) This part aims to pick up the generators with small inertia for increasing inertia within the limits of the area-level inertia demand and original inertia of the individual generator. Firstly, the

difference between the i^{th} and $(i+1)^{th}$ smallest inertia is treated as the aimed inertia for enhancement of i generator(s), where i=1,2,…, N-1. If the current area-level inertia demand can satisfy the demand (i.e., aimed inertia×i < area-level inertia demand), aimed inertia is installed on the i generators, and area-level inertia demand is decreased

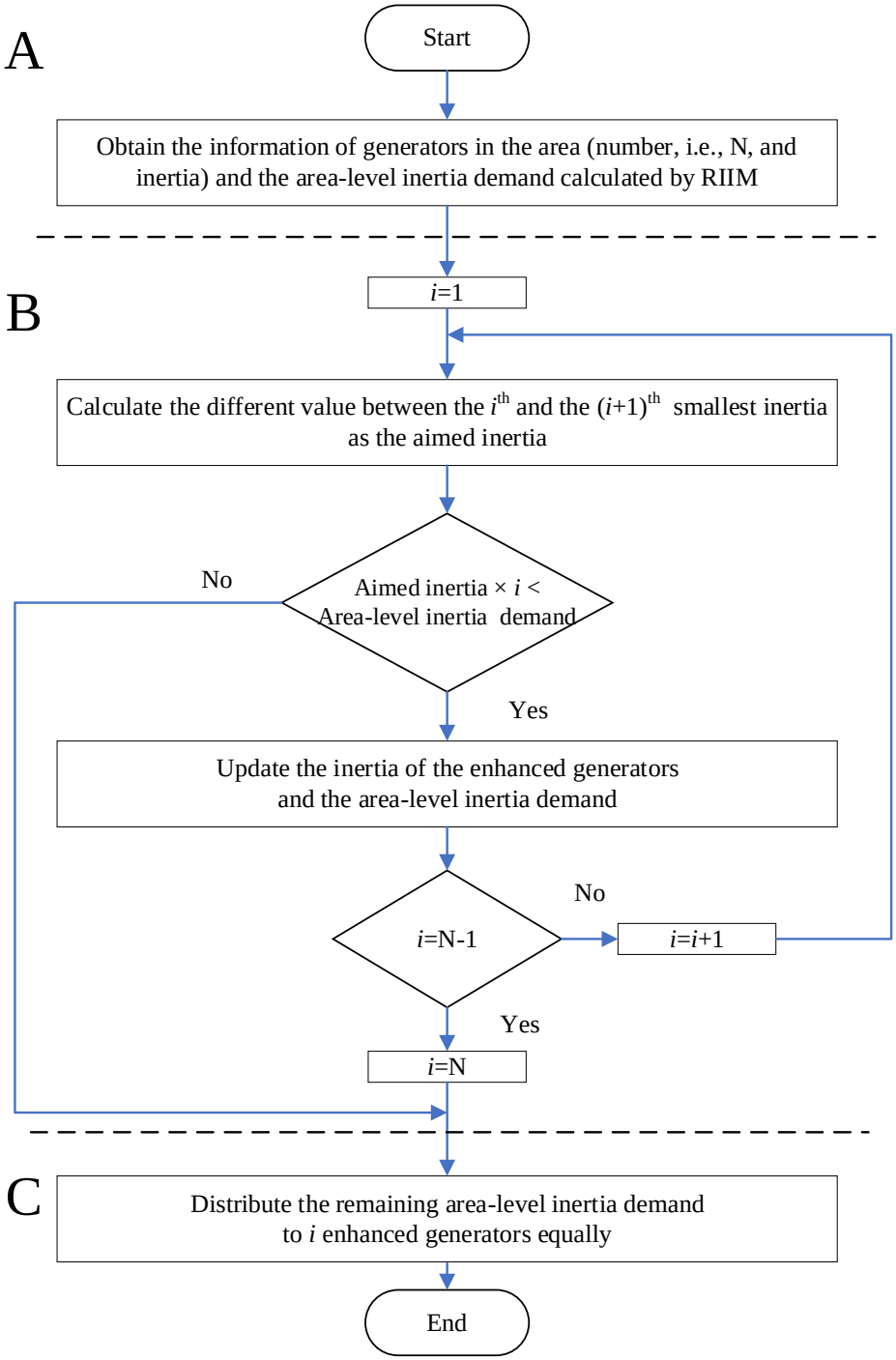

Fig. 4.5 The calculation Procedure of BID-AP.

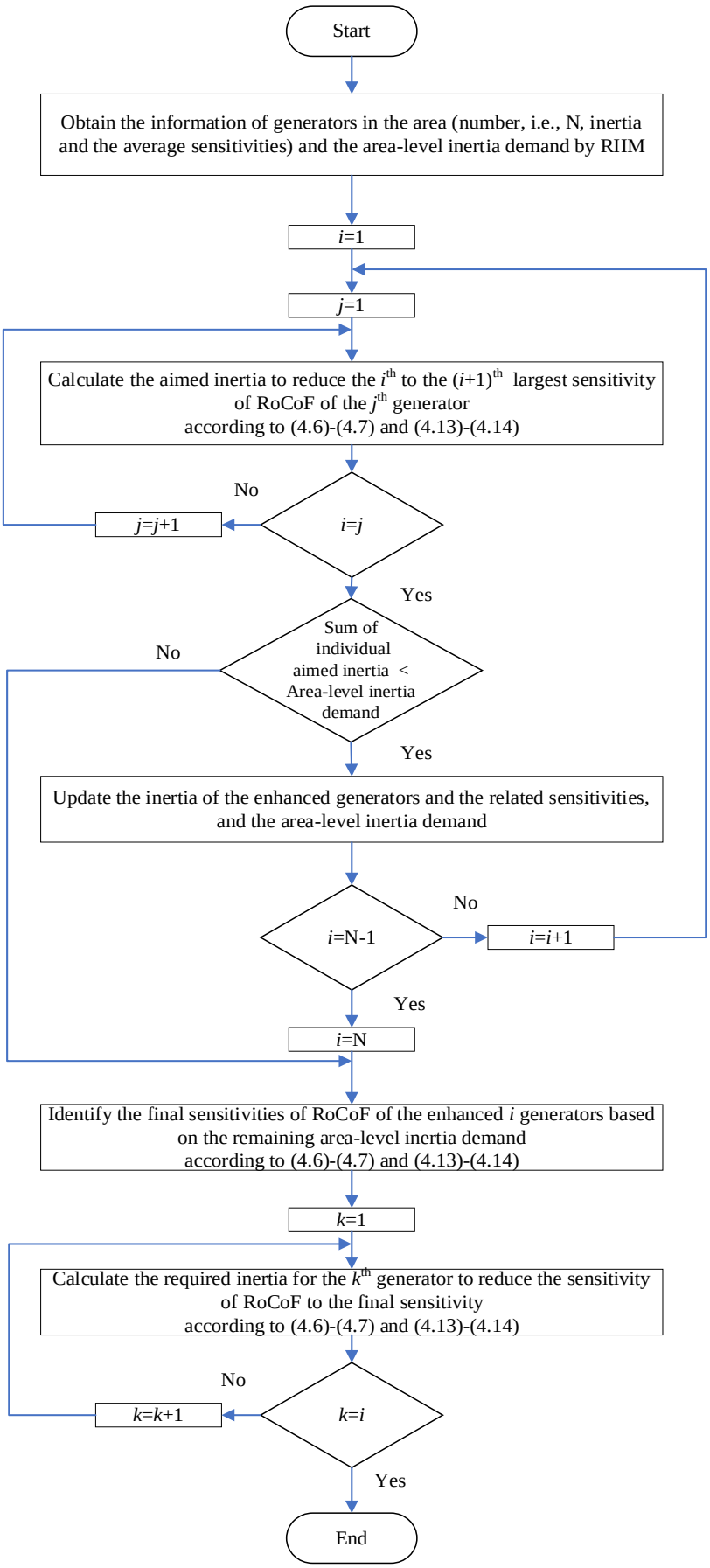

Fig. 4.6 The calculation Procedure of BSD-AP.

by aimed inertia×i. Then the procedure is repeated. If not, only the generators with the i^{th} smallest inertia are chosen for further calculation. C) The remaining area-level inertia demand is distributed to the selected i generators equally.

3) BSD-AP. From the perspective of the area control center, the safe operation of the regional RoCoF is of the greatest concern, regardless of the situation of generator-level responses. However, this plan improves area-level RoCoF from the perspective of enhancing the RoCoF performance of the individual generators in the region separately with the assist of the sensitivity of RoCoF. Hence, the sensitivities of generator RoCoFs in the enhanced region are required to be equal by this AP. The calculation procedure of the BSD-AP is illustrated in Fig. 4.6, some part of which is similar to BID-AP. To avoid duplication, a detailed description is not presented.

4.4 Case Studies

The effectiveness of the proposed risk assessment and enhancement methods is verified in Chapter 4.5.1 (IS-LSM) and 4.5.2-4.5.4 (RIIM and six APs) by 5000 SBS, respectively, where the employed number for Monte Carlo is selected according to [41].

. The benchmark system is a modified IEEE 5-area 16-machine 68-bus network, where three WFs are connected to buses 29, 31, and 41, respectively, as shown in Fig. 4.7. The system operational status decreases to 0.75 of normal status, which implies the load power and generated active power of generators as well as the related inertia all decrease to 0.75 of the original system. The capacity of each WF is 500MVA, and steady output is 1/3 of the capacity, where the Weibull distribution is adopted for wind

speed, and the detailed parameters refer to [129]. The penetration level of RES is 11%. The slow coherency identification method presented in Chapter 3.2 is applied for system partition, and the wind speed distribution in [124] is employed. The operational planning is conducted based on the N-1 criteria, where the RoCoF at disturbance instance is assessed and mitigated, and thus, only the spatial correlation among each WF is considered as (4.15). Three different types of area-level RoCoFs could be examined using this benchmark system, which includes: 1) system-level RoCoF, 2) area-level RoCoF (Area 4 and 5), 3) single-generator area-level RoCoF (Area 1-3).

$$[\rho_{ij}]_{3\times3} = \begin{bmatrix} 1 & 0.6 & 0 \\ 0.6 & 1 & 0 \\ 0 & 0 & 1 \end{bmatrix} \tag{4.15}$$

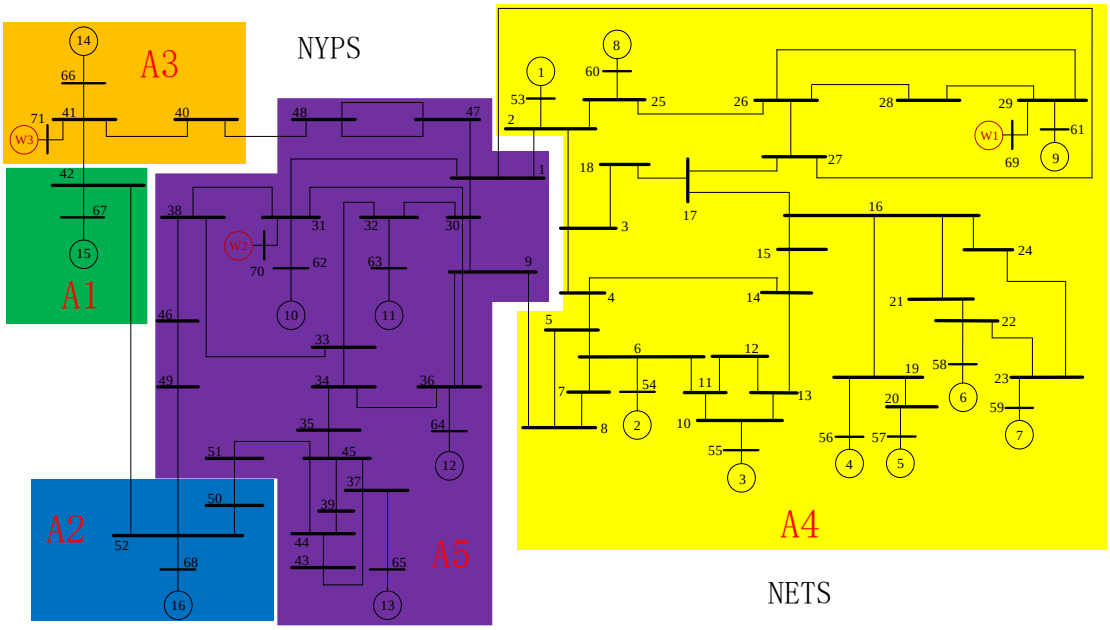

Fig. 4.7 A modified IEEE 16-machine 5-area test system involving three WFs in different locations (for IS-LSM and RIIM).

4.4.1 Validation of IS-LSM

The power distribution coefficients w.r.t individual WFs are calculated according to (4.3) and are displayed in Table 4.1, where C_{ij} is the power distribution coefficient between the ith generator and the jth WF. The power distribution coefficients between different WFs and the same generator are different, specifically for the first nine generators in Area 4.

Table 4.1 The Power distribution coefficients w.r.t each WF (%).

	C_{i1}	C_{i2}	C_{i3}
G1	9.59	5.49	1.12
G2	4.15	2.99	0.63
G3	5.45	3.42	0.73
G4	7.79	2.58	0.64
G5	4.29	1.42	0.35
G6	6.98	2.38	0.56
G7	5.46	1.87	0.44
G8	10.38	4.12	0.85
G9	36.35	2.77	0.64
G10	1.65	8.46	0.83
G11	5.08	16.72	2.59
G12	3.32	8.89	1.55
G13	9.45	26.19	4.4
G14	2.91	7.48	72.93
G15	1.06	2.93	15.17
G16	3.61	11.43	5.63
System	117.52	109.14	109.06

The power distribution coefficients of G1-G9 w.r.t WF1 range from 4.1% to 36.35%, while those values w.r.t WF3 around 1%. It is also notable that the system-level power distribution coefficients w.r.t individual WFs (117.52%, 109.14%, and 109.06%) are all above 100%, which indicates that the active power output of the RES fails to result in an equal change in the sum of the active power on all generator buses, due mainly to the adjustability of the network itself.

Based on the acquired power distribution coefficients and inertia, the sensitivities

of area-level RoCoF w.r.t each WF are calculated and listed in Table 4.2, which displays that the difference between the sensitivities is not as obvious as that between the power distribution coefficients since large H weakens the impact of the power distribution coefficients on sensitivity according to (4.7).

Table 4.2 The IS of area-level RoCoF w.r.t each WF.

	WF1	WF2	WF3
System	0.0396	0.0368	0.0367
Area 1	0.0024	0.0065	0.0337
Area 2	0.0053	0.0169	0.0083
Area 3	0.0065	0.0166	0.1621
Area 4	0.2133	0.0638	0.0141
Area 5	0.0201	0.0620	0.0097

The probability distributions of the area-level RoCoF are calculated by SBS and the IS-LSM are exhibited in Fig. 4.8. The proposed method still performs well. The related boundary values of area-level RoCoF are listed in Table 4.3. It is revealed that the absolute errors of the maximum RoCoF are slightly smaller than those of the min RoCoF, which implies that the proposed method could identify the maximum value of area-level RoCoF more accurately than the minimum value. The different degrees of the errors essentially stem from the selection of the active power disturbance (P_{Dist}) in (4.3), which is explained as follows.

As mentioned before, the accuracy of the estimated worst RoCoF, i.e., minimum RoCoF or maximum RoCoF, is one of the key indicators, and hence, it is essential to judge the direction of the worst RoCoF (positive or negative) first. It is assumed that the larger the active power fluctuation of RESs, the worse the RoCoF induced, and in this scenario, the worst RoCoF is the max RoCoF (positive). Therefore, the max power fluctuation of each WF, i.e., 10/3 (5-5/3) p.u. is selected as the active power disturbance

(P_{Dist}) in (4.3) to guarantee a higher accuracy of the estimated RoCoF around the worst RoCoF. However, this also results in slightly lower accuracy on the estimated value far away from the worst RoCoF, i.e., the min RoCoF in this thesis. The errors of the worst/max area-level RoCoF are all below 0.004Hz/s, less than 1% of the critical value, which can be ignored and meanwhile proves the effectiveness of the proposed IS-LSM in evaluating RoCoF.

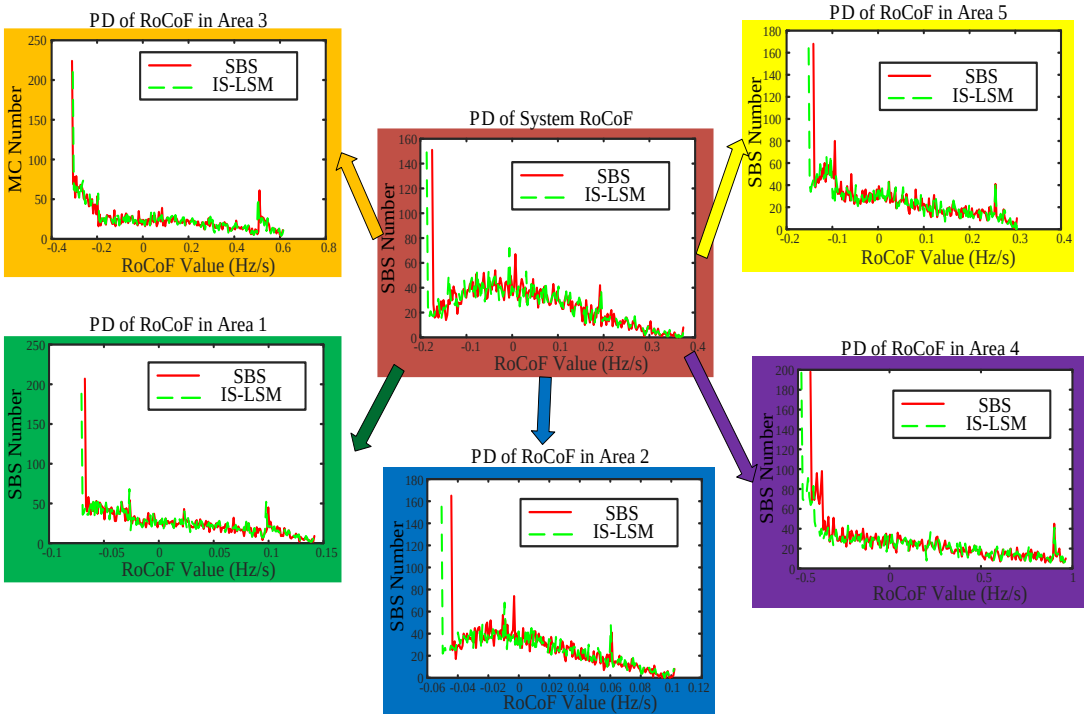

Fig. 4.8 The PD of area-level RoCoF.

Additionally, Table 4.3 also discovers that the max RoCoFs in both Area 3 and 4 violate the RoCoF limit. Therefore, it is necessary to calculate the probability of the RoCoF breaching the critical value in both areas for further evaluation, and the results are given in Table 4.4. The probabilistic results of the risky RoCoF (>0.5Hz/s) in both areas approach the real results acquired by SBS (i.e., 7.98% vs. 8.04% for Area 3 and

17.68% vs. 17.50% for Area 4). Both areas are evaluated as highly risky regions according to the presented RAM of RoCoF, which needs to be further improved.

Thereby, the IS-LSM can identify the boundary values of area-level RoCoF accurately and the probability distribution of highly risky area-level RoCoF with an acceptably small margin of error, which also indicates the effectiveness of the proposed IS-LSM in evaluating RoCoF. In Table 4.5, the computational time of SBS and the SBS is compared, and the IS-LSM is over 700 times faster than SBS, which proves the efficiency of the proposed method.

Table 4.3 The boundary-value of area-level RoCoF and absolute errors (HZ/s).

		SBS	S-LSM	Absolute Error
Max	System	0.3756	0.3768	0.0012
	Area 1	0.1423	0.1420	0.0003
	Area 2	0.1025	0.1021	0.0004
	Area 3	0.6145	0.6172	0.0027
	Area 4	0.9671	0.9707	0.0036
	Area 5	0.3047	0.3059	0.0012
Min	System	-0.1765	-0.1884	0.0119
	Area 1	-0.0679	-0.0710	0.0031
	Area 2	-0.0446	-0.0510	0.0064
	Area 3	-0.3119	-0.3086	0.0033
	Area 4	-0.4357	-0.4853	0.0496
	Area 5	-0.1426	-0.1530	0.0104

Therefore, the effectiveness and efficiency of the proposed IS-LSM in calculating area-level RoCoF is verified by SBS in terms of the probability distribution, boundary values of area-level RoCoF, and computational time.

Table 4.4 The probability distribution of RoCoF violation in Area 3 and 4 (%).

	Area 3	Area 4
SBS	8.04	17.50
IS-LSM	7.98	17.68

Table 4.5 The computational time of SBS and IS-LSM.

	SBS	IS-LSM
Computational time	2689.68s	3.62s

4.4.2 Analytical Results Calculated by RIIM and Six APs

The RIIM is adopted to compute the area-level inertia demand in Areas 3 and 4 with various probabilistic enhancement coefficients (β = 0,0.5,0.7,0.9,1) for Cases 1-5, and the results are listed in Table 4.6.

Table 4.6 The area-level inertia demand on Area 3 and 4 with different β (s).

Case No	Target	Area 3	Area 4
1	β=0	26.4	99.8
2	β=0.5	22.4	94.9
3	β=0.7	21.4	93.15
4	β=0.9	20.35	91.65
5	β=1	19.85	91.45

Table 4.7 The descending sort of generators in Area 4 based on the concerned index for NC-AP, IC-AP, and SC-AP.

NC-AP		IC-AP		SC-AP	
No	C	No	Inertia	No	Sensitivity
G9	0.133	G1	15.750	G9	0.256
G1	0.054	G3	13.425	G8	0.140
G8	0.051	G6	13.050	G1	0.086
G4	0.037	G9	12.938	G4	0.086
G6	0.033	G2	11.325	G7	0.065
G3	0.032	G4	10.725	G6	0.063
G7	0.026	G7	9.900	G3	0.060
G2	0.026	G5	9.750	G2	0.057
G5	0.020	G8	9.113	G5	0.052

With the increase in the probabilistic enhancement coefficient, less inertia demand is required for probabilistic improvement for both area-level RoCoFs, which implies less cost of investment. For single-generator area-level (i.e., Area 3) enhancement, the area-level inertia demand is imposed on the generator directly, while at the entire area-level (i.e., Area 4), the six APs depicted in Chapter 4.4 are employed to allocate the

area-level inertia demand to the individual conventional plant in the region. The centralized APs (i.e., NC-AP, IC-AP, and SC-AP) focus on the maximal/minimal value of the concerned index, and hence the descending sort of the individual generator based on the concerned index for NC-AP, IC-AP, and SC-AP (i.e., power distribution coefficient, inertia, and sensitivity) are given in Table 4.7. As shown, the G9, G8, and G9 are the selected generators for NC-AP, IC-AP, and SC-AP, respectively, to install inertia demand. AID-AP allocates the inertia demand to individual generators in Area 4 equally. The generator-level inertia demand in the regions distributed by BID-AP and BSD-AP is given in Table 4.8 and Table 4.9 respectively.

Table 4.8 The inertia demand of individual conventional plants in Area 4 by BID-AP (s).

No	Case 1	Case 2	Case 3	Case 4	Case 5
G1	7.110	6.569	6.373	6.206	6.185
G2	11.535	10.994	10.798	10.631	10.610
G3	9.435	8.894	8.698	8.531	8.510
G4	12.135	11.594	11.398	11.231	11.210
G5	13.110	12.569	12.373	12.206	12.185
G6	9.810	9.269	9.073	8.906	8.885
G7	12.960	12.419	12.223	12.056	12.035
G8	13.747	13.207	13.011	12.844	12.822
G9	9.922	9.382	9.186	9.019	8.997

Table 4.9 The inertia demand of individual conventional plants in Area 4 by BSD-AP (s).

No	Case 1	Case 2	Case 3	Case 4	Case 5
G1	11.236	10.598	10.367	10.165	10.138
G2	1.625	1.319	1.208	1.111	1.098
G3	2.561	2.182	2.045	1.926	1.910
G4	7.634	7.200	7.043	6.905	6.887
G5	0.365	0.125	0.039	0.000	0.000
G6	3.484	3.092	2.951	2.827	2.811
G7	3.054	2.747	2.636	2.539	2.526
G8	16.474	15.869	15.650	15.458	15.433
G9	53.332	51.764	51.196	50.700	50.635

4.4.3 Validation of RIIM and six APs for Area 3 (single-generator area)

In this section, whether the probabilistic enhancement (i.e., adding the inertia demand) of Area 3 RoCoF is impacted by the improvement in Area 4 is investigated. Hence the probabilistic results of Area 3 RoCoF enhanced by RIIM with and without improvement on Area 4 are calculated by SBS for further comparison, as illustrated in Table 4.10, which includes the six proposed APs for Area 4.

Table 4.10 shows that even though the different distribution plans (including adding no inertia demand and the proposed six APs) are carried out on Area 4, the probabilistic results on Area 3 are constant, which verifies the effectiveness of the proposed risk-oriented enhancement method in the single-generator area-level, i.e., that enhancement on one area would not impact other areas and vice versa. Furthermore, the proposed strategy satisfies the enhancement target (0%, 0.5%, 0.7%, 0.9%, and 1%), which also verifies the effectiveness of the proposed RIIM in terms of probabilistic enhancement in a single-generator area-level RoCoF.

Table 4.10 The probability of breaching critical RoCoF in Area 3 calculated by SBS based on different APs for Area 4 (%).

Plan for Area 4	Case 1	Case 2	Case 3	Case 4	Case 5
No adding inertia	0	0.44	0.56	0.86	0.90
Proposed Six APs	0	0.44	0.56	0.86	0.90

4.4.4 Validation of RIIM and six APs for Area 4 (multi-generator area)

The probability distribution of Area 4 RoCoF with BID-AP computed by SBS is illustrated in Fig. 4.9. As presented, the shape of the probabilistic results of RoCoF is compressed into a small range from two boundary values (maximum and minimum),

and the degree of compression increases with the decrease of β (i.e., from 1 to 0). The probability distribution of RoCoF breaching the operational limit (±0.4 Hz/s) and the statutory limit (i.e., critical RoCoF, ±0.5 Hz/s) are reduced, indicating a reducing risk of RoCoF violation. The probability distributions around the statutory limit, including the RoCoF boundaries in all enhancement situations, are amplified in the figure to give a clear presentation, in which the conventional method (β=1) keeps the boundary values of RoCoF within the statutory limit to ensure grid stability, whereas the others do not.

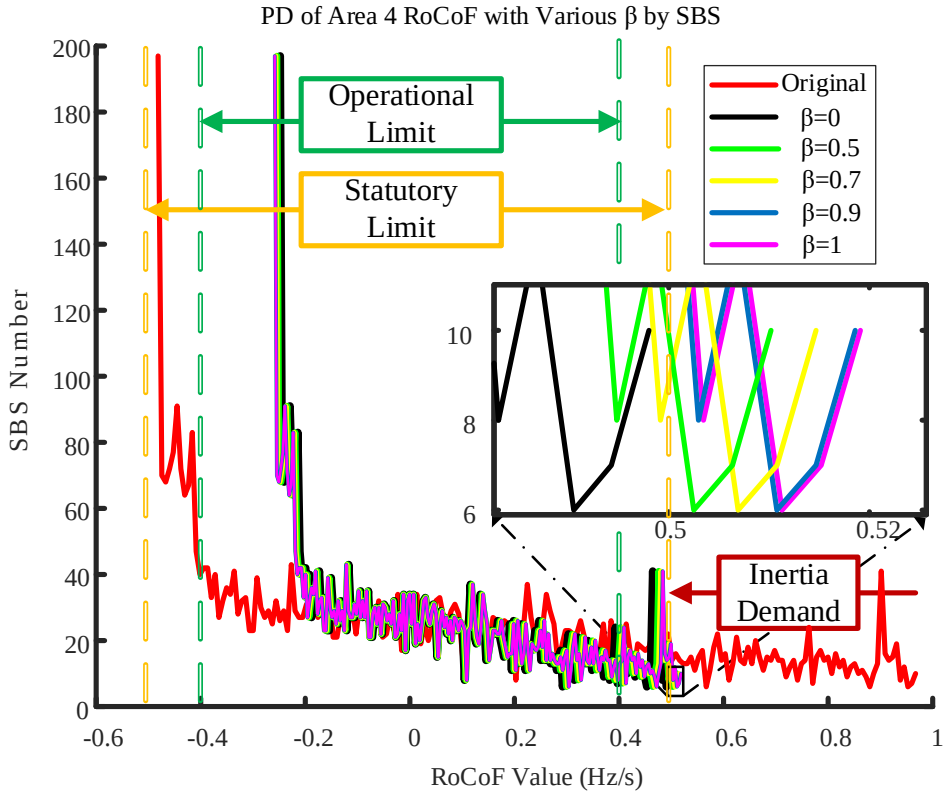

Fig. 4.9 The PD of Area 4 RoCoF with various β by SBS according to BID-AP.

The probabilistic result of RoCoF violation in Area 4 based on different APs given in Table 4.9 also meets the probabilistic target. Besides, even though the distributed inertia on individual conventional plants by the six APs are widely different, the

probabilities of Area 4 RoCoF violation are the same in each case except Case 3, where the small difference (0.02%) can be ignored. Both of the above demonstrate the validity of the proposed probabilistic enhancement on area-level RoCoF and the six proposed APs.

Table 4.11 The probability of breaching critical RoCoF in Area 4 calculated by SBS based on six different APs (%).

Case	NC-AP	IC-AP	SC-AP	AID-AP	BID-AP	BSD-AP
1	0	0	0	0	0	0
2	0.46	0.46	0.46	0.46	0.46	0.46
3	0.64	0.64	0.66	0.66	0.66	0.64
4	0.82	0.82	0.82	0.82	0.82	0.82
5	0.84	0.84	0.84	0.84	0.84	0.84

4.4.5 Investigation of Six APs on Probabilistic Risk Mitigation of Individual Generator-Level RoCoF in the Area Based on Area-Level Inertia Demand

After achieving a similar probabilistic enhancement of area-level RoCoF by the proposed six APs, probabilistic enhancement of RoCoF for each individual plant is investigated to further identify the characteristics of each distribution plan. Therefore, the probabilities breaching critical RoCoF of the individual generators in Area 4 calculated by SBS based on Plans A-F are given in Tables 4.12-4.16, respectively, where the probabilistic results calculated by NC-AP and SC-AP are the same, and thereby are integrated and presented as one.

As exhibited in Tables 4.12 and 4.13, the probabilistic enhancement only happens on the selected generator, while the probabilistic results of other generators are unchanged and still remain a high risk, which verifies the ‘risk-oriented’ feature of the RoCoF enhancement method again. In other words, these centralized APs reduce the area-level

Table 4.12 The probability of breaching critical RoCoF of individual generators in Area 4 based on NC/SC-AP calculated by SBS (%).

No	Case 1	Case 2	Case 3	Case 4	Case 5
G1	13.3	13.3	13.3	13.3	13.3
G2	3.2	3.2	3.2	3.2	3.2
G3	4.04	4.04	4.04	4.04	4.04
G4	13.82	13.82	13.82	13.82	13.82
G5	0.8	0.8	0.8	0.8	0.8
G6	6.52	6.52	6.52	6.52	6.52
G7	7.62	7.62	7.62	7.62	7.62
G8	25	25	25	25	25
G9	0	0	0	0	0

Table 4.13 The probability of breaching critical RoCoF of individual generators in Area 4 based on IC-AP calculated by SBS (%).

No	Case 1	Case 2	Case 3	Case 4	Case 5
G1	13.3	13.3	13.3	13.3	13.3
G2	3.2	3.2	3.2	3.2	3.2
G3	4.04	4.04	4.04	4.04	4.04
G4	13.82	13.82	13.82	13.82	13.82
G5	0.8	0.8	0.8	0.8	0.8
G6	6.54	6.54	6.54	6.54	6.54
G7	7.62	7.62	7.62	7.62	7.62
G8	0	0	0	0	0
G9	36.4	36.4	36.4	36.4	36.4

Table 4.14 The probability of breaching critical RoCoF of individual generators in Area 4 based on AID-AP calculated by SBS (%).

No	Case 1	Case 2	Case 3	Case 4	Case 5
G1	0.2	0.46	0.54	0.74	0.74
G2	0	0	0	0	0
G3	0	0	0	0	0
G4	0	0	0	0	0
G5	0	0	0	0	0
G6	0	0	0	0	0
G7	0	0	0	0	0
G8	6.42	7.36	7.66	7.84	7.92
G9	27.2	27.56	27.8	27.96	28

risk by largely reducing the RoCoF of only one generator, and the risks of other generators in this area are ignored, which is the characteristic of the centralized AP.

Distributed APs can have a better performance in terms of the enhancement of individual generators in the area given the same area-level results, which are shown in the following Tables 4.14-4.16.

Table 4.15 The probability of breaching critical RoCoF of individual generators in Area 4 based on BID-AP calculated by SBS (%).

No	Case 1	Case 2	Case 3	Case 4	Case 5
G1	4.14	4.6	4.76	4.9	4.9
G2	0	0	0	0	0
G3	0	0	0	0	0
G4	0	0	0	0	0
G5	0	0	0	0	0
G6	0	0	0	0	0
G7	0	0	0	0	0
G8	3.38	3.9	4.04	4.16	4.18
G9	28.18	28.6	28.76	28.94	28.94

Table 4.16 The probability of breaching critical RoCoF of individual generators in Area 4 based on BSD-AP calculated by SBS (%).

No	Case 1	Case 2	Case 3	Case 4	Case 5
G1	0.2	0.46	0.54	0.74	0.74
G2	0	0.32	0.44	0.48	0.54
G3	0	0.34	0.46	0.54	0.56
G4	0	0.34	0.46	0.64	0.66
G5	0.2	0.52	0.7	0.78	0.78
G6	0.16	0.46	0.64	0.78	0.8
G7	0.2	0.52	0.7	0.84	0.88
G8	0	0.4	0.52	0.7	0.72
G9	0	1.22	2.78	3.3	3.4

The enhanced probabilistic result of individual generator RoCoF in the area allocated by AID-AP (Table 4.14) manifests that the RoCoFs of most generators are robust stable, i.e., they have 0% unstable probability, while the probability of unstable RoCoF of minority generators is still extremely large, i.e., 27.2% (G9) and the other unstable probabilities are 6.42% and 0.2% for G8 and G1 respectively. Except for Case 1, G1 realizes the probabilistic stability in all cases. The equal allocation of area-level

inertia demand lowers the sensitivity, but the descending sort of the individual generator based on the sensitivity remains unchanged and is the same as in Table 4.7. The sorted result of generators by analytical sensitivity is consistent with that achieved by SBS in terms of the probabilistic distribution of risky RoCoF, and the highest risk is on G9, followed by G8 and G1, subsequently, which proves the effectiveness of the sensitivity analysis of RoCoF.

The enhanced probabilistic result of individual generator RoCoF in Area 4 based on BID-AP (Table 4.15) is similar to that based on AID-AP, where the unstable probabilities of RoCoF for most generators are still 0%, and values for G1, 8-9 are still above 0. However, compared with Table 4.14 the only difference is the risky probability and the related sort, in which the risk of G1 turns out to be higher than that of G8. BID-AP tries to maintain equal inertia after distribution, and hence the sort of generators based on the sensitivity changes to be based on power distribution coefficients (C) according to (4.7) in Table 4.7. The top three descending sorts of generators corresponding to power distribution coefficients are G9, G1, and G8, which are consistent with those computed by SBS in Table 4.15, and further verify the effectiveness of the analytical sensitivity analysis.

The probabilistic result of unstable individual generator RoCoF in Area 4 for BSD-AP is listed in Table 4.16. It is revealed that most generators achieve the probabilistic target, and there is no extremely large violating probability compared with the probabilistic result by other plans. Therefore, BSD-AP performs better than other plans in terms of the probabilistic enhancement of individual generator RoCoF under the

premise of the same area-level enhancement.

4.5 Summary

In this chapter, the RAM is established as a new criterion to assess and mitigate the risk of area-level RoCoF violation simultaneously caused by fluctuating RES for operational planning. The proposed RAM-based assessment can achieve an accurate result effectively and efficiently, which can accommodate any arbitrary distribution of stochastic disturbance. The proposed RAM-based enhancement can achieve different levels of probabilistic stability according to the given target, which can reduce the cost of mitigating the risk. Six different APs are proposed to allocate the area-level inertia demand to individual power plants in the region according to various concerns such as technical feasibility and individual cost & RoCoF performance. The distribution results of six APs are vastly different, but a similar and accurate enhancement performance can be achieved. Furthermore, the location of WF considerably impacts the generator/system-level RoCoFs considering the same size, which can be revealed by the proposed method for operational planning.

Chapter 5

Risk Assessment on System and Area-Level FN/FV

The above two chapters assess and mitigate the risk of area-level RoCoF violation, and this chapter proposes a framework for assessing the risk of area-level FN/FV, which is difficult to be characterized by SFR model for operational planning in a practical and effective manner. Firstly, an MPS is proposed based on the classical generator model to evaluate the system FN/FV, where the impact of different RESs on system FN/FV is considered. The method can be extended for regional frequency evaluation, but the influence of generator frequency oscillation cannot be effectively evaluated, which might affect assessment accuracy. To address this issue, a MIS is further proposed to calculate the probabilistic distribution of the area-level FN/FV. The probabilistic results are evaluated by the FN/FV RAM to provide a two-dimensional analysis for system operational planners. The accuracy and efficiency of the proposed MPS and MIS are critically validated via SBS in a modified IEEE 16-machine 68-bus benchmark system.

5.1 The Sensitivity of the FN/FV

The sensitivity of system FN/FV w.r.t a single disturbance is usually derived using the widely applied SFR model, as presented in (2.10), which can be simplified as below.

$$\Delta f_{n/v} = S_{n/v}\Delta P \tag{5.1}$$

The required sensitivity, i.e., $S_{\mathrm{n/v}}$, is required based on two assumptions

1) The system is aggregated as a mass, and the electric distance among different disturbance sources and the generators is ignored, which means the location of the disturbance has no impact on the derived results. For example, the system FN/FV caused by a single active power disturbance with the same size and different locations are evaluated as the same according to (5.1), but they are not the same in practice.

In a multi-disturbance system, the disturbance is aggregated by adding the stochastic output of individual disturbance sources, and thus, the system FN/FV can be expressed as below.

$$f_{n/v} = S_{n/v}\Delta P = \sum_{i=1}^{\mathrm{M}} S_{n/v}\,\Delta P_i \tag{5.2}$$

where, ΔP_i is the disturbance of the ith disturbance source, M is the number of the disturbance sources.

When individual ΔP_i is not equal to zero, but the sum of ΔP_i equals zero, the assessment result, according to (5.1), is zero, while in practice, it is not.

2) The excitation system is not considered, which is usually equipped in a traditional power plant in practice and impacts the FN/FV. Thus, the consideration of the excitation system can make the research more practical.

Therefore, the FN/FV evaluated by (5.1) - (5.2) can be improved via selecting a proper sensitivity considering the locations of disturbance sources and the response of the excitation system.

5.1.1 MPS of System FN/FV

The sensitivity is a link connecting the system FN/FV and the active power disturbance, while according to the above analysis, a single sensitivity is difficult to accurately reflect this relationship, especially in a multi-disturbance power system. Thereby, it is reasonable to use multiple sensitivities to describe the impact of the stochastic output of individual RES on system FN/FV as below, where the number of sensitivities is equal to that of the disturbance source.

$$f_{n/v} = \sum_{i=1}^{\mathrm{M}} S_{n/v_i} \Delta P_i \tag{5.3}$$

where, S_{n/v_i} is the sensitivity of the FN/FV w.r.t the ith disturbance which can consider the impacts from not only the electric disturbance but also the control system, including governor speed and excitation system.

It is assumed that the sensitivity of concerned FN/FV w.r.t the output of the same RES (i.e., the same location) is constant, which is fixed after being determined. The procedure of computing the sensitivity of the FN/FV is presented below.

1. Collect M sets of data, each of which contains the stochastic output of M disturbance sources and the corresponding FN/FV from historical data sets or simulations [130].

2. The collected M sets of data can be rewritten in matrix form as below.

$$\begin{bmatrix} f_{n/v_i} \\ \vdots \\ f_{n/v_{\mathrm{M}}} \end{bmatrix} = \begin{bmatrix} \begin{pmatrix} \Delta P_{1,1} & \cdots & \Delta P_{1,\mathrm{M}} \\ \vdots & \ddots & \vdots \\ \Delta P_{\mathrm{M},1} & \cdots & \Delta P_{\mathrm{M},\mathrm{M}} \end{pmatrix} \end{bmatrix} \begin{bmatrix} S_{n/v_1} \\ \vdots \\ S_{n/v_{\mathrm{M}}} \end{bmatrix}$$

$$\mathbf{F_{n/v}} = \mathbf{P_{DIS}} \mathbf{S_{n/v}} \tag{5.4}$$

where the $\Delta P_{i,j}$ refers to the stochastic output of the j^{th} disturbance source in the i^{th} data set, i,j =1…M.

3. According to (5.4), the MPS is determined by

$$\mathbf{S_{n/v}} = \mathbf{P_{DIS}}^{-1}\,\mathbf{F_{n/v}} \tag{5.5}$$

It is noted that the rank of the P_{DIS} in (5.4) based on selected data in Step 1 needs to be M, i.e., full rank, which refers to a low similarity among each set of data. Moreover, the calculated sensitivity includes the impacts from the electric disturbance and excitation system and governor speed of individual plants in the system.

5.1.2 MIS of Area-Level FN/FV

The area-level FN/FV is an important indicator for operational planning, especially in a large-scale power system, but nearly no effective analytical model is derived. One reason is that the impact from frequency oscillation of each generator on FN/FV after disturbance can be ignored in evaluating system FN/FV but cannot in area-level assessment. However, the impact is difficult to be expressed analytically due to strong nonlinearity.

It is discovered that different combinations of the simultaneous output of multiple RESs cause different levels of frequency oscillation of individual generators, which impacts the FN/FV evaluation performance. For example, in an M-RES power system, there are 2M output combinations of M RESs based on their output value (i.e., above/below steady state value treated as positive/negative, respectively). MPS is calculated based on only one combination from above. In other words, the impacts from

other 2^M-1 combinations are not properly considered.

Thereby, the MPS can be improved by comprehensively considering the impact of all output combinations of the RESs (i.e., 2M scenarios), which is the core idea of the proposed MIS. In detail, the stochastic output of M RESs is divided into 2M intervals according to the output directions of individual RESs. In each interval, the calculation procedure of MPS is repeated, which is used for further evaluation.

Three assessment methods based on different kinds of sensitivities are illustrated and summarized in Fig. 5.1.

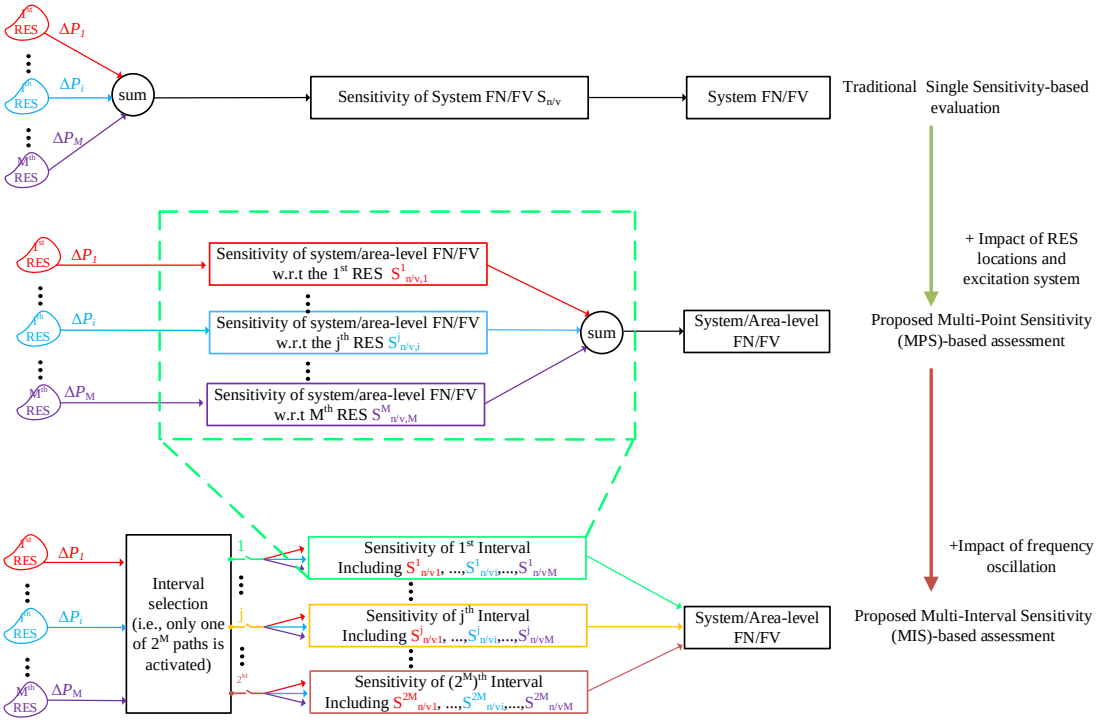

Fig. 5.1 The evaluation method based on single sensitivity, MPS, and MIS.

Firstly, the single sensitivity is derived based on the classical SFR model to calculate the system FN/FV suffering an aggregated disturbance via (5.2). Based on the above, to better assess the system FN/FV, the MPS is proposed to quantify the relationship between the system FN/FV and individual RES, where the impacts from

the electric distance and excitation system in a multi-RES system are quantified comprehensively according to (5.5). It also can be extended for area-level evaluation. On the basis of the MPS, the MIS is further proposed to assess the regional FN/FV, which additionally considers the impact of frequency oscillation caused by different output directions of multiple RESs.

5.2 Operational Planning based on MIS/MPS of Area-Level FN/FV

This section presents an overview of the evaluation process of area-level FN/FV based on MIS in a multi-RES power system for operational planning, as illustrated in Fig. 5.2.

1. Identify the information of the RESs, including number (i.e., M), type, distribution of the natural source, and their correlation. Then, the stochastic and steady output of the individual RES are identified.

2. Based on the above information and the forecasted load, the operational planner can determine the generation of the individual plant in the system, which means the power flow of the system to be assessed is available.

3. Calculate MIS. Firstly, the number of the sensitivity interval is determined, i.e., 2^M, which is also the number of the cycles to acquire MIS. In each cycle/interval, three sets of data are collected via historical information or simulation results, which contain the output of individual RES and the corresponding FN/FV, and then the MPS of the concerned FN/FV is computed according to (5.5). After 2^M cycles, the MIS is obtained.

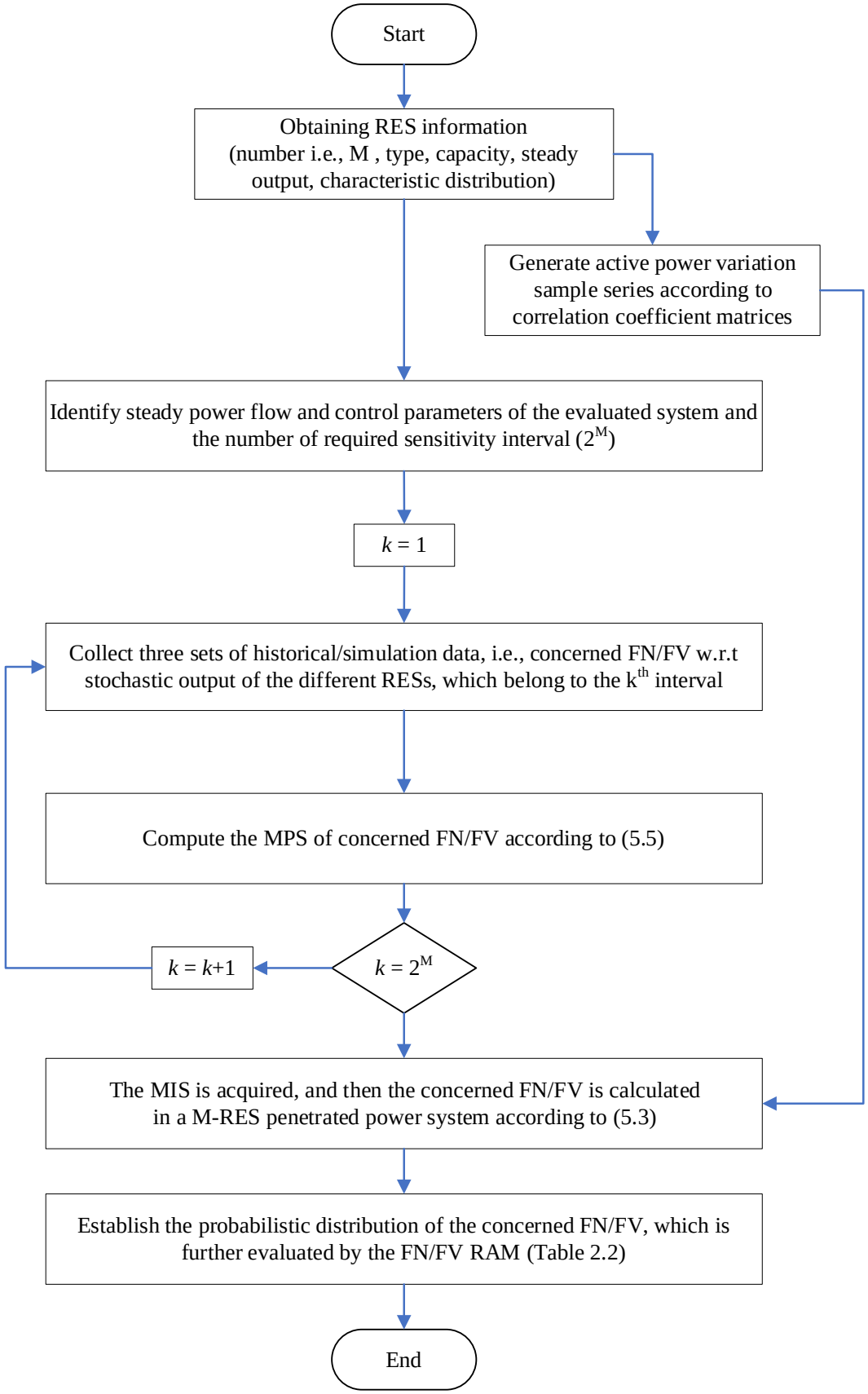

Fig. 5.2 The risk assessment on area-level FN/FV for operational planning based on MIS in a multi-RES power system.

4. Compute the concerned FN/FV by (5.3) using the generated stochastic output of individual RES in Step 1 and the MIS in Step 4, which is further assessed by the FN/FV RAM.

It is noted that the MPS-based assessment is a special case of MIS-based assessment considering only one interval rather than 2M intervals (in Step 3), and thus it is not presented to avoid duplication.

5.3 Case Studies

The effectiveness of the proposed framework is verified using the IEEE 5-area 16-machine 68-bus benchmark system with three WFs connected to buses 29, 31, and 41, respectively, as shown in Fig. 5.3. The slow coherency identification method presented in Chapter 3.2 is applied for system partition, which is perfectly suitable for validation of three types of area-level FN/FV, including 1) system-level FN/FV, 2) area-level FN/FV (Area 4 and Area 5), 3) single-generator area-level FN/FV (Area 1-3).

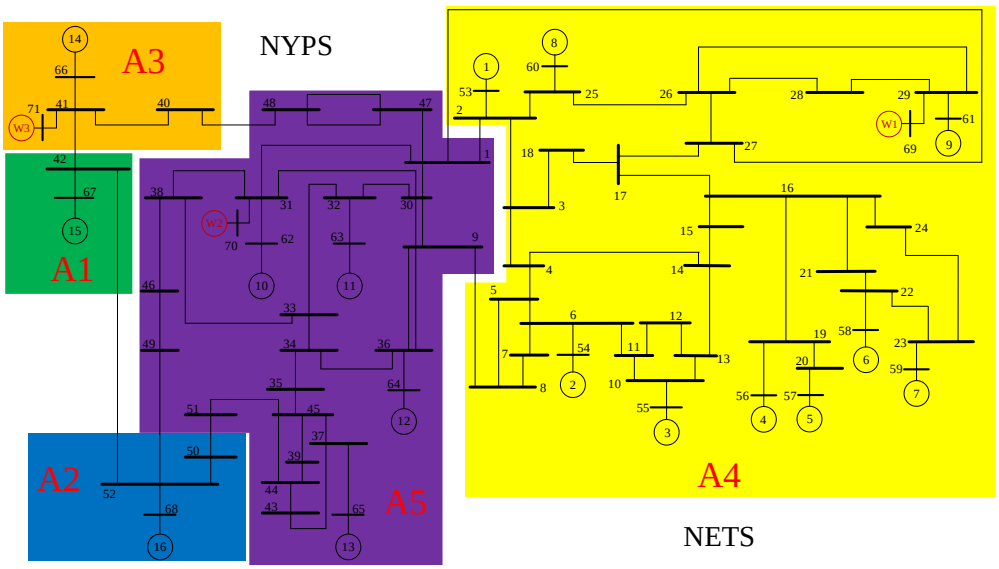

Fig. 5.3 A modified IEEE 16-machine 5-area test system involving three WFs in different locations (for MIS method).

The capacity of each WF is 2 p.u based on 100MVA, and the steady output is 2/3 of the capacity, which replaces the output of the adjacent generator, respectively. The Weibull distribution is employed for wind speed [124] with a spatial correlation coefficient matrix as below.

$$[\rho_{ij}]_{3\times3} = \begin{bmatrix} 1 & 0.7 & 0 \\ 0.7 & 1 & 0 \\ 0 & 0 & 1 \end{bmatrix} \tag{5.6}$$

5.3.1 Sensitivity Analysis

According to the proposed scheme, eight intervals are classified in Table 5.1. The positive, i.e., the stochastic output is higher than the steady output of the WF, is labeled as "+." Otherwise, it is "-." For each interval, three sets of data, including the stochastic output of each WFs and correlated FN/FV, are required via collecting historical data or simulation.

Table 5.1 The classified interval based on the relationship between the steady output and stochastic output of WFs.

Interval No	WF1	WF2	WF3
1	-	-	-
2	-	-	+
3	-	+	-
4	-	+	+
5	+	-	-
6	+	-	+
7	+	+	-
8	+	+	+

Then, the sensitivity of the individual area-level FN/FV w.r.t WF1-3 in each interval is calculated, shown in Table 5.2-5.4 separately. The sensitivity of the individual area-level FN/FV w.r.t WF1-3 for MPS can be directly extracted from the specific line of the individual three tables since it is a special case/interval of MIS. For example, the

second line of Tables 5.2-5.4 is picked up as MPS in Table 5.5. It is noted that the selection of line/interval is arbitrary. Moreover, there is only one sensitivity of system FN/FV based on the derived SFR model, which is 0.1910.

In the most aggregated level, the sensitivity of system FN/FV is derived based on the SFR model, and there is only one value, i.e., 0.1910. In order to improve the assessment accuracy, the impact of WF location is considered, and then the original sensitivity is "expanded" to 0.1423, 0.1310, and 0.2056 (in Table 5.5) for WF1-3 separately by the proposed MPS. Furthermore, the MPS can also be extended for area-level assessment, and the related sensitivities are also listed in Table 5.5. The different

Table 5.2 The MIS of area-level FN/FV w.r.t WF1 within different intervals.

Interval No	System	Area 1	Area 2	Area 3	Area 4	Area 5
1	0.1411	0.1412	0.1411	0.1425	0.1439	0.1417
2	0.1423	0.1439	0.1452	0.1421	0.1432	0.1403
3	0.1430	0.1432	0.1410	0.1444	0.1445	0.1436
4	0.1404	0.1402	0.1396	0.1377	0.1372	0.1397
5	0.1475	0.1482	0.1474	0.1457	0.1418	0.1461
6	0.1452	0.1453	0.1450	0.1469	0.1493	0.1461
7	0.1471	0.1467	0.1471	0.1486	0.1512	0.1478
8	0.1462	0.1464	0.1468	0.1478	0.1495	0.1470

Table 5.3 The MIS of area-level FN/FV w.r.t WF2 within different intervals.

Interval No	System	Area 1	Area 2	Area 3	Area 4	Area 5
1	0.1320	0.1319	0.1317	0.1319	0.1322	0.1320
2	0.1310	0.1303	0.1299	0.1311	0.1316	0.1317
3	0.1354	0.1362	0.1120	0.1346	0.1142	0.1335
4	0.1340	0.1336	0.1330	0.1328	0.1338	0.1337
5	0.1342	0.1339	0.1331	0.1335	0.1342	0.1338
6	0.1312	0.1308	0.1303	0.1310	0.1308	0.1310
7	0.1377	0.1379	0.1391	0.1355	0.1383	0.1350
8	0.1355	0.1357	0.1351	0.1353	0.1351	0.1354

Table 5.4 The MIS of area-level FN/FV w.r.t WF3 within different intervals.

Interval No	System	Area 1	Area 2	Area 3	Area 4	Area 5
1	0.2002	0.2007	0.2010	0.1983	0.1977	0.1977
2	0.2056	0.2068	0.2080	0.2055	0.2052	0.2040
3	0.1994	0.2000	0.1951	0.1974	0.1915	0.1964
4	0.2062	0.2069	0.2071	0.2046	0.2045	0.2041
5	0.1971	0.1972	0.1985	0.1958	0.1965	0.1950
6	0.2054	0.2060	0.2063	0.2040	0.2023	0.2029
7	0.1977	0.1977	0.1995	0.1969	0.1996	0.1958
8	0.2053	0.2061	0.2054	0.2040	0.2023	0.2028

Table 5.5 The MPS of area-level FN/FV w.r.t three WFs.

WF No	System	Area 1	Area 2	Area 3	Area 4	Area 5
WF1	0.1423	0.1439	0.1452	0.1421	0.1432	0.1403
WF2	0.1310	0.1303	0.1299	0.1311	0.1316	0.1317
WF3	0.2056	0.2068	0.2080	0.2055	0.2052	0.2040

values of each line in Table 5.5 indicate the fact that the same WF impacts system and area-level FN/FV differently can be revealed by the proposed MPS. However, MPS is derived in one interval, i.e., interval 2, the information in other intervals cannot be fully considered. Thereby, the assessment accuracy can be improved by comprehensively considering the impact (i.e., MPS) from each interval, and thus the 8 MPSs corresponding to different intervals are required to achieve better performance. In other words, each line of Table 5.5, including 6 values, is "expanded" to a table, including 48 values, shown in Tables 5.2-5.4, respectively. For each column of each three tables, the values are also various, which reflects the impact of different output ranges of three WFs on the same area-level FN/FV, i.e., the level of frequency oscillation.

5.3.2 Validation of MIS, MPS, and SFR -based Methods for System FN/FV

After obtaining the required sensitivities, the probabilistic distributions of system FN/FV assessed by SBS, proposed MIS and MPS, and traditional SFR-based method are presented in Fig. 5.4, and the assessment result and error analysis are in Table 5.6

and 5.7 separately.

The most concerning part is the evaluation accuracy on the 'red region,' i.e., frequency below 49.5 Hz and above 50.5 Hz. The error of high risk evaluated by MIS, MPS, and SFR method are 0.06%, 0.22%, and 3.44% separately. The error of the MPS method is below 0.3% and more than 15 times smaller than that of the SFR-based method, while the error of MIS is below 0.1% and more than 3 times smaller than that of the MPS method. The compared results indicate the proposed MIS and MPS achieve much better performance than the SFR model in evaluating system FN/FV, where the MIS method is more accurate. This summary is also correct for other frequency ranges, i.e., 49.5-49.8, 49.8-50.2, 50.2-50.5 Hz. in Table 5.7.

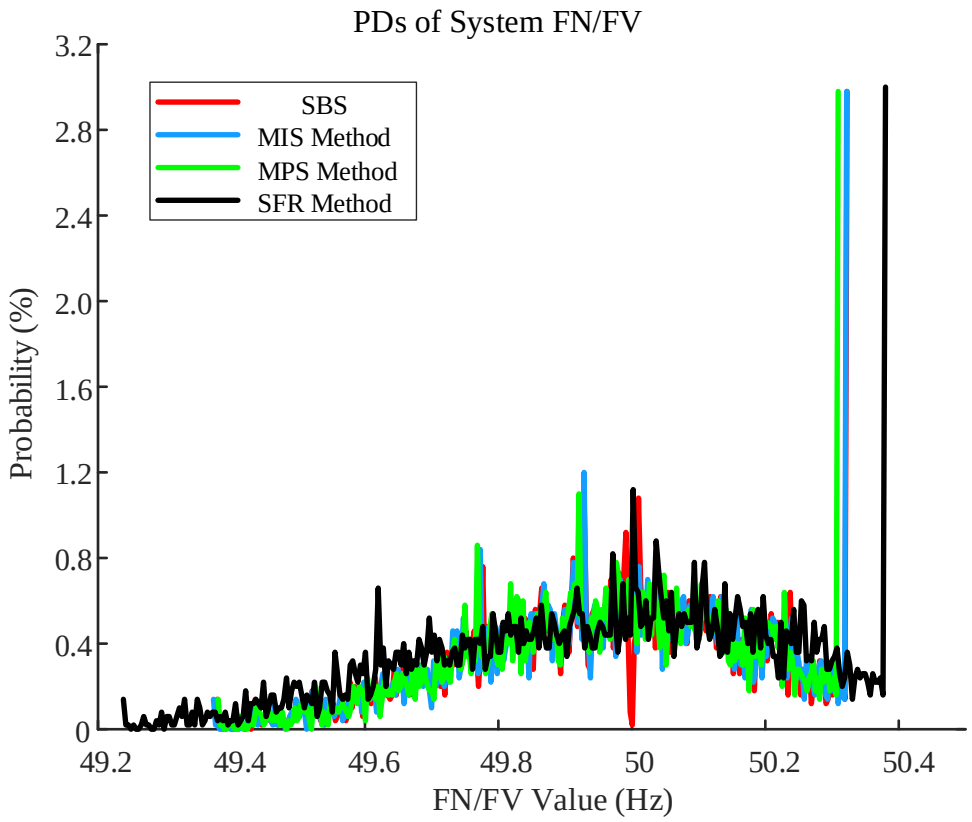

Fig. 5.4 The PDs of system FN/FV assessed by SBS, MIS, MPS, and SFR-based method.

Table 5.6 The assessment results of system FN/FV by SBS, MIS, MPS, and SFR-based method.

Level \ Hz	<49.5	49.5~49.8	49.8~50.2	50.2~50.5	>50.5
SBS	1.68%	20.80%	63.02%	14.50%	0.00%
MIS	1.74%	20.66%	63.06%	14.54%	0.00%
MPS	1.90%	20.92%	63.12%	14.06%	0.00%
SFR	5.16%	23.60%	52.72%	18.52%	0.00%

Moreover, for each line of Table 5.7, the absolute errors of MIS, MPS, and SFR methods change from 0.04% to 0.14%, from 0.10% to 0.44%, and from 2.78% to 10.10% separately. The smaller the error range, the more stable the assessment method (i.e., variance), and thus, the MIS method is the most stable, followed by the MPS method, while the SFR method is the most unstable for the system FN/FV evaluation. To sum up, the proposed MPS and MIS method can replace SFR-model based method for risk assessment of system FN/FV violation in terms of accuracy.

Table 5.7 The assessment results of system FN/FV by SBS, MIS, MPS, and SFR-based method.

Area \ Hz	<49.5	49.5~49.8	49.8~50.2	50.2~50.5	>50.5
MIS	0.06%	0.14%	0.04%	0.04%	0.00%
MPS	0.22%	0.12%	0.10%	0.44%	0.00%
SFR	3.44%	2.78%	10.10%	3.88%	0.00%

5.3.3 Validation of MIS and MPS-based Methods for Area-Level FN/FV

The probabilistic distributions of individual area-level FN/FV evaluated by SBS, MIS, and MPS are illustrated in Table 5.8-5.10 separately. The absolute errors of the assessment by MIS and MPS compared with SBS are given in Table 5.11 and 5.12, respectively.

Compare with Table 5.11 and 5.12, the assessment performance of MIS is better than MPS due to less error intuitively. The average absolute error in Table 5.11 (exclude

the last column) is 0.05%, which is around 6 times smaller than that in Table 5.12 (exclude the last column), 0.28%.

In Table 5.11, the best performance by MIS is on Area 1, with the error of 0.06%, 0.02%, 0.02%, and 0.02% in the intervals between below 49.5 to 50.5 Hz. The evaluation result of Area 3 is the worst due to larger errors, which are 0.06%, 0.10%, 0.18%, and 0.02%, respectively. For the first column (i.e., referring to the assessment error in the range of frequency below 49.5Hz), which is the most concerning section, the errors evaluated by MIS are at 0.04% or 0.06% for all five areas, which is a satisfying result. While the assessment errors by MPS in Table 5.12 vary from 0.26% to 0.34%, and the average is around 0.3%. Although both methods are in similar stability levels (i.e., variance), MIS is preferred due to less average error.

The average absolute errors of system FN/FV evaluated by MIS and MPS are 0.07% and 0.22%, while those of area-level FN/FV by MIS and MPS are 0.05% and 0.28%, respectively. It can be seen that the MIS performs much better in area-level assessment than in system-level assessment, while the MPS turns worse. One reason is that the characteristic of generator frequency oscillation cannot be comprehensively captured and reflected by MPS but can by MIS, which further validates the effectiveness of the proposed MIS.

Compares with Table 5.8 and the first line (i.e., the line including SBS) of Table 5.6, it is revealed the risk of area-level FN/FV cannot be identified by system-level evaluation result, which more conservative. In detail, the risk of system FN/FV in 'red part' is smaller than that of area-level FN/FV, while the risk of system FN/FV in 'green

part' (frequency between 49.8 and 50.2 Hz) is larger than that of area-level FN/FV.

One reason is the frequency oscillation, as illustrated in Fig. 5.5, where the regional frequency is below 49.5 Hz assessed as high risk, while the system frequency, as an average response of the system, is still above 49.5Hz and evaluated as a middle risk. Thus, when system data are not available, regional risk assessment can be treated as an alternative with a less conservative result.

Table 5.8 The RAM of area-level FN/FV evaluated by SBS.

Level \ Hz	<49.5	49.5~49.8	49.8~50.2	50.2~50.5	>50.5
Area 1	1.72%	20.82%	62.82%	14.64%	0.00%
Area 2	1.74%	20.84%	62.74%	14.68%	0.00%
Area 3	1.72%	20.92%	62.70%	14.66%	0.00%
Area 4	1.70%	20.86%	62.74%	14.70%	0.00%
Area 5	1.74%	21.00%	62.56%	14.70%	0.00%

Table 5.9 The RAM of area-level FN/FV evaluated by MIS method.

Level \ Hz	<49.5	49.5~49.8	49.8~50.2	50.2~50.5	>50.5
Area 1	1.78%	20.80%	62.80%	14.62%	1.78%
Area 2	1.78%	20.90%	62.64%	14.68%	1.78%
Area 3	1.78%	21.02%	62.52%	14.68%	1.78%
Area 4	1.76%	20.88%	62.68%	14.68%	1.76%
Area 5	1.78%	21.04%	62.52%	14.66%	1.78%

Table 5.10 The RAM of area-level FN/FV evaluated by MPS method.

Level \ Hz	<49.5	49.5~49.8	49.8~50.2	50.2~50.5	>50.5
Area 1	1.98%	21.10%	62.76%	14.16%	0.00%
Area 2	2.04%	21.10%	62.46%	14.40%	0.00%
Area 3	2.06%	21.26%	62.20%	14.48%	0.00%
Area 4	1.98%	21.06%	62.82%	14.14%	0.00%
Area 5	2.00%	21.14%	62.62%	14.24%	0.00%

In Table 5.13, the computational time of SBS and the proposed MIS and MPS method is compared, and around 154120s (42.8 hours) and 154773.6 (42.9 hours) can

be saved by the proposed MIS and MPS method separately, which proves the efficiency of the proposed methods. The MIS is time-consuming compared with MPS but accurate. If the data can be directly obtained from historical information, MIS is better than MPS. Both methods can be selected according to different requirements for operational planning.

Table 5.11 The absolute error of area-level FN/FV evaluated by MIS method.

Level \ Hz	<49.5	49.5~49.8	49.8~50.2	50.2~50.5	>50.5
Area 1	0.06%	0.02%	0.02%	0.02%	0.00%
Area 2	0.04%	0.06%	0.10%	0.00%	0.00%
Area 3	0.06%	0.10%	0.18%	0.02%	0.00%
Area 4	0.06%	0.02%	0.06%	0.02%	0.00%
Area 5	0.04%	0.04%	0.04%	0.04%	0.00%

Table 5.12 The absolute error of area-level FN/FV evaluated by MPS method.

Level \ Hz	<49.5	49.5~49.8	49.8~50.2	50.2~50.5	>50.5
Area 1	0.26%	0.28%	0.06%	0.48%	0.00%
Area 2	0.30%	0.26%	0.28%	0.28%	0.00%
Area 3	0.34%	0.34%	0.50%	0.18%	0.00%
Area 4	0.28%	0.20%	0.08%	0.56%	0.00%
Area 5	0.26%	0.14%	0.06%	0.46%	0.00%

Table 5.13 The computational time of the SBS, MIS, and MPS method.

	SBS	MIS	MPS
Computational Time	154875.3s	755.2s	101.4s

Therefore, the effectiveness and efficiency of the proposed MIS and MPS methods in calculating area-level FN/FV are verified by SBS.

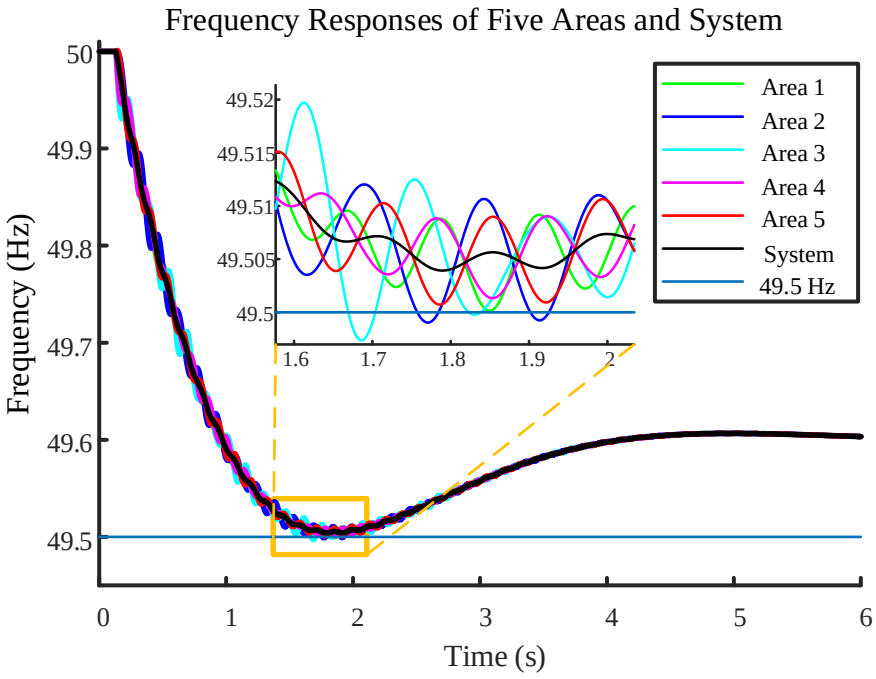

Fig. 5.5 The frequency responses of five areas and the system.

5.4 Summary

In this chapter, a framework for assessing the probabilistic distribution of the area-level FN/FV in a multi-RES power system is presented, and the MPS and MIS methods are proposed accordingly.

1. The proposed MPS and MIS can replace the classical SFR model for risk assessment of system FN/FV due to much smaller errors validated by SBS since both methods consider the impact of RES locations and excitation systems.

2. MIS performs better than MPS in the area-level FN/FV evaluation owning to additional consideration of frequency oscillation, while more data are required. Both methods are much more efficient than SBS.

3. The area-level FN/FV evaluation is more meaningful and practical since it can provide more detailed information and reveal potential violation risks, which cannot be

achieved by a conservative system-level evaluation. Moreover, less data is required for area-level assessment than system-level assessment when aggregating FN/FV for sensitivity calculation.

Chapter 6

Conclusions and Future Work

6.1 Conclusions

The integration of RESs, which brings more uncertainties and reduces system inertia, will more easily incur the frequency instability, i.e., the higher RoCoF and large FN/FV, than ever before, which should be assessed in operational planning. Moreover, uneven distribution of multiple RESs and inertia sources in a large-scale interconnected power system enable various regional frequency responses, which is difficult to be presented by an aggregated system frequency repones and further necessitates the area-level risk assessment on RoCoF and FN/FV. Thereby, this thesis proposes several methods to achieve the effective and effective risk assessment on both system and area-level RoCoF and FN/FV compared with SBS and further the related probabilistic enhancement strategies. The primary conclusions and contributions of this thesis are summarized as follows:

1) The proposed risk assessment framework can comprehensively and efficiently evaluate system frequency stability margins for the first time, which can significantly facilitate the system planner’s decision-making process in the operational planning and effectively mitigate the renewable curtailments. The proposed AS-based assessment (i.e., AS-CBM) and NS-based assessment (i.e., NS-CBM) can achieve satisfying performance in probabilistic evaluation on system RoCoF and FN/FV, which requires

much less computational time compared with the SBS method.

2) The probabilistic distributions of system RoCoF and area-level RoCoF are different, i.e., bell-shaped vs. non-bell-shaped, which necessities the evaluation of area-level RoCoF. Moreover, the apparent “impulses” in the probabilistic distribution curve of both system and area-level RoCoF can be evaluated by the proposed AS-LSM and AS-CBM, where the AS-LSM performs better in accuracy and contains a more straightforward calculation process.

3) The proposed IS-LSM based on active power measurement can achieve an efficient risk assessment on area-level RoCoF verified by SBS. Based on the assessment results, the proposed RIIM can achieve different levels of probabilistic stability according to the given target, which can reduce the cost of mitigating the risk. Moreover, the distribution results of the proposed six APs are vastly different, but a similar and accurate enhancement performance can be achieved. Furthermore, the location of WF impacts the generator/system-level RoCoFs considering the same size, which can be revealed by the proposed method for operational planning.

4) The risk of area-level FN/FV violation is difficult to be revealed by a single system frequency response (i.e., system FN/FV) validated by SBS. The proposed MPS and MIS methods can efficiently assess the risk of the system and area-level FN/FV since both methods consider the impact of RES locations and excitation system, where the MIS method performs better owning to additional consideration of generator frequency oscillation in the grid.

5) When the actual distribution of RES output does not match the predefined distribution, the data-driven method can be employed to improve the accuracy of the established stochastic model according to historical data, which may not follow any type of existing distribution. The proposed AS-LSM, IS-LSM, and MPS/MIS methods still work since these methods do not consider the distribution characteristics of the input data for assessment. Moreover, the calculation speed of the proposed methods is very fast, and thus, the required assessment results can be updated timely.

6.2 Future Work

This thesis has proposed several efficient methods to assess and mitigate the risk of frequency instability. To enrich the current work, the following topics should be investigated in the future.

1) It is necessary to develop a new probabilistic enhancement strategy to mitigate the risk of system and area-level FN/FV violation by guaranteeing a minimal level of spinning reserve in the system and different regions.

2) This research focuses on the assessment based on the ‘N-1’ criterion, and in the future, the risk assessment on frequency stability based on the ‘N-1-1’ criterion will be investigated.

3) The integration of distributed RES will drive the rapid development of high voltage direct current (HVDC), which largely changes the current distribution of the power flow and associated frequency response characteristics. Hence, the risk

assessment and enhancement of frequency stability in an HVDC-dominant power system will be investigated in the future.

4) The RES-dominant power system includes a large number of converters, which will largely change the frequency response of a system compared with a conventional power system. Thus, the risk assessment and enhancement on frequency stability in a converter-dominant power system will be further investigated in the future.

5) The sampling technique will be developed and improved in the future to reduce the required samples for simulation.

6) The robust of the proposed sensitivity-based assessment will be further conducted in my future work.

Appendix

A.1 IEEE 10-Machine Benchmark System Data

Table A.1 Bus Data

Bus No	Type	Voltage	Angle	Gen MW	Gen MVar	Load MW	Load MVar
B1	PQ	1	0	0	0	0	0
B2	PQ	1	0	0	0	0	0
B3	PQ	1	0	0	0	3.22	0.024
B4	PQ	1	0	0	0	5	1.84
B5	PQ	1	0	0	0	0	0
B6	PQ	1	0	0	0	0	0
B7	PQ	1	0	0	0	2.338	0.84
B8	PQ	1	0	0	0	5.22	1.76
B9	PQ	1	0	0	0	0	0
B10	PQ	1	0	0	0	0	0
B11	PQ	1	0	0	0	0	0
B12	PQ	1	0	0	0	0.075	0.88
B13	PQ	1	0	0	0	0	0
B14	PQ	1	0	0	0	0	0
B15	PQ	1	0	0	0	3.2	1.53
B16	PQ	1	0	0	0	3.29	0.32
B17	PQ	1	0	0	0	0	0
B18	PQ	1	0	0	0	1.58	0.3
B19	PQ	1	0	0	0	0	0
B20	PQ	1	0	0	0	6.28	1.03
B21	PQ	1	0	0	0	2.74	1.15
B22	PQ	1	0	0	0	0	0
B23	PQ	1	0	0	0	2.475	0.846
B24	PQ	1	0	0	0	3.086	-0.92
B25	PQ	1	0	0	0	2.24	0.472

B26	PQ	1	0	0	0	1.39	0.17
B27	PQ	1	0	0	0	2.81	0.755
B28	PQ	1	0	0	0	2.06	0.276
B29	PQ	1	0	0	0	2.835	0.269
B30	PV	1.0475	0	2.5	0	0	0
B31	slack	1.0400	0	5.7293	0	0	0
B32	PV	0.9831	0	6.5	0	0	0
B33	PV	0.9972	0	6.32	0	0	0
B34	PV	1.0123	0	5.08	0	0	0
B35	PV	1.0493	0	6.5	0	0	0
B36	PV	1.0635	0	5.6	0	0	0
B37	PV	1.0278	0	5.4	0	0	0
B38	PV	1.0265	0	8.3	0	0	0
B39	PV	1.0300	0	10	0	11.04	2.5

Table A.2 Network Structure

Bus	Bus	Resistance	Reactance	Susceptance	Ratio
B1	B2	0.0035	0.0411	0.6987	1
B1	B39	0.001	0.025	0.75	1
B2	B3	0.0013	0.0151	0.2572	1
B2	B25	0.007	0.0086	0.146	1
B2	B30	0	0.0181	0	1.025
B3	B4	0.0013	0.0213	0.2214	1
B3	B18	0.0011	0.0133	0.2138	1
B4	B5	0.0008	0.0128	0.1342	1
B4	B14	0.0008	0.0129	0.1382	1
B5	B8	0.0008	0.0112	0.1476	1
B6	B5	0.0002	0.0026	0.0434	1
B6	B7	0.0006	0.0092	0.113	1

B6	B11	0.0007	0.0082	0.1389	1
B7	B8	0.0004	0.0046	0.078	1
B8	B9	0.0023	0.0363	0.3804	1
B9	B39	0.001	0.025	1.2	1
B10	B11	0.0004	0.0043	0.0729	1
B10	B13	0.0004	0.0043	0.0729	1
B10	B32	0	0.02	0	1.07
B12	B11	0.0016	0.0435	0	1.006
B12	B13	0.0016	0.0435	0	1.006
B13	B14	0.0009	0.0101	0.1723	1
B14	B15	0.0018	0.0217	0.366	1
B15	B16	0.0009	0.0094	0.171	1
B16	B17	0.0007	0.0089	0.1342	1
B16	B19	0.0016	0.0195	0.304	1
B16	B21	0.0008	0.0135	0.2548	1
B16	B24	0.0003	0.0059	0.068	1
B17	B18	0.0007	0.0082	0.1319	1
B17	B27	0.0013	0.0173	0.3216	1
B19	B33	0.0007	0.0142	0	1.07
B19	B20	0.0007	0.0138	0	1.06
B20	B34	0.0009	0.018	0	1.009
B21	B22	0.0008	0.014	0.2565	1
B22	B23	0.0006	0.0096	0.1846	1
B22	B35	0	0.0143	0	1.025
B23	B24	0.0022	0.035	0.361	1
B23	B36	0.0005	0.0272	0	1

B25	B26	0.0032	0.0323	0.513	1
B25	B37	0.0006	0.0232	0	1.025
B26	B27	0.0014	0.0147	0.2396	1
B26	B28	0.0043	0.0474	0.7802	1
B26	B29	0.0057	0.0625	1.029	1
B28	B29	0.0014	0.0151	0.249	1
B29	B38	0.0008	0.0156	0	1.025
B31	B6	0	0.025	0	1.07

Table A.3 Generator Data

	X_l	R	X_d	X_d’	X_q	X_q’	H
G1	0.0125	0	0.1	0.031	0.069	0.031	84
G2	0.035	0	0.295	0.0697	0.282	0.0697	60.6
G3	0.0304	0	0.2495	0.0531	0.237	0.0531	71.6
G4	0.0295	0	0.262	0.0436	0.258	0.0436	57.2
G5	0.054	0	0.67	0.132	0.62	0.132	52
G6	0.0224	0	0.254	0.05	0.241	0.05	69.6
G7	0.0322	0	0.295	0.049	0.292	0.049	52.8
G8	0.028	0	0.29	0.057	0.28	0.057	48.6
G9	0.0298	0	0.2106	0.057	0.205	0.057	69
G10	0.003	0	0.02	0.006	0.019	0.006	500

A.2 IEEE 16-Machine Benchmark System Data

Table A.2 Bus Data

Bus No	Type	Voltage	Angle	Gen MW	Gen MVar	Load MW	Load MVar

B1	PQ	1	0	0	0	2.527	1.1856
B2	PQ	1	0	0	0	0	0
B3	PQ	1	0	0	0	3.22	0.02
B4	PQ	1	0	0	0	5	1.84
B5	PQ	1	0	0	0	0	0
B6	PQ	1	0	0	0	0	0
B7	PQ	1	0	0	0	2.34	0.84
B8	PQ	1	0	0	0	5.22	1.77
B9	PQ	1	0	0	0	1.04	1.25
B10	PQ	1	0	0	0	0	0
B11	PQ	1	0	0	0	0	0
B12	PQ	1	0	0	0	0.09	0.88
B13	PQ	1	0	0	0	0	0
B14	PQ	1	0	0	0	0	0
B15	PQ	1	0	0	0	3.2	1.53
B16	PQ	1	0	0	0	3.29	0.32
B17	PQ	1	0	0	0	0	0
B18	PQ	1	0	0	0	1.58	0.3
B19	PQ	1	0	0	0	0	0
B20	PQ	1	0	0	0	6.8	1.03
B21	PQ	1	0	0	0	2.74	1.15
B22	PQ	1	0	0	0	0	0
B23	PQ	1	0	0	0	2.48	0.85
B24	PQ	1	0	0	0	3.09	-0.92
B25	PQ	1	0	0	0	2.24	0.47
B26	PQ	1	0	0	0	1.39	0.17
B27	PQ	1	0	0	0	2.81	0.76
B28	PQ	1	0	0	0	2.06	0.28
B29	PQ	1	0	0	0	2.84	0.27
B30	PQ	1	0	0	0	0	0
B31	PQ	1	0	0	0	0	0
B32	PQ	1	0	0	0	0	0

B33	PQ	1	0	0	0	1.12	0
B34	PQ	1	0	0	0	0	0
B35	PQ	1	0	0	0	0	0
B36	PQ	1	0	0	0	1.02	-0.1946
B37	PQ	1	0	0	0	60	3
B38	PQ	1	0	0	0	0	0
B39	PQ	1	0	0	0	2.67	0.126
B40	PQ	1	0	0	0	0.6563	0.2353
B41	PQ	1	0	0	0	10	2.5
B42	PQ	1	0	0	0	11.5	2.5
B43	PQ	1	0	0	0	0	0
B44	PQ	1	0	0	0	2.6755	0.0484
B45	PQ	1	0	0	0	2.08	0.21
B46	PQ	1	0	0	0	1.507	0.285
B47	PQ	1	0	0	0	2.0312	0.3259
B48	PQ	1	0	0	0	2.412	0.022
B49	PQ	1	0	0	0	1.64	0.29
B50	PQ	1	0	0	0	1	-1.47
B51	PQ	1	0	0	0	3.37	-1.22
B52	PQ	1	0	0	0	24.7	1.23
B53	PV	1.04	0	2.5	0	0	0
B54	PV	0.98	0	5.45	0	0	0
B55	PV	0.98	0	6.5	0	0	0
B56	PV	0.99	0	6.32	0	0	0
B57	PV	1.01	0	5.052	0	0	0
B58	PV	1.05	0	7	0	0	0
B59	PV	1.06	0	5.6	0	0	0
B60	PV	1.03	0	5.4	0	0	0
B61	PV	1.02	0	8	0	0	0
B62	PV	1.01	0	5	0	0	0
B63	PV	1	0	10	0	0	0
B64	PV	1.01	0	13.5	0	0	0

B65	Slack	1.01	0	35.91	0	0	0
B66	PV	1	0	17.85	0	0	0
B67	PV	1	0	10	0	0	0
B68	PV	1	0	40	0	0	0

Table A.2 Network Structure

Bus	Bus	Resistance	Reactance	Susceptance	Ratio
B1	B2	0.0035	0.0411	0.6987	1
B1	B30	0.0008	0.0074	0.48	1
B2	B3	0.0013	0.0151	0.2572	1
B2	B25	0.007	0.0086	0.146	1
B2	B53	0	0.0181	0	1.025
B3	B4	0.0013	0.0213	0.2214	1
B3	B18	0.0011	0.0133	0.2138	1
B4	B5	0.0008	0.0128	0.1342	1
B4	B14	0.0008	0.0129	0.1382	1
B5	B6	0.0002	0.0026	0.0434	1
B5	B8	0.0008	0.0112	0.1476	1
B6	B7	0.0006	0.0092	0.113	1
B6	B11	0.0007	0.0082	0.1389	1
B6	B54	0	0.025	0	1.07
B7	B8	0.0004	0.0046	0.078	1
B8	B9	0.0023	0.0363	0.3804	1
B9	B30	0.0019	0.0183	0.29	1
B10	B11	0.0004	0.0043	0.0729	1
B10	B13	0.0004	0.0043	0.0729	1
B10	B55	0	0.02	0	1.07
B12	B11	0.0016	0.0435	0	1.06

B12	B13	0.0016	0.0435	0	1.06
B13	B14	0.0009	0.0101	0.1723	1
B14	B15	0.0018	0.0217	0.366	1
B15	B16	0.0009	0.0094	0.171	1
B16	B17	0.0007	0.0089	0.1342	1
B16	B19	0.0016	0.0195	0.304	1
B16	B21	0.0008	0.0135	0.2548	1
B16	B24	0.0003	0.0059	0.068	1
B17	B18	0.0007	0.0082	0.1319	1
B17	B27	0.0013	0.0173	0.3216	1
B19	B20	0.0007	0.0138	0	1.06
B19	B56	0.0007	0.0142	0	1.07
B20	B57	0.0009	0.018	0	1.009
B21	B22	0.0008	0.014	0.2565	1
B22	B23	0.0006	0.0096	0.1846	1
B22	B58	0	0.0143	0	1.025
B23	B24	0.0022	0.035	0.361	1
B23	B59	0.0005	0.0272	0	1
B25	B26	0.0032	0.0323	0.531	1
B25	B60	0.0006	0.0232	0	1.025
B26	B27	0.0014	0.0147	0.2396	1
B26	B28	0.0043	0.0474	0.7802	1
B26	B29	0.0057	0.0625	1.029	1
B28	B29	0.0014	0.0151	0.249	1
B29	B61	0.0008	0.0156	0	1.025
B9	B30	0.0019	0.0183	0.29	1

B9	B36	0.0022	0.0196	0.34	1
B9	B36	0.0022	0.0196	0.34	1
B36	B37	0.0005	0.0045	0.32	1
B34	B36	0.0033	0.0111	1.45	1
B35	B34	0.0001	0.0074	0	0.946
B33	B34	0.0011	0.0157	0.202	1
B32	B33	0.0008	0.0099	0.168	1
B30	B31	0.0013	0.0187	0.333	1
B30	B32	0.0024	0.0288	0.488	1
B1	B31	0.0016	0.0163	0.25	1
B31	B38	0.0011	0.0147	0.247	1
B33	B38	0.0036	0.0444	0.693	1
B38	B46	0.0022	0.0284	0.43	1
B46	B49	0.0018	0.0274	0.27	1
B1	B47	0.0013	0.0188	1.31	1
B47	B48	0.0025	0.0268	0.4	1
B47	B48	0.0025	0.0268	0.4	1
B48	B40	0.002	0.022	1.28	1
B35	B45	0.0007	0.0175	1.39	1
B37	B43	0.0005	0.0276	0	1
B43	B44	0.0001	0.0011	0	1
B44	B45	0.0025	0.073	0	1
B39	B44	0	0.0411	0	1
B39	B45	0	0.0839	0	1
B45	B51	0.0004	0.0105	0.72	1
B50	B52	0.0012	0.0288	2.06	1

B50	B51	0.0009	0.0221	1.62	1
B49	B52	0.0076	0.1141	1.16	1
B52	B42	0.004	0.06	2.25	1
B42	B41	0.004	0.06	2.25	1
B41	B40	0.006	0.084	3.15	1
B31	B62	0	0.026	0	1.04
B32	B63	0	0.013	0	1.04
B36	B64	0	0.0075	0	1.04
B37	B65	0	0.0033	0	1.04
B41	B66	0	0.0015	0	1
B42	B67	0	0.0015	0	1
B52	B68	0	0.003	0	1
B1	B27	0.032	0.32	0.41	1

Table A.2 Generator Data

	X_l	R	X_d	X_d’	X_q	X_q’	H
G1	0.0125	0	0.1	0.031	0.069	0.028	42
G2	0.035	0	0.295	0.0697	0.282	0.06	30.2
G3	0.0304	0	0.2495	0.0531	0.237	0.05	35.8
G4	0.0295	0	0.262	0.0436	0.258	0.04	28.6
G5	0.027	0	0.33	0.066	0.31	0.06	26
G6	0.0224	0	0.254	0.05	0.241	0.045	34.8
G7	0.0322	0	0.295	0.049	0.292	0.045	26.4
G8	0.028	0	0.29	0.057	0.28	0.05	24.3
G9	0.0298	0	0.2106	0.057	0.205	0.05	34.5
G10	0.0199	0	0.169	0.0457	0.115	0.045	31
G11	0.0103	0	0.128	0.018	0.123	0.015	28.2
G12	0.022	0	0.101	0.031	0.095	0.028	92.3
G13	0.003	0	0.0296	0.0055	0.0286	0.005	248
G14	0.0017	0	0.018	0.00285	0.0173	0.0025	300

G15	0.0017	0	0.018	0.00285	0.0173	0.0025	300
G16	0.0041	0	0.0356	0.0071	0.0334	0.006	225

References

[1] S. Guner and A. Ozdemir, "Turkish Power System: From conventional past to smart future," in *2011 2nd IEEE PES International Conference and Exhibition on Innovative Smart Grid Technologies*, 2011, pp. 1-4.

[2] D. Dizdaroglu, "The Role of Indicator-Based Sustainability Assessment in Policy and the Decision-Making Process: A Review and Outlook," *Sustainability,* vol. 9, no. 6, 2017.

[3] A. Ahmed, S. W. Sutrisno, and S. You, "A two-stage multi-criteria analysis method for planning renewable energy use and carbon saving," *Energy,* vol. 199, p. 117475, 2020/05/15/ 2020.

[4] K. Kaygusuz, "Energy for sustainable development: A case of developing countries," *Renewable and Sustainable Energy Reviews,* vol. 16, no. 2, pp. 1116-1126, 2012/02/01/ 2012.

[5] S. Sen and S. Ganguly, "Opportunities, barriers and issues with renewable energy development – A discussion," *Renewable and Sustainable Energy Reviews,* vol. 69, pp. 1170-1181, 2017/03/01/ 2017.

[6] J. Pinho, J. Resende, and I. Soares, "Capacity investment in electricity markets under supply and demand uncertainty," *Energy,* vol. 150, pp. 1006-1017, 2018/05/01/ 2018.

[7] E. Samani and F. Aminifar, "Tri-level robust investment planning of DERs in distribution networks with AC constraints," *IEEE Transactions on Power Systems,* vol. 34, no. 5, pp. 3749-3757, 2019.

[8] M. S. Nazir, A. J. Mahdi, M. Bilal, H. M. Sohail, N. Ali, and H. M. N. Iqbal, "Environmental impact and pollution-related challenges of renewable wind energy paradigm – A review," *Science of The Total Environment,* vol. 683, pp. 436-444, 2019/09/15/ 2019.

[9] M. Z. Jacobson *et al.*, "100% Clean and Renewable Wind, Water, and Sunlight All-Sector Energy Roadmaps for 139 Countries of the World," *Joule,* vol. 1, no. 1, pp. 108-121, 2017/09/06/ 2017.

[10] G. Cai and L. Kong, "Techno-economic analysis of wind curtailment/hydrogen production/fuel cell vehicle system with high wind penetration in China," *CSEE Journal of Power and Energy Systems,* vol. 3, no. 1, pp. 44-52, 2017.

[11] G. Li, G. Li, and M. Zhou, "Model and application of renewable energy accommodation capacity calculation considering utilization level of inter-provincial tie-line," *Protection and Control of Modern Power Systems,* vol. 4, no. 1, p. 1, 2019.

[12] D. Xu, Q. Wu, B. Zhou, C. Li, L. Bai, and S. Huang, "Distributed Multi-Energy Operation of Coupled Electricity, Heating and Natural Gas Networks," *IEEE Transactions on Sustainable Energy,* pp. 1-1, 2019.

[13] B. Zhou, D. Xu, K. W. Chan, C. Li, Y. Cao, and S. Bu, "A two-stage framework for multiobjective energy management in distribution networks with a high penetration of wind energy," *Energy,* vol. 135, pp. 754-766, 2017/09/15/ 2017.

[14] H. Xu, J. Su, N. Liu, and Y. Shi, "A Grid-Supporting Photovoltaic System Implemented by a VSG with Energy Storage," *Energies,* vol. 11, no. 11, 2018.

[15] M. B. Mcelroy and X. Chen, "Wind and solar power in the united states: status and prospects," *CSEE Journal of Power and Energy Systems,* vol. 3, no. 1, pp. 1-6, 2017.

[16] D. Wu, M. Javadi, and J. N. Jiang, "A preliminary study of impact of reduced system inertia in a low-carbon power system," *Journal of Modern Power Systems and Clean Energy,* vol. 3, no. 1, pp. 82-92, 2015/03/01 2015.

[17] N. Mithulananthan, R. Shah, and K. Y. Lee, "Small-Disturbance Angle Stability Control With High Penetration of Renewable Generations," *IEEE Transactions on Power Systems,* vol. 29, no. 3, pp. 1463-1472, 2014.

[18] D. Gautam, V. Vittal, and T. Harbour, "Impact of Increased Penetration of DFIG-Based Wind Turbine Generators on Transient and Small Signal Stability of

Power Systems," *IEEE Transactions on Power Systems,* vol. 24, no. 3, pp. 1426-1434, 2009.

[19] A. Perilla, J. L. Rueda Torres, S. Papadakis, E. Rakhshani, M. van der Meijden, and F. Gonzalez-Longatt, "Power-Angle Modulation Controller to Support Transient Stability of Power Systems Dominated by Power Electronic Interfaced Wind Generation," *Energies,* vol. 13, no. 12, 2020.

[20] X. Xu, Z. Yan, M. Shahidehpour, H. Wang, and S. Chen, "Power System Voltage Stability Evaluation Considering Renewable Energy With Correlated Variabilities," *IEEE Transactions on Power Systems,* vol. 33, no. 3, pp. 3236-3245, 2018.

[21] S. Azzam, E. Feilat, and A. Al-Salaymeh, "Impact of connecting renewable energy plants on the capacity and voltage stability of the national grid of Jordan," in *2017 8th International Renewable Energy Congress (IREC)*, 2017, pp. 1-6.

[22] M. Furukakoi, O. B. Adewuyi, H. Matayoshi, A. M. Howlader, and T. Senjyu, "Multi objective unit commitment with voltage stability and PV uncertainty," *Applied Energy,* vol. 228, pp. 618-623, 2018/10/15/ 2018.

[23] G. Magdy, E. A. Mohamed, G. Shabib, A. A. Elbaset, and Y. Mitani, "SMES based a new PID controller for frequency stability of a real hybrid power system considering high wind power penetration," *IET Renewable Power Generation*, vol. 12, no. 11, pp. 1304-1313Available: https://digital-library.theiet.org/content/journals/10.1049/iet-rpg.2018.5096

[24] N. Nguyen and J. Mitra, "Reliability of Power System with High Wind Penetration Under Frequency Stability Constraint," *IEEE Transactions on Power Systems,* vol. 33, no. 1, pp. 985-994, 2018.

[25] E. M. Wazeer, R. El-Azab, M. Daowd, and A. M. A. Ghany, "Short-Term Frequency Stability Regulation for Power System with Large-Scale Wind Energy Penetration Using PID Controller," in *2018 Twentieth International Middle East Power Systems Conference (MEPCON)*, 2018, pp. 1059-1063.

[26] E. A. Feilat, S. Azzam, and A. Al-Salaymeh, "Impact of large PV and wind power plants on voltage and frequency stability of Jordan's national grid," *Sustainable Cities and Society,* vol. 36, pp. 257-271, 2018/01/01/ 2018.

[27] N. Amjady and F. Fallahi, "Determination of frequency stability border of power system to set the thresholds of under frequency load shedding relays," *Energy Conversion and Management,* vol. 51, no. 10, pp. 1864-1872, 2010/10/01/ 2010.

[28] V. V. Terzija, "Adaptive underfrequency load shedding based on the magnitude of the disturbance estimation," *IEEE Transactions on Power Systems,* vol. 21, no. 3, pp. 1260-1266, 2006.

[29] S. Chandak, P. Bhowmik, and P. K. Rout, "Load shedding strategy coordinated with storage device and D-STATCOM to enhance the microgrid stability," *Protection and Control of Modern Power Systems,* vol. 4, no. 1, p. 22, 2019/11/22 2019.

[30] S. Zhiming, L. Yong, L. Chen, M. Zhenbin, and D. Lei, "Review on over-frequency generator tripping for frequency stability control," in *2016 IEEE PES Asia-Pacific Power and Energy Engineering Conference (APPEEC)*, 2016, pp. 2240-2243.

[31] M. N. H. Shazon, H. M. Ahmed, and M. Nahid Al, "Over-Frequency Mitigation Using Coordinated Generator Shedding Scheme in a Low Inertia Power System," in *2020 IEEE Region 10 Symposium (TENSYMP)*, 2020, pp. 560-563.

[32] P. Tielens and D. Van Hertem, "The relevance of inertia in power systems," *Renewable and Sustainable Energy Reviews,* vol. 55, pp. 999-1009, 2016/03/01/ 2016.

[33] A. Mokari-Bolhasan, H. Seyedi, B. Mohammadi-ivatloo, S. Abapour, and S. Ghasemzadeh, "Modified centralized ROCOF based load shedding scheme in an islanded distribution network," *International Journal of Electrical Power & Energy Systems,* vol. 62, pp. 806-815, 2014/11/01/ 2014.

[34] "Technical Report on the event of 9 August 2019," 2019, Available: https://www.nationalgrideso.com/information-about-great-britains-energy-system-and-electricity-system-operator-eso.

[35] J. Wen, S. Bu, B. Zhou, Q. Chen, and D. Yang, "A Fast-Algorithmic Probabilistic Evaluation on Regional Rate of Change of Frequency (RoCoF) for Operational Planning of High Renewable Penetrated Power Systems," *Energies,* vol. 13, no. 11, 2020.

[36] H. Zhang, "Introduction to Transmission Expansion Planning in Power Systems," in *Electric Power Engineering Research and Education: A festschrift for Gerald T. Heydt*, E. Kyriakides, S. Suryanarayanan, and V. Vittal, Eds. Cham: Springer International Publishing, 2015, pp. 155-183.

[37] R. Preece and J. V. Milanović, "Risk-Based Small-Disturbance Security Assessment of Power Systems," *IEEE Transactions on Power Delivery,* vol. 30, no. 2, pp. 590-598, 2015.

[38] S. Bu, J. Wen, and F. Li, "A Generic Framework for Analytical Probabilistic Assessment of Frequency Stability in Modern Power System Operational Planning," *IEEE Transactions on Power Systems,* pp. 1-1, 2019.

[39] M. Negnevitsky, D. H. Nguyen, and M. Piekutowski, "Risk Assessment for Power System Operation Planning With High Wind Power Penetration," *IEEE Transactions on Power Systems,* vol. 30, no. 3, pp. 1359-1368, 2015.

[40] B. Hu, L. Wu, and M. Marwali, "On the Robust Solution to SCUC With Load and Wind Uncertainty Correlations," *IEEE Transactions on Power Systems,* vol. 29, no. 6, pp. 2952-2964, 2014.

[41] S. Q. Bu, W. Du, H. F. Wang, Z. Chen, L. Y. Xiao, and H. F. Li, "Probabilistic Analysis of Small-Signal Stability of Large-Scale Power Systems as Affected by Penetration of Wind Generation," *IEEE Transactions on Power Systems,* vol. 27, no. 2, pp. 762-770, 2012.

[42] M. Aien, M. Fotuhi-Firuzabad, and F. Aminifar, "Probabilistic Load Flow in Correlated Uncertain Environment Using Unscented Transformation," *IEEE Transactions on Power Systems,* vol. 27, no. 4, pp. 2233-2241, 2012.

[43] M. T. Bina and D. Ahmadi, "Stochastic Modeling for the Next Day Domestic Demand Response Applications," *IEEE Transactions on Power Systems,* vol. 30, no. 6, pp. 2880-2893, 2015.

[44] L. Wu and D. G. Infield, "Towards an Assessment of Power System Frequency Support From Wind Plant—Modeling Aggregate Inertial Response," *IEEE Transactions on Power Systems,* vol. 28, no. 3, pp. 2283-2291, 2013.

[45] Y. Li, W. Li, W. Yan, J. Yu, and X. Zhao, "Probabilistic Optimal Power Flow Considering Correlations of Wind Speeds Following Different Distributions," *IEEE Transactions on Power Systems,* vol. 29, no. 4, pp. 1847-1854, 2014.

[46] Z. Qin, W. Li, and X. Xiong, "Generation System Reliability Evaluation Incorporating Correlations of Wind Speeds With Different Distributions," *IEEE Transactions on Power Systems,* vol. 28, no. 1, pp. 551-558, 2013.

[47] A. Soroudi, M. Aien, and M. Ehsan, "A Probabilistic Modeling of Photo Voltaic Modules and Wind Power Generation Impact on Distribution Networks," *IEEE Systems Journal,* vol. 6, no. 2, pp. 254-259, 2012.

[48] V. A. Evangelopoulos and P. S. Georgilakis, "Optimal distributed generation placement under uncertainties based on point estimate method embedded genetic algorithm," *IET Generation, Transmission & Distribution,* vol. 8, no. 3, pp. 389-400, 2014.

[49] M. Fan, V. Vittal, G. T. Heydt, and R. Ayyanar, "Probabilistic Power Flow Analysis With Generation Dispatch Including Photovoltaic Resources," *IEEE Transactions on Power Systems,* vol. 28, no. 2, pp. 1797-1805, 2013.

[50] H. Huang, C. Y. Chung, K. W. Chan, and H. Chen, "Quasi-Monte Carlo Based Probabilistic Small Signal Stability Analysis for Power Systems With Plug-In Electric Vehicle and Wind Power Integration," *IEEE Transactions on Power Systems,* vol. 28, no. 3, pp. 3335-3343, 2013.

[51] J. L. Rueda, D. G. Colome, and I. Erlich, "Assessment and Enhancement of Small Signal Stability Considering Uncertainties," *IEEE Transactions on Power Systems,* vol. 24, no. 1, pp. 198-207, 2009.

[52] G. Papaefthymiou and D. Kurowicka, "Using Copulas for Modeling Stochastic Dependence in Power System Uncertainty Analysis," *IEEE Transactions on Power Systems,* vol. 24, no. 1, pp. 40-49, 2009.

[53] S. O. Faried, R. Billinton, and S. Aboreshaid, "Probabilistic Evaluation of Transient Stability of a Wind Farm," *IEEE Transactions on Energy Conversion,* vol. 24, no. 3, pp. 733-739, 2009.

[54] J. Rueda and D. Colome, "Probabilistic performance indexes for small signal stability enhancement in weak wind-hydro-thermal power systems," *IET generation, transmission & distribution,* vol. 3, no. 8, pp. 733-747, 2009.

[55] E. Vaahedi, W. Li, T. Chia, and H. Dommel, "Large scale probabilistic transient stability assessment using BC Hydro's on-line tool," *IEEE Transactions on Power Systems,* vol. 15, no. 2, pp. 661-667, 2000.

[56] K. N. Hasan and R. Preece, "Impact of stochastic dependence within load and non-synchronous generation on frequency stability," in *Bulk power systems dynamics and control symposium*, 2017.

[57] Z. Y. Dong, J. H. Zhao, and D. J. Hill, "Numerical Simulation for Stochastic Transient Stability Assessment," *IEEE Transactions on Power Systems,* vol. 27, no. 4, pp. 1741-1749, 2012.

[58] E. Carpaneto and G. Chicco, "Evaluation of the probability density functions of distribution system reliability indices with a characteristic functions-based approach," *IEEE Transactions on Power Systems,* vol. 19, no. 2, pp. 724-734, 2004.

[59] J. M. Nahman and M. R. Tanaskovic, "Probability Models for Optimal Sparing of Distribution Network Transformers," *IEEE Transactions on Power Delivery,* vol. 24, no. 2, pp. 758-763, 2009.

[60] R. Billinton, P. R. S. Kuruganty, and M. F. Carvalho, "An Approximate Method for Probabilistic Assessment of Transient Stability," *IEEE Transactions on Reliability,* vol. R-28, no. 3, pp. 255-258, 1979.

[61] S. Faried, R. Billinton, and S. Aboreshaid, "Probabilistic evaluation of transient stability of a power system incorporating wind farms," *IET Renewable Power Generation,* vol. 4, no. 4, pp. 299-307, 2010.

[62] Z. Xia and Z. Jiaqi, "Probabilistic transient stability assessment based on distributed DSA computation tool," in *2010 IEEE 11th International Conference on Probabilistic Methods Applied to Power Systems*, 2010, pp. 685-690.

[63] A. S. Ahmadyar, S. Riaz, G. Verbi, x010D, A. Chapman, and D. J. Hill, "A Framework for Assessing Renewable Integration Limits With Respect to Frequency Performance," *IEEE Transactions on Power Systems,* vol. 33, no. 4, pp. 4444-4453, 2018.

[64] T. Amraee, M. G. Darebaghi, A. Soroudi, and A. Keane, "Probabilistic Under Frequency Load Shedding Considering RoCoF Relays of Distributed Generators," *IEEE Transactions on Power Systems,* vol. 33, no. 4, pp. 3587-3598, 2018.

[65] J. S. Liu and R. Chen, "Sequential Monte Carlo Methods for Dynamic Systems," *Journal of the American Statistical Association,* vol. 93, no. 443, pp. 1032-1044, 1998/09/01 1998.

[66] C. Andrieu, A. Doucet, and E. Punskaya, "Sequential Monte Carlo Methods for Optimal Filtering," in *Sequential Monte Carlo Methods in Practice*, A. Doucet, N. de Freitas, and N. Gordon, Eds. New York, NY: Springer New York, 2001, pp. 79-95.

[67] J. C. O. Mello, M. V. F. Pereira, and A. M. L. da Silva, "Evaluation of Reliability Worth in Composite Systems based on Pseudo-Sequential Monte Carlo Simulation," *IEEE Transactions on Power Systems,* Article vol. 9, no. 3, pp. 1318-1326, 1994.

[68] F. Vallée, C. Versèle, J. Lobry, and F. Moiny, "Non-sequential Monte Carlo simulation tool in order to minimize gaseous pollutants emissions in presence of fluctuating wind power," *Renewable Energy,* Article vol. 50, pp. 317-324, 2013.

[69] W. K. Hastings, "Monte Carlo sampling methods using Markov chains and their applications," *Biometrika,* vol. 57, no. 1, pp. 97-109, 1970.

[70] L. Tierney, *The Annals of Statistics,* p. 1701, 1994.

[71] S. V. Dhople and A. D. Dominguez-Garcia, "A parametric uncertainty analysis method for markov reliability and reward models," *IEEE Transactions on Reliability,* Article vol. 61, no. 3, pp. 634-648, 2012, Art. no. 6246660.

[72] Y. Zhao, F. Fan, J. Wang, and K. Xie, "Uncertainty analysis for bulk power systems reliability evaluation using Taylor series and nonparametric probability density estimation," *International Journal of Electrical Power and Energy Systems,* Article vol. 64, pp. 804-814, 2015.

[73] C. Wan, Z. Xu, Z. Y. Dong, and K. P. Wong, "Probabilistic load flow computation using first-order second-moment method," in *2012 IEEE Power and Energy Society General Meeting*, 2012, pp. 1-6.

[74] X. Li, Y. Li, and S. Zhang, "Analysis of Probabilistic Optimal Power Flow Taking Account of the Variation of Load Power," *IEEE Transactions on Power Systems,* Article vol. 23, no. 3, pp. 992-999, 2008.

[75] A. Soroudi and M. Afrasiab, "Binary PSO-based dynamic multi-objective model for distributed generation planning under uncertainty," *IET Renewable Power Generation*, vol. 6, no. 2*,* pp. 67-78.

[76] X. Li, J. Cao, and D. Du, "Two-Point Estimate Method for Probabilistic Optimal Power Flow Computation Including Wind Farms with Correlated Parameters," in *Intelligent Computing for Sustainable Energy and Environment*, Berlin, Heidelberg, 2013, pp. 417-423: Springer Berlin Heidelberg.

[77] S. J. Julier and J. K. Uhlmann, "Unscented filtering and nonlinear estimation," *Proceedings of the IEEE,* vol. 92, no. 3, pp. 401-422, 2004.

[78] R. Preece, K. Huang, and J. V. Milanović, "Probabilistic Small-Disturbance Stability Assessment of Uncertain Power Systems Using Efficient Estimation Methods," *IEEE Transactions on Power Systems,* vol. 29, no. 5, pp. 2509-2517, 2014.

[79] K. N. Hasan, R. Preece, and J. V. Milanović, "Existing approaches and trends in uncertainty modelling and probabilistic stability analysis of power systems with renewable generation," *Renewable and Sustainable Energy Reviews,* vol. 101, pp. 168-180, 2019/03/01/ 2019.

[80] T. Ackermann, T. Prevost, V. Vittal, A. J. Roscoe, J. Matevosyan, and N. Miller, "Paving the Way: A Future Without Inertia Is Closer Than You Think," *IEEE Power and Energy Magazine,* vol. 15, no. 6, pp. 61-69, 2017.

[81] R. Azizipanah-Abarghooee, M. Malekpour, M. Paolone, and V. Terzija, "A New Approach to the Online Estimation of the Loss of Generation Size in Power Systems," *IEEE Transactions on Power Systems,* vol. 34, no. 3, pp. 2103-2113, 2019.

[82] "IEEE Standard for Synchrophasor Measurements for Power Systems," *IEEE Std C37.118.1-2011 (Revision of IEEE Std C37.118-2005),* pp. 1-61, 2011.

[83] C. Wu, M. E. Magaña, and E. Cotilla-Sánchez, "Dynamic Frequency and Amplitude Estimation for Three-Phase Unbalanced Power Systems Using the Unscented Kalman Filter," *IEEE Transactions on Instrumentation and Measurement,* vol. 68, no. 9, pp. 3387-3395, 2019.

[84] J. Khodaparast and M. Khederzadeh, "Least square and Kalman based methods for dynamic phasor estimation: a review," *Protection and Control of Modern Power Systems,* vol. 2, no. 1, p. 1, 2017/01/26 2017.

[85] W. Maohai and S. Yuanzhang, "A practical, precise method for frequency tracking and phasor estimation," *IEEE Transactions on Power Delivery,* vol. 19, no. 4, pp. 1547-1552, 2004.

[86] S. Wen *et al.*, "Optimal sizing of hybrid energy storage sub-systems in PV/diesel ship power system using frequency analysis," *Energy,* vol. 140, pp. 198-208, 2017/12/01/ 2017.

[87] C. Li, Y. Tao, W. Ao, S. Yang, and Y. Bai, "Improving forecasting accuracy of daily enterprise electricity consumption using a random forest based on ensemble empirical mode decomposition," *Energy,* vol. 165, pp. 1220-1227, 2018/12/15/ 2018.

[88] Y. Yin, T. Liu, L. Wu, C. He, and Y. Liu, "Frequency-constrained multi-source power system scheduling against N-1 contingency and renewable uncertainty," *Energy,* vol. 216, p. 119296, 2021/02/01/ 2021.

[89] U. Markovic, Z. Chu, P. Aristidou, and G. Hug, "Fast Frequency Control Scheme through Adaptive Virtual Inertia Emulation," in *2018 IEEE Innovative Smart Grid Technologies - Asia (ISGT Asia)*, 2018, pp. 787-792.

[90] H. Gu, R. Yan, and T. K. Saha, "Minimum Synchronous Inertia Requirement of Renewable Power Systems," *IEEE Transactions on Power Systems,* vol. 33, no. 2, pp. 1533-1543, 2018.

[91] P. M. Anderson and A. A. Fouad, *Power System Control and Stability*. Ames, IA: Iowa State Uni. Press, 1977.

[92] G. Frigo, A. Derviškadić, Y. Zuo, and M. Paolone, "PMU-Based ROCOF Measurements: Uncertainty Limits and Metrological Significance in Power System Applications," *IEEE Transactions on Instrumentation and Measurement,* vol. 68, no. 10, pp. 3810-3822, 2019.

[93] A. G. Phadke and B. Kasztenny, "Synchronized Phasor and Frequency Measurement Under Transient Conditions," *IEEE Transactions on Power Delivery,* vol. 24, no. 1, pp. 89-95, 2009.

[94] A. E. M. Operator, "Integrating renewable energy-Wind integration studies report," 2013, Available: https://www.aemo.com.au/-/media/files/pdf/integrating-renewable-energy--wind-integration-studies-report-2013pdf.pdf.

[95] P. M. Ashton, C. S. Saunders, G. A. Taylor, A. M. Carter, and M. E. Bradley, "Inertia Estimation of the GB Power System Using Synchrophasor Measurements," *IEEE Transactions on Power Systems,* vol. 30, no. 2, pp. 701-709, 2015.

[96] Q. Hong *et al.*, "Fast frequency response for effective frequency control in power systems with low inertia," *The Journal of Engineering,* vol. 2019, no. 16, pp. 1696-1702, 2019.

[97] J. Driesen and K. Visscher, "Virtual synchronous generators," in *2008 IEEE Power and Energy Society General Meeting - Conversion and Delivery of Electrical Energy in the 21st Century*, 2008, pp. 1-3.

[98] H. Beck and R. Hesse, "Virtual synchronous machine," in *2007 9th International Conference on Electrical Power Quality and Utilisation*, 2007, pp. 1-6.

[99] Q. Zhong and G. Weiss, "Synchronverters: Inverters That Mimic Synchronous Generators," *IEEE Transactions on Industrial Electronics,* vol. 58, no. 4, pp. 1259-1267, 2011.

[100] V. Karapanos, P. Kotsampopoulos, and N. Hatziargyriou, "Performance of the linear and binary algorithm of virtual synchronous generators for the emulation of rotational inertia," *Electric Power Systems Research,* vol. 123, pp. 119-127, 2015/06/01/ 2015.

[101] T. Kerdphol, F. S. Rahman, M. Watanabe, Y. Mitani, D. Turschner, and H. Beck, "Enhanced Virtual Inertia Control Based on Derivative Technique to Emulate Simultaneous Inertia and Damping Properties for Microgrid Frequency Regulation," *IEEE Access,* vol. 7, pp. 14422-14433, 2019.

[102] L. Ruttledge and D. Flynn, "Emulated Inertial Response From Wind Turbines: Gain Scheduling and Resource Coordination," *IEEE Transactions on Power Systems,* vol. 31, no. 5, pp. 3747-3755, 2016.

[103] E. Rakhshani and P. Rodriguez, "Inertia Emulation in AC/DC Interconnected Power Systems Using Derivative Technique Considering Frequency

Measurement Effects," *IEEE Transactions on Power Systems,* vol. 32, no. 5, pp. 3338-3351, 2017.

[104] O. N. Buwa and G. N. Jadhav, "Primary frequency support by virtual synchronous generator with precise frequency detection techniques," in *2016 IEEE 7th Power India International Conference (PIICON)*, 2016, pp. 1-6.

[105] I. Serban and C. P. Ion, "Microgrid control based on a grid-forming inverter operating as virtual synchronous generator with enhanced dynamic response capability," *International Journal of Electrical Power & Energy Systems,* vol. 89, pp. 94-105, 2017/07/01/ 2017.

[106] J. Fang, H. Li, Y. Tang, and F. Blaabjerg, "Distributed Power System Virtual Inertia Implemented by Grid-Connected Power Converters," *IEEE Transactions on Power Electronics,* vol. 33, no. 10, pp. 8488-8499, 2018.

[107] F. S. Rahman, T. Kerdphol, M. Watanabe, and Y. Mitani, "Optimization of virtual inertia considering system frequency protection scheme," *Electric Power Systems Research,* vol. 170, pp. 294-302, 2019/05/01/ 2019.

[108] Y. Wen, W. Li, G. Huang, and X. Liu, "Frequency Dynamics Constrained Unit Commitment With Battery Energy Storage," *IEEE Transactions on Power Systems,* vol. 31, no. 6, pp. 5115-5125, 2016.

[109] F. Teng, V. Trovato, and G. Strbac, "Stochastic Scheduling With Inertia-Dependent Fast Frequency Response Requirements," *IEEE Transactions on Power Systems,* vol. 31, no. 2, pp. 1557-1566, 2016.

[110] P. Daly, H. W. Qazi, and D. Flynn, "RoCoF-Constrained Scheduling Incorporating Non-Synchronous Residential Demand Response," *IEEE Transactions on Power Systems,* pp. 1-1, 2019.

[111] J. H. Chow, *Time-scale modeling of dynamic networks with applications to power systems*. New York Springer-Verlag, 1982.

[112] J. H. Chow, J. Cullum, and R. A. Willoughby, "A Sparsity-Based Technique for Identifying Slow-Coherent Areas in Large Power Systems," *IEEE Power Engineering Review,* vol. PER-4, no. 3, pp. 23-24, 1984.

[113] Z. Ma, L. Ding, Z. Liu, Y. Guo, Q. Liu, and W. Bao, "The application of a generator coherency identification method based on linearization in complex power system," in *2016 China International Conference on Electricity Distribution (CICED)*, 2016, pp. 1-5.

[114] H. U. Banna, T. Iqbal, A. Khan, and Z. Zahra, "Generators coherency identification using relative correlation based clustering," in *2018 International Conference on Engineering and Emerging Technologies (ICEET)*, 2018, pp. 1-5.

[115] S. Wang, S. Lu, G. Lin, and N. Zhou, "Measurement-based coherency identification and aggregation for power systems," in *2012 IEEE Power and Energy Society General Meeting*, 2012, pp. 1-7.

[116] A. M. Khalil and R. Iravani, "A Dynamic Coherency Identification Method Based on Frequency Deviation Signals," *IEEE Transactions on Power Systems,* vol. 31, no. 3, pp. 1779-1787, 2016.

[117] J. Wen and S. Bu, "Performance Evaluation of Coherency Identification Methods in Frequency Stability Analysis Based on A Novel Assessment Index," in *2018 IEEE 2nd International Electrical and Energy Conference (CIEEC)*, 2018, pp. 132-137.

[118] P. M. Anderson and M. Mirheydar, "A low-order system frequency response model," *IEEE Transactions on Power Systems,* vol. 5, no. 3, pp. 720-729, 1990.

[119] I. Egido, F. Fernandez-Bernal, P. Centeno, and L. Rouco, "Maximum Frequency Deviation Calculation in Small Isolated Power Systems," *IEEE Transactions on Power Systems,* vol. 24, no. 4, pp. 1731-1738, 2009.

[120] L. Liu, W. Li, Y. Ba, J. Shen, C. Jin, and K. Wen, "An Analytical Model for Frequency Nadir Prediction Following a Major Disturbance," *IEEE Transactions on Power Systems,* vol. 35, no. 4, pp. 2527-2536, 2020.

[121] Q. Shi, F. Li, and H. Cui, "Analytical Method to Aggregate Multi-Machine SFR Model With Applications in Power System Dynamic Studies," *IEEE Transactions on Power Systems,* vol. 33, no. 6, pp. 6355-6367, 2018.

[122] H. Cramer, *Numerical Methods of Statistics*. NJ, Princeton: Princeton University, 1946.

[123] M. Kendall, *Kendall's Advanced Theory Statistics*. New York: Oxford University, 1987.

[124] I. Abouzahr and R. Ramakumar, "An approach to assess the performance of utility-interactive wind electric conversion systems," *IEEE Transactions on Energy Conversion,* vol. 6, no. 4, pp. 627-638, 1991.

[125] NationalgridESO. Review of the NETS SQSS Criteria for Frequency Control that drive reserve, response and inertia holding on the GB electricity system [Online]. Available: https://www.nationalgrideso.com/industry-information/codes/security-and-quality-supply-standards-old/modifications/gsr027-review

[126] T. Ackermann, *Wind Power in Power Systems, 2nd Edition*. England: Hon Wiley & Sons, 2012.

[127] L. Freris and D. Infield, *Renewable Energy in Power Systems*. New York: Wiley, 2008.

[128] A. Ulbig, T. Rinke, S. Chatzivasileiadis, and G. Andersson, "Predictive control for real-time frequency regulation and rotational inertia provision in power systems," in *52nd IEEE Conference on Decision and Control*, 2013, pp. 2946-2953.

[129] D. W. B. S. W. Haifeng, "Effect of Stochastic Variation of Grid-connected Wind Generation on Power System Small-signal Probabilistic Stability " *Proceedings of the CSEE,* vol. 31, pp. 7-11, 2011.

[130] K. Zhang, B. Wang, D. Liu, J. Zhao, Y. Guo, and Z. Wu, "Prediction Modeling of Frequency Response Characteristic of Power System Based on Historical Data," in *2020 IEEE/IAS Industrial and Commercial Power System Asia (I&CPS Asia)*, 2020, pp. 1486-1490.

List of Publications

Journal paper

1. S. Bu, **J. Wen** and F. Li, "A Generic Framework for Analytical Probabilistic Assessment of Frequency Stability in Modern Power System Operational Planning," *IEEE Transactions on Power Systems*, vol. 34, no. 5, pp. 3973-3976, Sept. 2019. DOI: 10.1109/TPWRS.2019.2924149.

2. **J. Wen**, S. Bu, B. Zhou, Q. Chen, and D. Yang, "A Fast-Algorithmic Probabilistic Evaluation on Regional Rate of Change of Frequency (RoCoF) for Operational Planning of High Renewable Penetrated Power Systems," *Energies*, vol. 13, 2780. DOI: 10.3390/en13112780.

3. **J. Wen**, S. Bu, F. Li, and P. Du, "Risk assessment and mitigation on area-level RoCoF for operational planning," *Energy*, vol. 228, 120632, 1 August 2021. DOI: 10.1016/j.energy.2021.120632.

4. **J. Wen**, S. Bu, and H. Xin, "Probabilistic Assessment on Area-level Frequency Nadir/Vertex for Operational Planning of High Renewable Penetrated Power Systems," in IEEE Open Access Journal of Power and Energy, vol. 8, pp. 341-351, 2021. DOI: 10.1109/OAJPE.2021.3108428.

5. **J. Wen** and S. Bu, "Uncertainty Modeling in Power System Assessment: A Review," submitted to *Frontiers in Energy Research*, 703350, 30 April 2021.

6. **J. Wen**, S. Bu, Q. Chen, and B. Zhou, "Data Learning-based Frequency Risk Assessment in a High-penetrated Renewable Power System," *Power Generation Technology*, 2021, 42(1): 40-47.

7. **J. Wen** and S. Bu, "Two-Level Ensemble Methods for Efficient Assessment and Region Visualization of Maximal Frequency Deviation Risk," submitted to *IEEE Transactions on Power System*, TPWRS-01354-2021, 23 August 2021.

8. **J. Wen**, S. Bu, J. Luo, and Q. Hu, “Comparison of Two Coherency Identification Methods for Frequency Response Assessment on a Large-scale Power System with Fluctuating Wind Power Generation”, in *the 11th International Conference on Advances in Power System Control, Operation & Management (APSCOM)*, 2018. DOI: 10.1049/cp.2018.1757.

9. **J. Wen** and S. Bu, "Performance Evaluation of Coherency Identification Methods in Frequency Stability Analysis Based on A Novel Assessment Index," in *the 2018 IEEE 2nd International Electrical and Energy Conference (CIEEC)*, 2018, pp. 132-137. DOI: 10.1109/CIEEC.2018.8745778.